

8-2017

Proteinaceous Resin and Hydrophilic Encapsulation: A Self-Healing-Related Study

Ting Zheng

Clemson University, zhengzting@gmail.com

Follow this and additional works at: https://tigerprints.clemson.edu/all_dissertations

Recommended Citation

Zheng, Ting, "Proteinaceous Resin and Hydrophilic Encapsulation: A Self-Healing-Related Study" (2017). *All Dissertations*. 1996.
https://tigerprints.clemson.edu/all_dissertations/1996

This Dissertation is brought to you for free and open access by the Dissertations at TigerPrints. It has been accepted for inclusion in All Dissertations by an authorized administrator of TigerPrints. For more information, please contact kokeefe@clemson.edu.

PROTEINACEOUS RESIN AND HYDROPHILIC ENCAPSULATION:
A SELF-HEALING-RELATED STUDY

A Dissertation
Presented to
the Graduate School of
Clemson University

In Partial Fulfillment
of the Requirements for the Degree
Doctor of Philosophy
Automotive Engineering

by
Ting Zheng
August 2017

Accepted by:
Professor Srikanth Pilla, Committee Chair
Professor Annel Greene
Professor Yi Zheng
Professor Mark Hoffman
Dr. Craig M. Clemons

ABSTRACT

Inspired by living organisms, self-healing materials have been designed as smart materials. Their automatic healing nature is achieved through the use of capsule in which the healing agent is encapsulated. The occurrence of cracks leads to ripping of the capsule, along with crack propagation and release of the healing agent that wets the crack surface to eventually heal (bond) the crack. Such automatic repair of the crack significantly extends the service life of the material.

A vast majority of existing self-healing systems have been designed for the epoxy matrix – the most common commercially used thermoset – that possesses low crack resistance. Currently, self-healing systems have not yet been introduced for fully protein-based materials, despite their great potential to replace currently used synthesis precursors for the latter and the eco-friendly nature of self-healing materials. This has been probably due to two major obstacles: poor mechanical properties of the protein-based matrix, and extreme difficulty associated with the encapsulation of hydrophilic healing agents suitable for the protein-based matrix. This study provides possible solutions towards addressing both these obstacles.

To improve the inherent mechanical properties of protein-based resin, soy protein isolate (SPI) was chosen as the model in this study. Dialdehyde carboxymethyl cellulose (DCMC) was synthesized and used as the crosslinking agent to modify the SPI film. As-synthesized DCMC – a fully bio-based material – exhibited high mechanical strength, excellent thermal stability, and reduced moisture sensitivity. Good compatibility and effective crosslinking were believed to be the key reasons for such property enhancements.

However, these were accompanied by poor crack resistance, where self-healing is a pertinent solution.

A novel healing system for the protein matrix was designed in this work via the use of formaldehyde as a healing agent. Subsequently, the well-acknowledged challenge, e.g. hydrophilic agent encapsulation, was addressed through the development of novel polyurethane-Poly(melamine-formaldehyde) (PU-PMF) dual-component capsules. Remarkably, the external PU insulation layer was fabricated through interfacial polymerization based on a water-in-oil-in-oil (W/O/O) emulsion template. Surface tension was identified as the main driving factor for the formation of the external oil phase. The internal PMF layer was observed to strongly influence the internal morphology of the capsule. A protocol was developed, and a typical capsule with dense and neat shell morphology with a shell/capsule diameter (around 3 %) was fabricated.

This study provides solutions for the two aforementioned obstacles related to the development of the healing system for the protein-based materials.

ACKNOWLEDGMENTS

I am extremely fortunate in my life to work with a group of great people in a great research group. It is my luck to meet a respectful person, Dr. Pilla. Without his guidance, patience, and providing me with an excellent atmosphere for doing my research, I would never have been able to finish my dissertation. It is an enjoyable journey.

I must list names of two critical people who led me to this wonderful journey: Dr. Chenbo Dong and Dr. Xiaoyan Yu.

I would also like to thank my colleague Rakesh Iyer, who supported me to refine my dissertation.

TABLE OF CONTENTS

	Page
TITLE PAGE	i
ABSTRACT	ii
ACKNOWLEDGMENTS	iv
LIST OF TABLES	v
LIST OF FIGURES	xi
LIST OF SYMBOLS AND ABBREVIATIONS	xii
CHAPTER	
I. INTRODUCTION AND LITERATURE	1
1.1 Protein-based resin.....	1
1.2 Designing self-healing system for the protein-based material.....	4
1.3 Encapsulation.....	5
1.4 Overview of the dissertation	13
II. MECHANICAL AND MOISTURE SENSITIVITY OF FULLY BIO-BASED DIALDEHYDE CARBOXYMETHYL CELLULOSE CROSS-LINKED SOY PROTEIN ISOLATE FILMS	14
2.1 Introduction.....	15
2.2 Materials and methods	16
2.3 Results and discussion	22
2.4 Conclusion	40
2.5 Supporting information:.....	40
III. ENCAPSULATING HYDROPHILIC SOLUTION BY PU-PMF DOUBLE COMPONENT CAPSULE BASED ON WATER-IN-OIL-IN-OIL EMULSION TEMPLATE	42
3.1 Introduction.....	43
3.2 Results and discussion	45

Table of Contents (Continued)	Page
3.3 Conclusion	54
3.4 Support information	55
IV. ENCAPSULATION OF HYDROPHILIC PAYLOAD BY PU-PMF CAPSULE: EFFECT OF SHELL FORMING CONTENT, PH VALUE AND TEMPERATURE ON CAPSULE MORPHOLOGY	75
4.1 Introduction	75
4.2 Experimental	78
4.3 Results and discussions	82
4.4 Conclusion	97
V. CONCLUSION AND FUTURE WORK	98
5.1 Conclusion	98
5.2 Future work	100
REFERENCES	102

LIST OF TABLES

Table		Page
1.1	Performance of existing protein-based materials.....	4
2.1	T% and transparency of SPI-DCMC films	26
2.2	Moisture content, insoluble matter percentage and WVP of SPI-DCMC films.....	35
4.1	Preparation parameters for different batches of microcapsules.....	79
S 3.1	Characteristics of hydrophobically modified nanoclay	58
S 3.2	Typical recipe for conventional method	62
S 3.3	Molecular weight of the polymeric isocyanate (PPI)	64
S 3.4	Composition of multilayer PM-PU capsules	74

LIST OF FIGURES

Figure	Page
1.1	Schematic of polycondensation interfacial polymerization (adapted from 37) 6
1.2	Schematic of Polymerization-induced phase separation..... 9
1.3	Schematic of solvent evaporation induced phase separation..... 9
1.4	Schematic on layer-by-layer polyelectrolyte deposition(adapted from literature 53) 10
2.1	FTIR spectra of DCMC 23
2.2	Appearance (up) and SEM image (bottom) of SPI, SPI-CMC and SPI- DCMC films with 5 wt. % of glycerol. For optical images, a glass sheet (thickness = 3.5 mm) was placed between the film samples and the 6.4 mm × 6.4 mm grid paper to illustrate the opacity. 27
2.3	Mechanical properties of SPI-DCMC and SPI-CMC films with different DCMC/CMC content: Elongation at Break (A); Tensile Strength (B); Young's Modulus and (D) Typical Strain-Stress curves..... 30
2.4	Effect of plasticizer on the mechanical properties of SPI film. Elongation at Break (A); Tensile Strength (B); Typical Strain-Stress Curves (C); and Young's Modulus (D)..... 33
2.5	Experimental results of IMP 35
2.6	Thermal properties of SPI-DCMC film with different DCMC/CMC content (in %) TG curves: (A); DTG curves (B). 39
3.1	Schematic of PU-PMF capsule formation. PPI drop-lets migrate to the interface of water droplet where they fuse, spread and engulf water droplets to form isocyanate-rich layer as the locus of the consequent PU shell-forming reaction. 45
3.2	Characterization of emulsions templates. Optical and fluorescence images of the W/O template droplet (A) and W/O/O template droplet with labelled PPI (B,D). The latter displayed corrugated and wrinkling surfaces with the PPI middle oil layer fluorescently visible. Scale bars are 200 μm.

List of Figures (Continued)	Page
SEM image of lyophilized W/O/O template stabilized by MOCA (C). Scale bar is 20 μm	48
3.3 Microscopy of double component capsule (suspension of xylene). Shell-core structure is visible under bright field (A). Rhodamine cargo is visible under fluorescent microscopy (A-insert). Arrows indicate the position of the “shell” of sample E6. FTIR spectra of capsule, PU, and PMF (B).	51
3.4 SEM image of the external appearance of double component capsules (A & B), and cross section exhibiting hollow (F capsule_BpH6), porous filled (E, capsule_E6) and solid filled (D, capsule_A6) structures. Exfoliated skins (C, I) indicates the multi-layer structure. Detailed synthesis parameters are presented in supporting document.	52
3.5 Aqueous cargo released after glass slide rolling. Optical images of (A-insert): intact dried capsules; (A) and (B): broken capsules; arrow: released water.	53
4.1 FTIR of capsule and its reactants.....	83
4.2 Size distribution curves of template emulsion (n ~ 400, droplets were measured in optical microscopy images), and size distribution curves of final capsules (n ~300, measured in SEM image) obtained with different pre-MF content.	85
4.3 SEM images of capsule with F/M=3:1 but different pre-MF contents: a) 0 % master pre-MF (A1); b) 10 % master pre-MF (A2); c) 25 % master pre-MF (A3); d) 50 % master pre-MF (A4); e) 75 % master pre-MF (A5); f) 100 % master pre-MF (A6). All the scale bars are 200 μm	86
4.4 SEM image of the cross-section of A5 (a-1 & a2) and A6 (b-1 to b-5) capsule. Capsules are crushed by a silicon wafer. Scale bars are 100 μm for a-1 and b-1, 50 μm for the rest.	88
4.5 SEM of capsules prepared with different pH. Step 2 was carried out in pH = 3.0 (a, capsule BpH3), 4.0 (b, capsule BpH4), 5.0 (c, capsule BpH5), 6.0 (d, capsule BpH6) and 6.6 (e, capsule BpH6.6). Surface feature and crushed capsule are presented as inserts respectively. Scale bars are 200 μm	89
4.6 TGA thermograms of capsule (right) and PMF resin (left).	92
4.7 SEM image of capsules prepared at 30C° (a), 50C° (b) and 70C° (c). Inserts include break capsules. The thickness of capsules’ shell (d).	95

List of Figures (Continued)	Page
4.8 Diffusion profile of rhodamine B from the capsule in water (a). Encapsulated solution released after the crush (b &c).....	96
S 2.1 The crosslinking chemistry of DCMC with SPI.....	40
S 2.2 Concentration of residual primary amino group after the DCMC or CMC treatment (top), and the typical colorimetric reaction (bottom).	41
S 3.1 Schematic presentation of the reaction between amine (e.g. MOCA) and an isocyanate (e.g. PPI and TDI).....	57
S 3.2 Schematic representation of the synthesis PPI.....	57
S 3.3 Preparation of inverse Pickering emulsions (W/O template emulsion).....	60
S 3.4 The effect of Cloisite 20 load on the template-emulsion. The scale bar is 200 μm	60
S 3.5 Capsules fabricated by TDI-BD interfacial polymerization on the basis of W/O emulsion (A) collapsed during the in air drying process (B). Optimizing parameters (see Table S2) led to appearance of few survivor capsule after drying (D), and can be torn by pipette tip (E), showing the elastic and soft texture of capsule shell.	63
S 3.6 PPI precipitates out from its cyclohexanone solution upon addition of xylene	65
S 3.7 The fluorescent microscope image of a drop of PPI-Fluor solution (A-C) and its precipitate residual after xylene wash on the slide (E-G). Scale bar = 2000 μm	66
S 3.8 The fluorescent microscope image of pre-emulsion (A-C, scale bar 400 μm), pre-emulsion with PPI (D-F, scale bar = 100 μm), and pre-emulsion with PPI-fluorescence (G-I, scale bar 200 μm , J-L, scale bar 100 μm). Red color indicates the aqueous payload and PPI, and green color indicates PPI	67
S 3.9 Optical and fluorescent images of PPI-MOCA capsules prepared on the basis of W/O/O emulsion, in xylene solution (A &D) and after the evaporation of xylene (B,C,E &F). Black objects in B & E are deemed to be the debris of brittle and solid capsule debris, companied with the aqueous leakage.....	69

List of Figures (Continued)	Page
S 3.10 Schematic presentation of capsulation via PU external layer and PMF skeleton	70
S 3.11 Schematic of two-step poly(melamine-formaldehyde) formation chemistry	72
S 3.12 Shell forming factors analysis. Optical images of dried capsule with different shell formation factors. Images are (A): template emulsion-PPI, (B): template emulsion-PPI with pre-MF in aqueous phase, (C): (B) with excessive formaldehyde, and (D): template emulsion with pre-MF and excess formaldehyde. (E), (F) and (G) samples were prepared same as (A), (B), (C) respectively, but adding MOCA as chain extender in the xylene phase. Results showed that, capsules can only be obtained in case (G), indicating MOCA, PPI, Pre-MF and excessive formaldehyde are critical factors to form robust capsules.....	73

LIST OF SYMBOLS AND ABBREVIATIONS

BD	1,4-butanediol
CMC	carboxymethyl cellulose
DCMC	dialdehyde carboxymethyl cellulose
DAS	dialdehyde starch
EB	elongation at break
FTIR	Fourier Transform Infrared
MOCA	4,4'-methylene bis(2-chloroaniline)
PLA	polylactic acid
PMF	poly (melamine-formaldehyde)
PMPPI	polymethylene-polyphenylene-isocyanate
PPI	polymeric isocyanate
PU	polyurethane
SPI	soy protein isolate
TEDA	triethylenediamine
TGA	thermogravimetric analysis
TS	tensile strength
WVP	water vapor permeability

CHAPTER ONE

1. INTRODUCTION AND LITERATURE

1.1 Protein-based resin

Protein-based materials have drawn the attention of researchers in recent times, in part due to the current focus on addressing environmental issues such as inadequate facilities for waste disposal amidst huge mounds of garbage, and the depletion of non-renewable resources. Various strategies have been designed for partial/full substitution of petroleum-based polymers with alternative bio-based materials, thus endowing sustainability to the final product. Decades of endeavor has led to some bio-based materials exhibiting comparable or better performance than their petroleum-based counterparts, enabling their successful application across several industries. Representative examples include the use of epoxidized plant oil as a substitute to conventional petroleum-based epoxy¹⁻²; phenolic resins originating from cashew nut shell liquid³; renewable polyol derived from bio-pitches; castor oil; and oxy-propylated lignin used for the synthesis of polyurethane⁴, to name a few. Recently, Raquez *at el.* has reviewed the current progress on bio-based thermosetting polymers⁵.

Proteins are composed of amino acid units with a broad range of chain length, ranging from tens of amino acid units up to 100,000 units. In nature, proteins are produced from animal feedstock or through plant products such as casein (from milk), soy protein

and gluten. Commercial application of protein-based materials dates back to 1930s when Henry Ford launched soy-based automobile parts via blending of phenol-formaldehyde resin and soybean meal⁶. This effort later came to a halt due to World War II and subsequent low prices of petroleum-based plastics but has revived in recent years owing to increasing concerns regarding environmental sustainability. Today, Ford and other automotive manufacturers including General Electric (GE), Honda, Daimler, and Renault are demonstrating a commitment to utilize natural resources and wastes to ensure that the automotive sector is eco-friendly and sustainable. Their achievements have been summarized in the “Biobased Automobile Parts Investigation” report issued by the United States Department of Agriculture (USDA) (2012)⁷.

Soy protein remains an excellent model for making protein-based materials. Soy protein is abundant and hence, is relatively inexpensive. Chemically, the molecular weight of soy protein ranges from 20k to 35k Dalton, and it is composed of amino acid residuals, including aspartic acid, glutamic acid, nonpolar amino acids, and < 1 wt. % of cysteine⁸. The functionality of amino acid residuals provides functional groups for subsequent/future modifications. However, a major drawback of soy protein-based materials is their high sensitivity to moisture⁹. To address this problem, soy protein materials are crosslinked with aldehydes, such as formaldehyde¹⁰, glyoxal¹¹ and glutaraldehyde¹². The aldehyde group reacts with amine groups – mainly from lysine (6.2 g/100 g in PRO-FAM 646, the commercial product used in this study) – and leads to the formation of intra- and intermolecular covalent bonds, resulting in a dense crosslinked network. As shown in Table

1.1, crosslinking is an effective approach to improve mechanical properties and sensitivity to moisture.

Gluten is another abundantly available protein in nature. Unlike soy protein, gluten is insoluble in water due to its high uncharged amino acid (glutamine and prolines) content. Hence, it exhibits lower sensitivity to moisture when compared with soy protein. Also, gluten contains a high amount of disulfide bonds, probably due to the high gliadins content, which explains its viscous flow properties without any sign of significant elasticity. Similarly, aldehyde-induced crosslinking is also a proper modification strategy to improve the mechanical properties of gluten-based material¹³. Besides, the reductive L-cysteine could also induce crosslinking by cleaving the existing disulfide bonds, thus promoting the formation of new disulfide bonds¹³⁻¹⁴.

In addition to soy proteins and gluten, the potential of other protein-based materials has also been evaluated in literature, including on egg-white protein¹⁵, gelatin, and keratin¹⁶ that originate from animals. Crosslinking has also been used to effectively improve their mechanical properties and moisture sensitivity. For instance, gelatin, derived from collagen, can be crosslinked by resorcinol, formaldehyde or glutaraldehyde¹⁷.

As discussed above, crosslinking is among the most efficient and commonly used approaches to address the inherent shortcomings of protein-based materials. However, the formation of the crosslinking network also causes brittleness – a common problem with most thermosets. Inspired by the solution designed for epoxies, self-healing strategy was considered to be a possible solution to heal cracks and extend the service life of the product.

Table 1.1 Performance of existing protein-based materials

Type of modification	Bio-matrix	Modifier	Mechanical properties	Thermal stability	Moisture sensitivity	Non-toxicity	References
Coating	SPI	PLA	+++		+	√	18
	SPI	PU	+++		+	√	19
Crosslinking	SPI	Aldehyde	++		+	-	10-12, 20
	SPI	Diglycidyl ester	++		+	-	21
	SPI	Dialdehyde starch (DAS)	+		-	√	22
	Egg white	DAS	+		-	√	15
	Keratin	DAS	-		+	√	16
	Gelatin	DAS	-	√	-	√	23
	Gelatin	DCMC	+		+	√	24
Gluten	Aldehyde	++	√	+	√	13	

1.2 Designing self-healing system for the protein-based material

A lot of capsule-based self-healing strategies have been developed to heal the cracked hydrophobic matrix. Most of these are based on hydrophobic material systems, such as epoxies, multi-amine hardener, or multimaleimide²⁵. Most of the successful epoxy capsules with external PU shell have been prepared in the emulsion system. In such capsules, surface polymerization takes place on the surface of water-in-oil (W/O) emulsion, producing an ideal shell that has low permeability, high loading capacity, good stability and excellent bonding with the matrix. On the other hand, encapsulation of hydrophilic content is currently a challenge²⁶, despite it being in high demand across various applications.

Encapsulation of the hydrophilic filling can be achieved through interfacial polymerization in inverse emulsion. For interfacial polymerization, surfactants were used in this work to stabilize the emulsion droplets. The consequent shell formation reaction, including the epoxy-amine chemistry^{27,28}, isocyanate-amine chemistry²⁹, and isocyanate-polyol chemistry^{26, 30-31} were observed to occur at the interface of the W/O system.

The aim of this study is to prepare the healing capsule suitable for the proteinaceous matrix. Single microcapsule self-healing system was considered in this study to take the advantage of presence of the amine in the protein-based matrix. Curing reaction between the amino group of protein and epoxy has been proven to be too slow at room temperature³² for the purpose of healing. Highly reactive isocyanates-filled capsules have been prepared³³⁻³⁴, without any evaluation of their healing performance. Also, its low protein bonding capacity is not satisfied in adhesive usage³⁵. Another candidate is glycidyl methacrylate that can cure the epoxy substrate at room temperature but needs to react with DETA in the matrix³⁶. Hence, researchers have focused on formaldehyde, glutaraldehyde, and paraformaldehyde that have shown exceptional bonding capacity with protein in existing literature¹⁰.

1.3 Encapsulation

In this section, current strategies to encapsulate payload have been reviewed. Methods for payload encapsulation include polycondensation interfacial polymerization, polymer precipitation by phase separation, layer-by-layer polyelectrolyte deposition, and polymer growth by surface polymerization. Such methods can be broadly categorized into

two groups, depending on the hydrophilic/hydrophobic nature of the payload. Both kinds of methods have been briefly discussed in this section, especially hydrophilic encapsulation as it is relevant to this study.

The general purpose of encapsulation is to isolate the payload from the surroundings; for instance, bioactive enzymes are encapsulated to prevent their denaturing. Self-healing solution remains stored in the capsule until its release is triggered by crack generation and propagation. Also, the capsule carrier integrates add-on properties such as target delivery and controlled release, which is valuable for pharmaceutical applications. Among all these payloads, self-healing reagents are usually hydrophobic, while the drug, water-soluble dye, flavors, preservatives, vitamins and bio-reactive enzymes are usually hydrophilic. The nature of the payload determines the encapsulation strategy. In the following section, various methods are introduced and discussed.

Polycondensation interfacial polymerization

This technique is usually based on the emulsion system. Shell-forming monomers are dissolved in either phase. Therefore, the water-oil (W/O) interface serves as the locus where the reactants meet and react to form a shell “membrane.” This process is depicted in Figure 1.1.

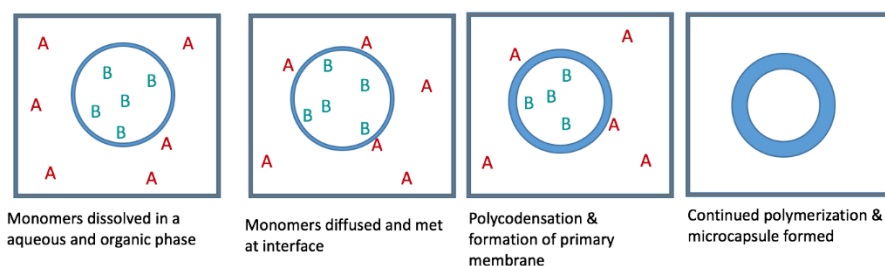


Figure 1.1 Schematic of polycondensation interfacial polymerization (adapted from³⁷)

Generally speaking, this technique can be performed in both oil-in-water (O/W) emulsion system (direct emulsion) and water-in-oil (W/O) emulsion system (inverse emulsion), depending on the nature of the payload to be encapsulated. Also, the size of the resultant capsule is determined by the dimension of the emulsion droplets that are developed. Hence, parameters that affect the size of emulsion capsule will also determine its dimensions. Such parameters include the rate of agitation, surfactant amount and species, and the viscosity of the dispersive phase. The most typical model of this technique is the polyurethane capsule formed using isocyanate, polyol (or polyamine) and nylon capsule fabricated by polyamine and terephthaloyldichloride, which dates back to 1980s when aqueous-containing amine was injected into the oil phase via a syringe³⁸. The process can also be performed in inverse emulsions, thus encapsulating the aqueous phase³⁹. Polyurethane capsule has been extensively investigated due to its versatility. Koh *et al.* produced oil-core capsules with isocyanate derivatives and diol as chain extender to encapsulate hydrophobic corrosion inhibitors. Capsules with neat morphology were facilely fabricated³⁰. Recently, Kuypers *et al.* added the thiol-isocyanate reaction into the chemistry family suitable for the interfacial polymerization and encapsulated aqueous payloads via thiourethane nanocarriers⁴⁰.

Polycondensation interfacial polymerization provides a facile, efficient manner for encapsulating hydrophobic payloads. This is especially evident in its prevalence in the fabrication of self-healing capsules where the hydrophobic epoxy, multiamine hardener, or multimaleimide²⁵ are loaded. However, encapsulation of hydrophilic payload through

this method has not proven successful. Although some cases have been reported, the resultant capsules have been found to be either too small⁴⁰ or too weak^{38, 40}, which inhibit their application.

Interfacial precipitation (by phase separation)

The main difference between interfacial precipitation and polycondensation interfacial polymerization is the location of shell-forming polymers. In the case of interfacial precipitation, the shell-forming polymer precipitates out and gets deposited onto the interface of the droplet. Polymerization-induced phase separation (Case (1)) and Solvent evaporation-induced phase separation (Case (2)) are among the key driving factors that affect this deposition. In Case (1), monomers are dissolved in the dispersive/continuous phase, and chain growth reduces the solubility of resulting polymer. This leads to its separation from the solution and deposition on the internal/external side of the droplet interface, as illustrated in Figure 1.2. The most typical example of this technique is the formation of poly(formaldehyde-melamine) (PMF) capsule, in which pre-PMF oligomer is dissolved in either the continuous phase or dispersed phase. Further crosslinking leads to the separation of PMF polymer and its subsequent deposition, resulting in the formation of the capsule shell⁴¹⁻⁴⁴. Other major chemistries include the poly(methyl methacrylate) (PMMA) capsule⁴⁵⁻⁴⁶.

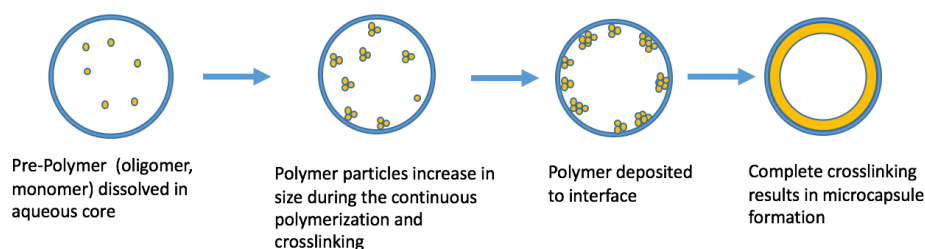


Figure 1.2 Schematic of Polymerization-induced phase separation

Case (2) mainly occurs in the oil-in-water (O/W) system. Shell-forming polymer is dissolved in the dispersed oil phase, which consists of one volatile organic solvent and one non-volatile solvent. Evaporation of the volatile solvent leads to the precipitation of shell-forming polymer on the oil/water interface. Examples of polymers that have employed this technique include PMMA⁴⁷, poly(vinyl phenyl ketone) (PVPK)⁴⁸, and polystyrene (PS)⁴⁹, in the CH₂Cl₂/Hexadecane (good solvent/ poor solvent) system.

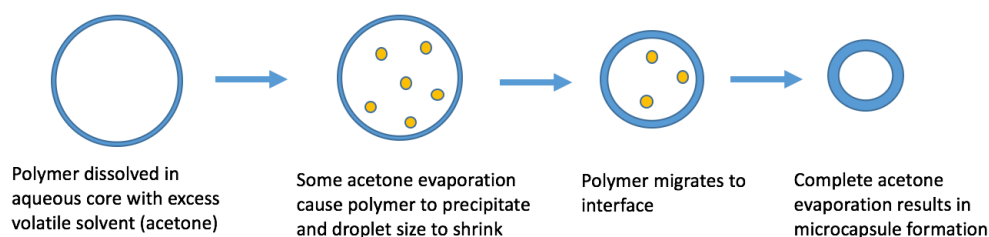


Figure 1.3 Schematic of solvent evaporation induced phase separation

Interfacial precipitation method is commonly used for encapsulation, mainly for preventing oxidation and trapping and controlled release of perfume odor, due to its narrow size distribution and tunable shell thickness. The disadvantage of this technique is its limitation in hydrophilic payload encapsulation (for Case (1)), and difficulty in choosing the proper ternary system (for Case (2))⁵⁰.

The previous two approaches are those that have been successfully employed for commercial large-scale industrial applications for several years. Since our interest is in encapsulating hydrophilic payloads, other less-common methods have also been discussed below.

Layer-by-layer polyelectrolyte deposition

Layer-by-layer polyelectrolyte deposition takes advantage of electrostatic driving force. A charged solid template is submerged into a solution of polyelectrolytes of opposite charge on an iterative basis. Commonly used polyelectrolytes include poly(styrene sulfonate) (as poly-anion) and poly (allylamine hydrochloride) (as poly-cation) respectively. After coating, the solid core dissolves, leaving behind a hollow capsule shell. Applications of this approach include the encapsulation of enzyme crystal, followed by a step called solubilization to form the enzyme solution inside the capsule⁵¹. The advantages of this product include its tunable shell thickness, non-usage of organic solvents, and good stimuli response properties inherited from the polyelectrolyte (such as pH response)⁵¹. The disadvantages are also evident, such as laborious fabrication procedure, low stability, and inability in encapsulating solution⁵².

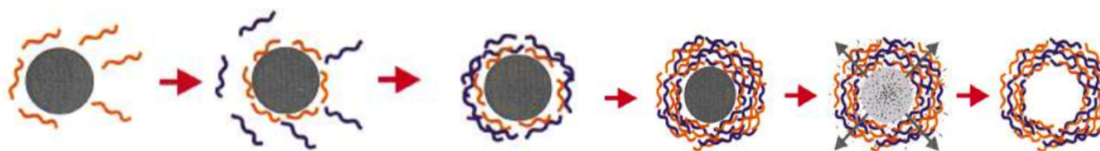


Figure 1.4 Schematic on layer-by-layer polyelectrolyte deposition(adapted from literature⁵³)

Hydrophilic encapsulation

When compared with hydrophobic encapsulation, encapsulation of hydrophilic load is challenging despite its high value in industrial applications such as a water-soluble dye, flavors, preservatives, vitamins, and pharmaceuticals⁵⁴. Currently, common examples of hydrophilic encapsulation exist in the pharmaceutical industry, where liquid medicine is encapsulated by liposomes that enable the delivery of hydrophilic medicine through the physiology barrier and into the target organ. A review article on hydrophilic encapsulation has been recently published, mainly focusing on the drug delivery issue⁵⁴. However, for other applications such as self-healing capsule, where dense, robust capsule shells are desired, the progress is much slower.

As a pioneer and an important contributor in the field of self-healing, Dr. Scott R. White at the University of Illinois at Urbana-Champaign has undertaken impressive endeavor to encapsulate hydrophilic amine as a component of the dual-capsule self-healing system on the basis of the epoxy-amine chemistry. Encapsulation of epoxy was conveniently developed by adopting interface polymerization³³ (published in 2008) or via polymerization-induced phase separation method⁵⁵ (2006). In contrast, encapsulating amine – another self-healing component – was an extreme challenge owing to its reactive nature and wide miscibility. Attempts to adopt interfacial polymerization to the inverse emulsion to encapsulate amine can hardly be considered successful due to the unconfirmed capsule structure, broad size distribution, and most importantly, limited healing performance (2010)^{29,56}. Further up-gradation of this approach by incorporating inorganic particles as well as polymeric isocyanate was not observed to result in capsules with hard

and dense shell⁵⁷ (2014). In 2012, amine microcapsules were prepared by vacuum infiltration of hollow polymer microcapsules, finally resulting in self-healing of the epoxy capsule⁵⁶. Despite the laborious procedure, Philipp *et al.* in ETH in Switzerland offered his solution – perhaps, the closest to the ideal capsule in 2014. They used microfluidics to make a double-emulsion template. Aqueous amine solution was confined in the innermost droplet and polymerization of acrylic monomer was carried out in the middle oil layer. This method avoided the interference of shell forming reaction with the active payload (amine), leading to the obtainment of typical capsules with dense shell, clean surface, tunable shell thickness, and narrow distribution⁵⁸. Unfortunately, the laborious nature of microfluidic method hindered its mass production.

Other application-oriented studies did not exhibit exciting results. To encapsulate flame-retardant (bistetrazol·diammonium), interfacial polymerization between epoxy (oil phase) and hydrazine (aqueous phase) was carried out in a W/O system. The obvious drawback of this design was the side reaction between the payload and epoxy²⁸. In another study aiming to encapsulate herbicide, two water emulsions were separately prepared, one containing poly(vinyl alcohol) and chitosan as wall material, while the other containing crosslinker and catalyst. Shell formation was carried out via the collision of these two kinds of droplets in the oil phase⁵⁹. While spheres were fabricated, their internal architecture was not characterized.

In conclusion, although various methods were developed continuously in the lab to encapsulate a hydrophilic solution, few easy and efficient routes exist for this purpose, leaving a big gap between the existing techniques and the demands of the industry.

1.4 Overview of the dissertation

In Chapter 2, the strategy developed to crosslink protein-based film is discussed. Crosslinking is achieved via the use of a bio-based cross-linker derived from cellulose to address the inherent problems (i.e., low mechanical properties and high moisture sensitivity) that hinder the application of protein-based materials. Mechanical properties, sensitivity to moisture and thermal stability are systematically evaluated. However, improvement in properties above is also accompanied by brittleness post-crosslinking modification.

Chapter 3 discusses a method to encapsulate hydrophilic liquid – acknowledged as a challenge, but difficult to avoid in the scenario where self-healing strategy is intended to be applied to address the brittleness problem discussed in Chapter 2. The capsule was fabricated from water-in-oil-in-oil (W/O/O) double emulsion template. As this is a novel method that has never been considered in the earlier literature, the underlying mechanism and verification of the process has been discussed in great detail to justify the techniques.

Chapter 4 is an extension of Chapter 3. Parameters that affect capsule fabrication were systematically investigated, focusing mostly on the internal PMF layer. A protocol was provided to fabricate the capsule and meet its requirements for self-healing purposes.

Chapter 5 concludes the dissertation. Recommendations are provided for the future investigation of this system.

CHAPTER TWO

2. MECHANICAL AND MOISTURE SENSITIVITY OF FULLY BIO-BASED DIALDEHYDE CARBOXYMETHYL CELLULOSE CROSS-LINKED SOY PROTEIN ISOLATE FILMS

ABSTRACT

Dialdehyde carboxymethyl cellulose (DCMC) crosslinked soy protein isolate (SPI) films were prepared by solvent casting method. Effect of DCMC treatment on mechanical properties, water sensitivity, light barrier properties and thermal stability were investigated. A significant increase in tensile strength (TS) was observed (up to 218%) by varying the content of DCMC and plasticizer, suggesting the occurrence of highly effective crosslinking between SPI and DCMC. Significant improvement in TS compared to other dialdehyde polysaccharide crosslinking agents such as dialdehyde starch is likely due to the higher compatibility of DCMC with SPI, as was further confirmed by SEM images. Crosslinking also led to a reduction in water vapor permeability and moisture content along with the increase of insoluble mass percentage, indicating improvement in the water resistance of these bio-based protein films. The thermal stability of protein films also showed improvement post crosslinking of DCMC.

2.1 Introduction

Protein-based films have received significant attention in recent times for purposes of food packaging due to their abundance, biodegradability, and good gas barrier properties (O₂, CO₂)²¹. However, these are accompanied with conspicuously weak mechanical properties and poor water resistance, hindering their use for packaging applications. Various strategies such as external coating and crosslinking have been deployed to overcome these drawbacks while not compromising on the merits above. For instance, an external coating of PLA⁶⁰ or polyurethane¹⁹ layers has been observed to lead to low water permeability and improvement in mechanical properties of soy protein isolate (SPI) films. On the other hand, the addition of crosslinking agents during film preparation has led to obtainment of better mechanical properties and thermal stability, low moisture sensitivity, and reduced hydrophilicity of protein-based films. In such crosslinking reactions, functional groups of crosslinking agents such as aldehydes²⁰ and diglycidyl ether⁶¹ react effectively with amino groups – abundantly available in protein chain – to form the crosslinking network (Fig. S 2.1 in supporting materials). However, the biggest concern about the small aldehyde molecule is its cytotoxicity, restricting the application of SPI films in food-related industries²¹. Efforts have been made to overcome this through developing crosslinking agents of low cytotoxicity, one of which is dialdehyde starch (DAS)⁶². Unfortunately, DAS treatment has not necessarily led to satisfactory results. For example, only marginal increase (20-40%) was observed in tensile strength of DAS-treated SPI²² and egg white⁶³ films. Treatment with DAS even led to a deterioration in mechanical properties of keratin¹⁶ and gelatin²³ films. These results were probably due to low

crosslinking efficiency induced by steric hindrances of these polymeric agents and/or compatibility-induced phase separation of the components²³. Compared to starch, cellulose – another naturally abundant polysaccharide – has shown better compatibility with protein films⁶⁴. A recent effort involved preparation of dialdehydecaboxymethyl cellulose (DCMC)^{24, 65}, and attempts to crosslink it to gelatin⁶⁶. However, this effort resulted in limited improvement in mechanical properties (e.g. only 20-30% increase in tensile strength).

Through our study, we focus on addressing the issues with poor mechanical and water-resistant properties of protein films. In this work, DCMC was used to modify SPI films via crosslinking to process fully bio-based films and improvements in mechanical properties and water sensitivity was investigated. SPI film was chosen for the fact that although it shows high promise as an important food packaging material, currently it has shortcomings due to the nature of its protein.

2.2 Materials and methods

Materials:

Soy protein isolate (PRO-FAM 646) was provided by Archer Daniels Midland (ADM) food processing company. It contains approximately < 6 wt. % moisture, > 90 wt. % protein, < 4 wt. % fat and < 5 wt. % ash. Glycerol (99 %, AC332031000, ACROS), sodium periodate (99 %, AC43285, ACROS Organics), and carboxymethyl cellulose sodium salt (CMC, average M.W. 250000, DS = 0.9, AC33262, ACROS Organics) was used as-received.

DCMC preparation:

DCMC was prepared by oxidation method as described in ^{16, 66} with minor modifications. Briefly, carboxymethyl cellulose (1.0 g) was dissolved in 30 mL purified water under magnetic stirring. pH of the cellulose-water solution was then adjusted to 3.0 using hydrochloric acid solution (1 N). 10 mL of sodium periodate solution (1.1 g/10 mL) was added drop-wise to the above-mentioned solution in order to trigger oxidization reaction at 35 °C in darkness. After 4 h, the product solution was poured in an excess amount of isopropyl alcohol to obtain the product precipitate, namely DCMC. White floc precipitant (DCMC) was recovered after washing it with isopropyl alcohol and dried under vacuum at room temperature for future use.

Film preparation:

SPI (2.04 g) was dissolved in purified water (41 mL) containing glycerin (50 %, 40 %, or 30 % as SPI weight) as the plasticizer. pH of SPI solution was adjusted to 11 using 1 M NaOH solution. SPI solution was then heated to 90 °C in water bath for 30 min to denature the protein. After the SPI solution was cooled to room temperature, certain volume of DCMC solution (0.1 g/10 mL), or corresponding amount of carboxymethyl cellulose (CMC) solution (0.1 g/10 mL, as control) was added. The solution was then cast using silicon mold (294 cm²), and dried in air for at least 72 h in lab room (20 ° C, 35% humidity). Films were obtained after peeling from the mold, and denoted as SPI-x%

DCMC or SPI-x% CMC films, with numerical values (“x”) denoting the weight percentage of DCMC or CMC based on SPI.

ATR-FTIR spectroscopy:

Attenuated Total Reflectance Fourier Transform-Infrared (ATR-FTIR) Spectroscopy was performed on a Thermo-Nicolet Magna 550 FTIR spectrometer in combination with a Thermo-SpectraTech Foundation Series Diamond ATR accessory with a 50-degree angle of incidence. Spectra of DCMC and as-received CMC were collected in absorbance mode from 4000 to 400 cm^{-1} at a resolution of 2 cm^{-1} .

Light transparency:

UV-visible light spectrophotometer (Lambda 900, Perkin Elmer) was used to determine the light transparency of the film. This method was obtained from a previous study⁶⁶ and is based on ASTM D 1746-92 standard. Film samples were cut into small pieces and placed perpendicularly into the film frame. Light absorbance was measured in the wavelength range of 200-800 nm, and light transparency was determined using Equation (1):

$$\text{Light transparency} = -\frac{\log T}{x} \quad (1)$$

Where T refers to transmittance at 600 nm, and x is the film thickness (in mm).

SEM imaging:

Micro-morphology of the film surface and frozen-fracture cross-sectional surface were obtained using Scanning Electron Micrograph (SEM) (Hitachi, S-4800) at an accelerating voltage of 5.0 kV. Film samples were coated with a gold layer before imaging.

Mechanical properties:

Tensile strength (TS) and elongation at break (EB) were measured using Instron Universal Testing Machine (Model 1125 with 0-500 g load cell) at a cross-head speed of 50 mm/min with 30 mm grip separation as per ASTM D882-12 standard. Tensile specimens were prepared by cutting the film into six rectangular sized-samples of dimensions 10 mm × 70 mm. All the cut samples were tested, and average properties were measured and reported.

Moisture content:

Moisture content was calculated as the percentage of weight loss of the prepared film²². Before undertaking the test, films were cut in a square shape (dimensions – 0.9 cm × 0.9 cm) and conditioned in laboratory atmosphere (temperature of 20 °C, 36% humidity) for 5 days. At least five specimens were tested for each composition. Film specimen was first weighed ($m_1, \pm 0.1$ mg) and then dried at 105 °C for 24 h. After cooling in a desiccator,

specimen was weighed to obtain the dried mass ($m_0, \pm 0.1$ mg). Moisture content was calculated using Equation (2):

$$\text{Moisture content (MC)} = \frac{m_1 - m_0}{m_1} \times 100\% \quad (2)$$

Total insoluble matter percentage (IMP):

The total insoluble matter was determined as the percentage of residual insoluble mass to its original dry mass after immersion in water for 24 h²². Briefly, eight square specimens (dimensions of 2 cm \times 2 cm) were cut from film samples; four of these were used to determine moisture content (MC), while the other four were weighed precisely ($m_i, \pm 0.1$ mg) for the water solubility test. Consequently, specimens for water soluble test were immersed in 50 mL water for 24 h at 20 °C with occasional, gentle shaking. Following this, insoluble samples were collected by filtration, rinsed and dried at 105 °C in oven for 24 h, and then the final weight ($m_f, \pm 0.1$ mg) was measured. The total soluble matter was calculated using Equation (3):

$$\text{Total insoluble matter percentage} = \frac{(m_i \times \theta) - m_f}{m_i} \times 100\% \quad (3)$$

At least three film samples were tested for each composition.

Water vapor permeability (WVP):

WVP of protein films was determined as per ASTM E96-15 standard. The film was sealed on top of a plastic cup containing CaCl₂ and placed in an ESPEC (ESX-4Cw) environmental chamber at 25 °C and controlled relative humidity (RH) level of 50% in order to maintain the RH gradient at 50:0 between both sides of the film. The weight of the cup was recorded at intervals of 1 h for 10 hours. WVP was calculated using Equation (4):

$$WVP = \frac{w \times x}{[A \times t \times (P_2 - P_1)]} \quad (4)$$

Where *w* is weight gain (g), *x* is film thickness (m), *A* is area of the exposed film (m²), *t* is time (s), and (*P*₂ – *P*₁) is the vapor pressure difference across the film (Pa). Three measurements were taken for each film composition.

Thermogravimetric analysis (TGA):

TGA measurement was undertaken using TGA Q5000 instrument. About 4.0 mg samples were analyzed from room temperature to 800 °C at 10 °C/min under nitrogen atmosphere (25 mL/min) using Al₂O₃ pans.

Intrinsic viscosity:

Intrinsic viscosity [*η*] of CMC and DCMC was measured in water solution at 25 °C using the Ubbelohde viscometer. Test samples were diluted five times to achieve

concentration ranging between 1.08×10^{-3} g/mL and 3×10^{-3} g/mL for CMC and between 5.00×10^{-3} g/mL and 1.08×10^{-3} for DCMC.

Statistical analysis:

At least three independent experiments were conducted to obtain replications for every SPI film. Films were compared by analyzing the variance with post-hoc comparison of mean values using Duncan's multiple-range test. At $P < 0.05$ or as indicated, differences between the mean values were considered significant.

2.3 Results and discussion

Preparation and characterization of DCMC:

DCMC was prepared by oxidation of sodium periodate in the solution⁶⁶. Formation of active aldehyde groups was accomplished by cleavage of the C2-C3 bond as per Malaprade reaction²⁴. This reaction was performed in a low pH environment, and conversion of cellulose to 2,3-dialdehyde cellulose was associated with reaction duration and oxidant concentration⁶⁷.

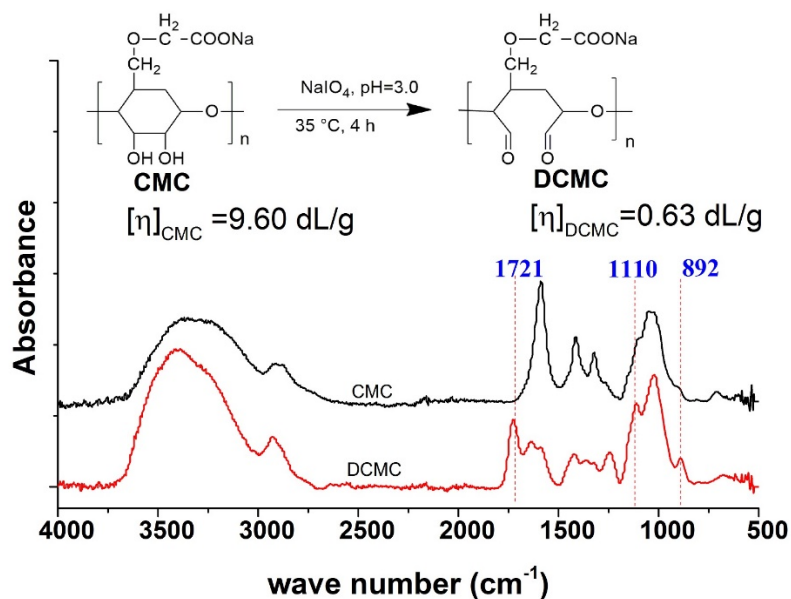


Figure 2.1 FTIR spectra of DCMC

FTIR spectrum was used to characterize oxidation products. Two characteristic bands were observed for the carbonyl group (Figure 2.1). Absorbance at 1721 cm⁻¹ was assigned to C=O vibrations of the aldehyde group, while absorbance at 892 cm⁻¹ was assigned to its hemiacetal form⁶⁶. In addition, absorbance observed at 1110 cm⁻¹ was assigned to C-O bond stretching on glucose residues¹⁶. FTIR spectrum was found to be in accordance with previously undertaken studies^{16,66}, indicating the formation of aldehyde groups.

A significant decrease in viscosity was observed after oxidation of sodium periodate. The intrinsic viscosity of CMC and DCMC was measured to be 9.60 and 0.63 dL/g respectively. A decrease in intrinsic viscosity has also been reported in previous

studies^{24, 65}. Oxidation-induced thinning is believed to be associated with two phenomena: one, degradation due to acid-catalyzed hydrolysis of β -1,4-glycosidic bonds (Li, Wu, Mu & Lin, 2011), and two, breaking of hydrogen bonds attributed to the irregular structure of newly-formed DCMC.

Film Preparation:

SPI film was prepared by referring to the optimized process in⁶⁰. Alkali treatment, heat treatment and polyol plasticizer have been proved as key factors in obtaining a homogeneous, transparent, mechanically strong and smooth SPI film. Alkaline and high-temperature conditions have been observed to cause denaturing of the globular protein chain to extended conformation⁶⁸, resulting in increased solubility, higher elongation at break (EB), and uniform appearance. On the other hand, plasticizers are found to lead to reduced protein-protein interaction and increased the mobility of protein chains, resulting in an increase in EB and reduction in tensile strength (TS)⁶⁹.

In this study, the alkaline condition and presence of plasticizer also impacted the subsequent cross-linking reaction in various ways. First, the reaction between aldehyde and amine groups generated the Schiff base rapidly in alkaline condition (pH of 7-10, Figure S1)⁷⁰, thereby leading to the efficient generation of crosslinking sites. Second, denatured protein provided an adequate amount of exposed residues with high chain flexibility, further facilitating the crosslinking reaction. Third, the addition of plasticizer improved both mobility and flexibility of the protein⁷¹, increasing the probability of amine groups

getting exposed to distal DCMC in the final stages. This, in turn, lowered the activation energy of crosslinking reaction and facilitated crosslink formation. Moreover, instead of the alcohol used by other researchers ⁶⁰, isopropyl alcohol was chosen as the precipitant in this study, allowing flocculent DCMC to conveniently precipitate out in the reaction.

Film appearance, light transparency and microstructure:

All processed films were observed to be yellowish in color, flexible and easy to peel off from the mold on the application of 50 wt. % glycerol. The surface of the SPI-CMC film was observed to be rough upon addition of CMC beyond 1 wt. %, and showed frosting. In stark contrast to SPI-CMC films, all SPI-DCMC films processed for this study exhibited a highly transparent, smooth surface (Figure 2.2). For SPI-DCMC films, an increase in DCMC content led to a change in color from greenish to reddish tinge, this is considered a general phenomenon in aldehyde-treated protein film systems due to the intermediate or final product formed as a result of the reaction between the protein and the aldehyde ^{20,22}.

The film transparencies are presented in in Table 2.1. SPI-DCMC films show low transmission value in the wavelength range of 200-280 nm, indicating good UV-barrier properties. Similar UV-barrier properties have also been observed in other protein-based films, such as gelatin ⁶⁶ and keratin ¹⁶ films. Such good UV-barrier properties are due to the presence of aromatic amino residual of proteins which absorbs UV radiation ⁷². From the application point of view, an effective UV-barrier property is essential for safe food

packaging, as highly energetic UV radiation is associated with discoloration ⁷³ and oxidation, leading to short retail time for the food ⁷⁴.

Our results indicate that UV-barrier properties were preserved after crosslinking with DCMC. At the same time, SPI-DCMC films also showed high transmission for light in the visible wavelength region, exhibiting good values of light transparency, as shown in Table 2.1. These results suggest that SPI-DCMC films are transparent and can be used as UV-barrier, see-through packaging.

Table 2.1 T% and transparency of SPI-DCMC films

	T%					Transparency 600 nm
	200 nm	280 nm	400 nm	600 nm	800 nm	
SPI	0.002±0.002	0.001±0.001	38.59±6.52	77.08±1.57	83.27±0.76	1.16 ± 0.10
SPI-1%DCMC	0.002±0.001	0.003±0.001	40.00±2.59	76.59±0.76	82.61±0.73	1.29±0.09
SPI-3%DCMC	0.001±0.001	0.002±0.001	38.65±3.74	75.41±1.18	81.25±1.46	1.36±0.30
SPI-5%DCMC	0.001±0.001	0.002±0.001	37.61±4.20	76.29±0.44	82.63±0.22	1.17±0.17
SPI-7%DCMC	0.001±0.001	0.002±0.001	42.51±7.55	75.90±0.90	82.15±1.00	1.23±0.36
SPI-10%DCMC	0.002±0.002	0.002±0.001	40.91±6.46	75.86±1.44	82.00±1.20	1.33±0.23

Non-uniform surfaces (Figure 2.2) are associated with non-homogeneous bulk. This is probably due to the unstable dispersed state or low compatibility between the film and crosslinking agents, leading to poor mechanical properties of the film ⁷⁵. To verify this, surfaces and cryo-fractured cross-sections were observed under a SEM. SPI film and SPI-DCMC cross-linked films exhibited uniform surface with clean and dense cross-sections (Figure 2.2). In contrast, SPI-CMC films with CMC content greater than 1 wt. % exhibited rough surfaces. Accordingly, aggregation/phase separation was also observed in the cross-section for SPI-CMC films with CMC content ranging from 1 to 10 wt. %. This was

probably due to thermodynamic incompatibility between SPI and CMC, and has been observed in the past for gelatin-dialdehyde starch film systems²³.

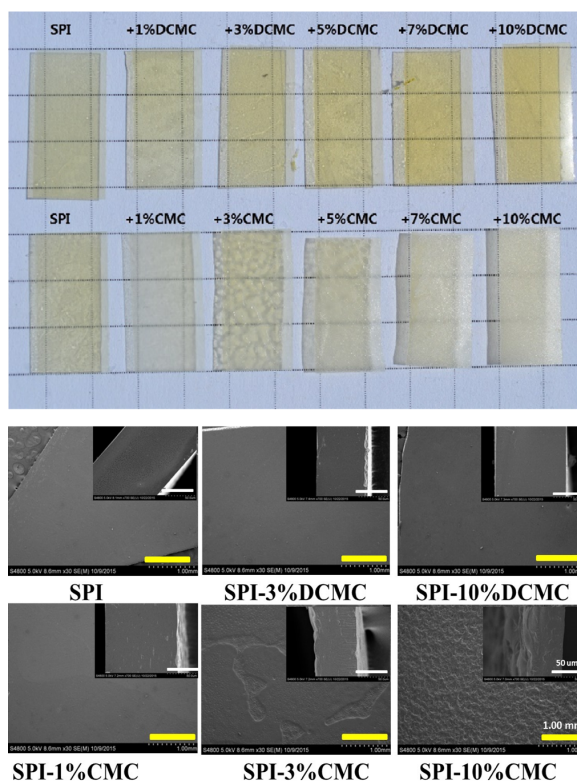


Figure 2.2 Appearance (up) and SEM image (bottom) of SPI, SPI-CMC and SPI- DCMC films with 5 wt. % of glycerol. For optical images, a glass sheet (thickness = 3.5 mm) was placed between the film samples and the 6.4 mm × 6.4 mm grid paper to illustrate the opacity.

Mechanical properties:

Films used for packaging purposes should have good mechanical properties such that their integrity is maintained after usage. Tensile strength (TS) and elongation at break (EB) are two critical mechanical properties in this regard. In this study, initially the percentage of glycerol was kept constant (e.g. 50 wt. %) while varying DCMC content (e.g.

0-10 wt. %). For the sake of control and comparison, SPI-CMC films with the same wt. % of CMC were also prepared. It is noteworthy that the difference between CMC and DCMC lies both in their chain length and in the presence of active aldehyde groups, both of which impact mechanical properties, and should therefore be taken into consideration while comparing the two films.

Figure 2.3 shows the effects of DCMC/CMC on EB and TS of SPI films. SPI-DCMC films exhibit an increase of ~ 1.8 fold in TS compared to SPI film at 10 wt. % addition of DCMC (Figure 2.3-B), with insignificant change in EB (Figure 2.3-A). However, for SPI-CMC films, no significant difference is observed in TS compared to pure SPI film, indicating the limited impact of unmodified CMC on mechanical properties of SPI film. The significant improvement observed in mechanical properties of SPI-DCMC films suggests the occurrence of crosslinking between DCMC and SPI.

When compared with values reported for other DCMC or DAS crosslinked protein film systems, the 178% increase observed in TS (SPI-10% DCMC) in this study can be considered significant. Moreover, this increase in TS is not accompanied by any decrease in EB, as is commonly observed in other similar systems such as gelatin-DCMC film (TS increases by 30% while EB reduces by 23% upon addition of 10 wt.% DCMC)⁶⁶, and SPI-dialdehyde starch film (TS increases by 20%, and EB decreases by 8% upon addition of 10 wt.% DAS)²². Even when compared with small molecular aldehyde crosslinking systems, such as SPI-glutaraldehyde (GA) (TS increases by 79% and EB increases by 84% upon addition of 0.4 wt. % of GA)⁷⁶, improvement in TS upon addition of DCMC to SPI films is significant. It should be noted that such comparison is not strictly undertaken due to the

prevalence of different conditions in different cases, such as plasticizer proportion, as these have a strong influence on mechanical properties of the film obtained ^{64, 77}. Moreover, comparing with some petroleum thermoplastics film, such as the polypropylene (35.13 MPa⁷⁸) and polyethylene (~26 Mpa⁷⁹), the absolute tensile strength (~2.5 MPa) of the modified SPI film is still very low, indicating its incapacity as structural materials.

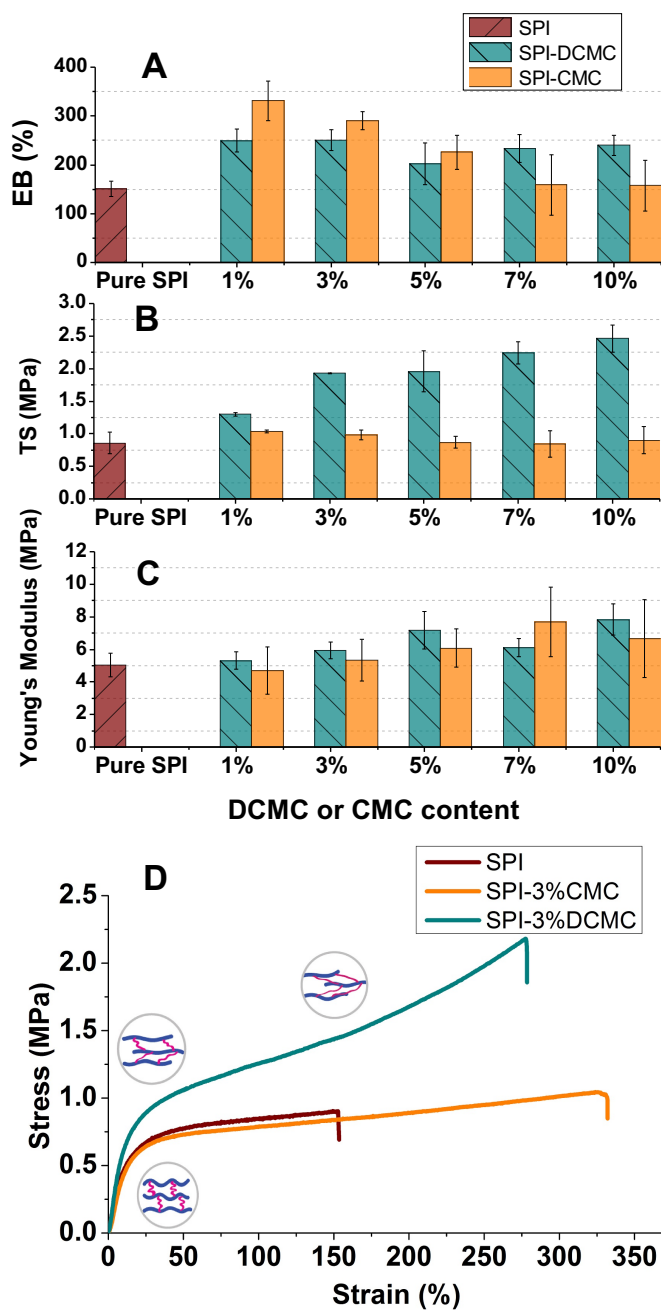


Figure 2.3 Mechanical properties of SPI-DCMC and SPI-CMC films with different DCMC/CMC content: Elongation at Break (A); Tensile Strength (B); Young's Modulus (C) and (D) Typical Strain-Stress curves.

To evaluate the effects of DCMC crosslinking in a broader sense, SPI-5% DCMC film was chosen and subjected to variation in glycerol content within a reasonable range

(30-50 wt. %). At lower glycerol content (10-20 wt. %), films were observed to be highly brittle and quite difficult to cut into qualified tensile specimens, and were henceforth excluded for the purpose of our study. For glycerol content in our chosen range, for both SPI and SPI-DCMC films, increase in glycerol content led to increase in EB and reduction in TS (Fig. 4), consistent with previous studies⁶⁴. As can be seen in Figure 2.4-B, significant increase was observed in TS of SPI-DCMC films (218%, 177%, and 133% at glycerol content of 30 wt. %, 40 wt. % and 50 wt. % respectively), strongly supporting the conclusion that crosslinking of DCMC leads to significant improvement in TS of films. Moreover, crosslinking did not lead to significant change in EB, as is shown in Figure 2.4-A. Also, the impact of crosslinking was observed to be more significant at lower glycerol content, with SPI-5%DCMC film showing a Young's modulus value of 101.7 MPa at 30 wt. % glycerol content, exhibiting good stiffness.

Typical strain-stress curves for various SPI-DCMC films is presented in Fig.2.3(D). Several characteristics of polymeric aldehyde crosslinking are shown in these typical strain-stress curves. Distinct features, such as high TS, comparable Young's modulus, and continuous increase in TS during extension, were observed in SPI-DCMC curves upon comparison with their uncross-linked counterparts (SPI-CMC). Young's modulus was measured at the initial stage of extension, which was calculated as being in the range of 1-5 % strain in this study. Comparable values of Young's modulus were obtained for SPI, SPI-CMC and SPI-DCMC films, likely due to the flexible, long polysaccharide chain exerting less restriction at low strain. In stark contrast, a significant difference was

observed in Young's modulus when different amount of small molecular crosslinking agents, e.g. glutaraldehyde, was applied ^{66, 80}. However, at higher strain values, these flexible segments between the cross-linking sites tend to exert restriction, leading to a continuous increase in stress until break (Figure 2.3). A hypothesis is illustrated Figure 2.3 (D). In the case of non-crosslinked SPI, SPI chain was observed to the first yield and then begin to slip against protein-protein interaction, showing a plateau until it breaks. This was also observed in SPI-CMC films where no crosslinking occurs (see typical curves in Figure 2.3).

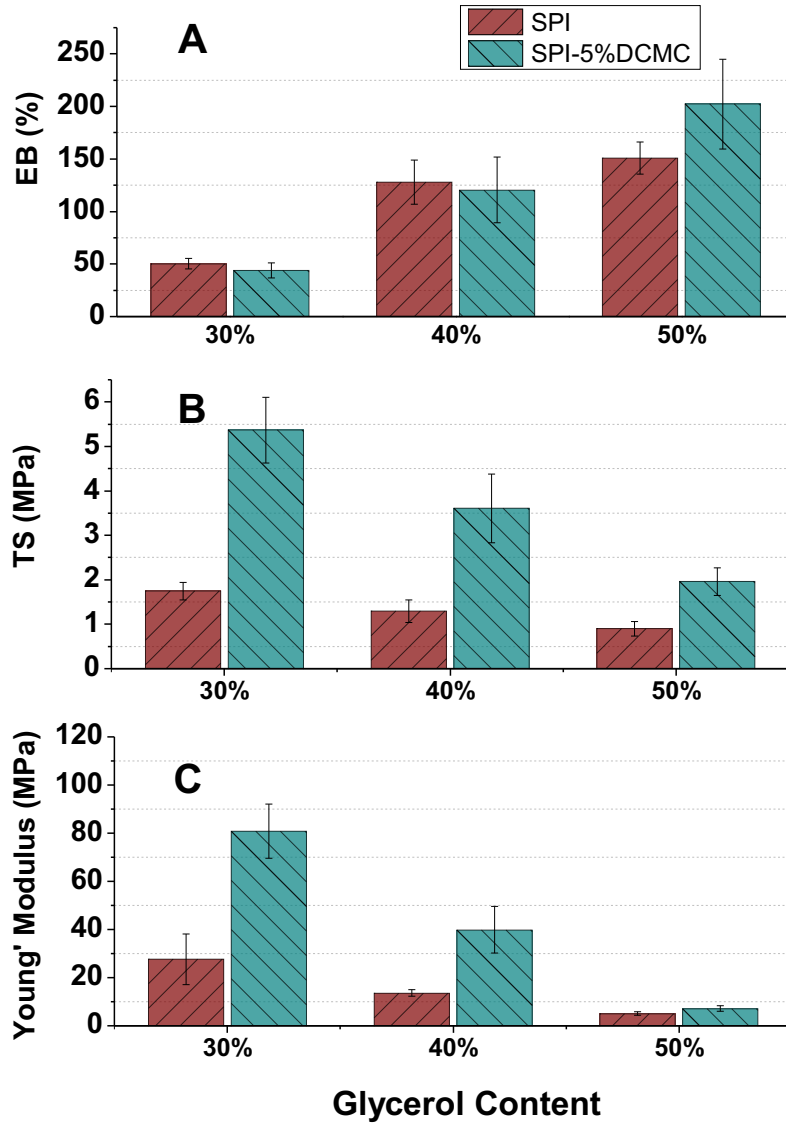


Figure 2.4 Effect of plasticizer on the mechanical properties of SPI film. Elongation at Break (A); Tensile Strength (B); Typical Strain-Stress Curves (C); and Young's Modulus (D).

Water resistance:

To understand the impact of crosslinking on moisture sensitivity, three criteria – moisture content, insoluble mass percentage (IMP), and water vapor permeability (WVP) – were evaluated for SPI-DCMC films and control SPI films. Results of these studies are summarized in Table 2.2. Moisture content showed a decrease with increasing DCMC content, which was consistent with TGA results in which weight-loss in the temperature range of 50-125 °C was found to reduce with increase in DCMC content (Figure 2.6-B). This reduction was probably due to crosslinking restricting the exposure of hydrophilic groups of protein and consuming amino acid residues that can form a hydrogen bond with water²³. However, this is not always true for macromolecular crosslinking agents such as dialdehyde starch²². This is probably due to the hydrophilic nature of polysaccharide having an affinity to water and ineffectively formed crosslinking network. Furthermore, increase in water content has been observed to be associated with a decrease of TS²² and vice-versa⁸¹. Although no strict causal relationship can be attributed based on current results, a cautious assumption was made that continuous decrease in moisture content of SPI-DCMC system reflects the formation of an effective crosslinking network. This network is believed to override inherent hydrophilicity, leading to the continuous increase in TS, as shown in Fig. 2.3.

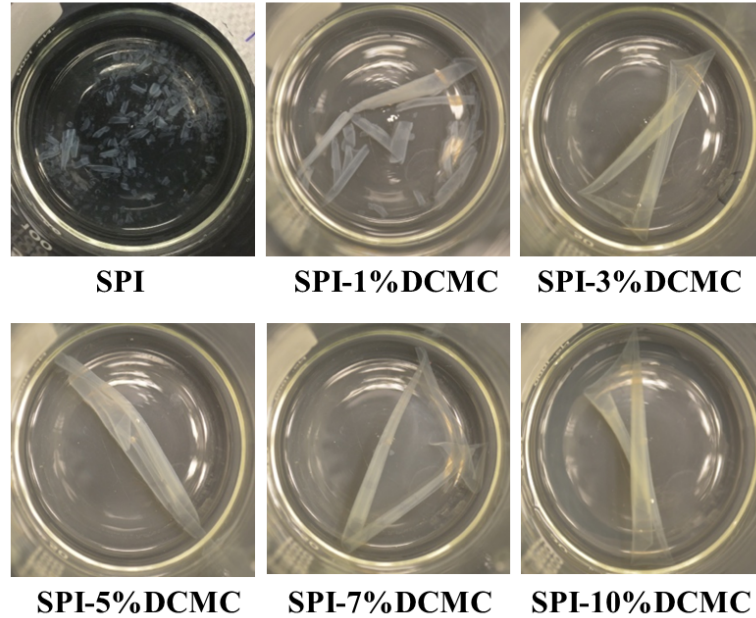


Figure 2.5 Experimental results of IMP

Table 2.2 Moisture content, insoluble matter percentage and WVP of SPI-DCMC films

	MC (%)	IMP (%)	WVP (10 ⁻⁹ g·m·m ⁻² ·s ⁻¹ ·Pa ⁻¹)
SPI	26.1 ± 0.6 a	15.2 ± 4.7 a	1.49 ± 0.11 a
SPI-1%DCMC	25.0 ± 0.6 b	38.6 ± 9.2 b	1.45 ± 0.05 a,b
SPI-3%DCMC	24.3 ± 0.7 c	63.3 ± 5.4 c	1.46 ± 0.22 a,b
SPI-5%DCMC	24.2 ± 0.6 c	62.5 ± 9.7 c	1.40 ± 0.93 b
SPI-7%DCMC	23.9 ± 0.7 c	62.1 ± 4.5 c	1.33 ± 0.13 b,c
SPI-10%DCMC	23.8 ± 1.3 c	61.6 ± 5.5 c	1.28 ± 0.05 c

Means of 3 to 6 replicates ± standard deviations. Any two means in the same column followed by the same letter are not significantly ($P > 0.05$) different by Duncan's multiple range test.

IMP was determined using two parallel steps (see the experiment section) to avoid possible heat-induced cross-linking via sulphhydryl-disulphide exchange reactions between protein molecules⁸²⁻⁸⁴, or through Maillard reaction between amine groups in protein and

hydroxyl groups in polysaccharide ⁸¹. Pure SPI film disintegrated within 1 h after immersion, while SPI-1% DCMC film was observed to maintain its integrity, but broke when gentle agitation applied. For SPI-DCMC films with more than 3 wt. % DCMC content, the integrity of the entire film remained even after immersion in water for 24 h, although significant swelling was observed (Figure 2.5). Accordingly, IMP showed an increase from 15.2% for pure SPI to reach its plateau at around 63% on use of more than 3 wt. % DCMC, indicating that ~ 3 wt. % is threshold concentration of DCMC for generating dynamic 3D networks. The occurrence of swelling, insolubility in water and continuous consumption of primary amine (Figure S 2.2) can together be considered to be a direct evidence of the occurrence of crosslinking.

WVP (water vapor permeability) is essential for food packaging in order to ensure adequate food moisture during storage. WVP test is a dynamic process in which water molecule penetrates the film due to the driving force of concentration gradient built between both sides of the film. Table 2 shows a significant and continuous decrease in WVP with an increase in DCMC content, induced by DCMC crosslinking. Similar crosslinking-induced reduction in WVP is also observed in aldehyde-treated gluten films ²⁰. Such crosslinking-induced decrease in WVP is attributed to the formation of reticulation which increases pathway of the water molecule. Consumption of hydrophilic protein during crosslinking may also play a role in reducing diffusion of H₂O molecule.

In this study, water barrier properties show significant improvement, but it cannot be said with authority that SPI-DCMC films can or should be used alone. Thus, other

methods, such as coating^{19, 60} can be considered for use with these films in order to make them suitable for food packaging applications.

Thermal stability:

The effect of DCMC crosslinking on thermal stability of SPI films was studied using TGA. TGA curves of pure SPI and SPI-DCMC films are presented in Figure 2.6-(A). Three regions relevant to glycerol, pure SPI and DCMC degradation are presented on the top of the figure (Figure 2.6-B). Glycerol and pure SPI showed their maximum rate of mass loss at 199 °C and 321 °C, respectively, giving non-overlapping decomposition regions. Degradation of DCMC was observed to occur within a wide temperature range overlapping with both glycerol and SPI.

For SPI-DCMC films, the first stage of mass loss below 125 °C is characteristic of absorbed water. Areas in this range shrink with an increase in DCMC content, indicating a fall in water/moisture content and resulting in obtainment of a denser film post-crosslinking. This is also confirmed by SEM imaging and through moisture content assays. Considering the low proportion of DCMC (< 10 wt. %), the mass loss occurring in the temperature range of 250-400 °C can be mainly attributed to thermal degradation of the protein. In this region, single broad peak observed in the case of pure SPI film sample split into several smaller ones after completion of the filming process, and was observed in both crosslinked (containing 1 wt. %, 3 wt. % and 10 wt. % DCMC) and uncrosslinked SPI films. This was probably due to the denaturing procedure leading to change in protein conformation, the disentanglement of peptide chains, and exposure of thermal sensitive segments. The first peak of DTG curves in this region shifted from low temperature to high

temperature (280 °C for 0 wt. %, 279 °C for 1 wt. % and 287 °C for 3 wt. % DCMC) and merged with the border peak on DCMC content reaching 10 wt. % at 303 °C. This suggested that the crosslinking network integrated those thermal sensitive proteinases composition to the network and delayed their decomposition. Lower moisture content and higher degradation temperature of protein after crosslinking contributed to the higher thermal stability of SPI-DCMC film, indicating delayed weight loss (Figure 2.6 (A)). Both these aspects indicated better thermal stability.

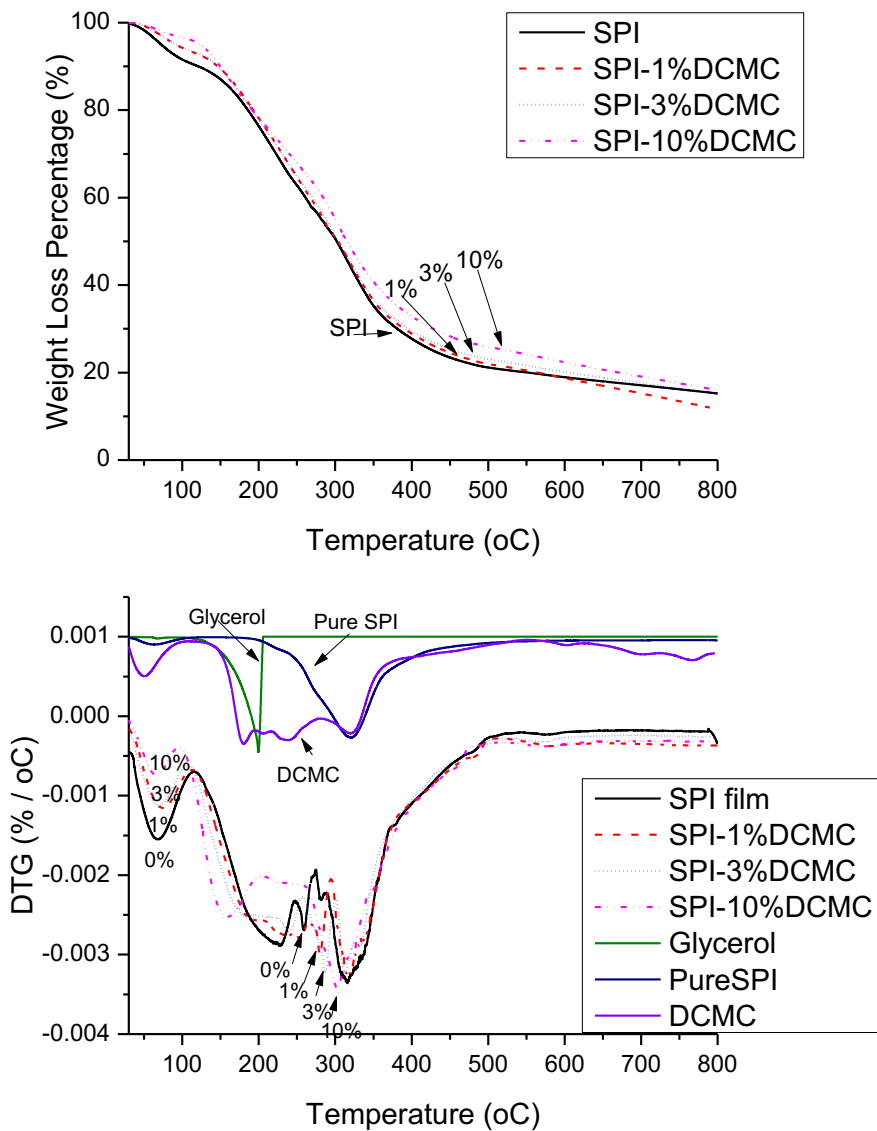


Figure 2.6 Thermal properties of SPI-DCMC film with different DCMC/CMC content (in %) TG curves: (A); DTG curves (B).

2.4 Conclusion

The present study demonstrates a method to improve properties of SPI films by DCMC crosslinking. DCMC treatment leads to significant increase in tensile strength (~218%) and simultaneous improvement in both water resistance and thermal stability. Effective generation of crosslinking network via aldehyde-amine reaction is believed to be the reason for these improvements. These improvements are also observed to be associated with DCMC content and are accompanied by consumption of primary amine groups in the system. Excellent performance of SPI-DCMC system is believed to be due to good compatibility between SPI and DCMC. Unlike other protein bio-based crosslinking systems, granules and phase separation phenomenon were not observed in SEM images of SPI-DCMC films. In summary, DCMC crosslinking was an effective method for obtaining fully bio-based, biodegradable SPI films with low cytotoxicity.

2.5 Supporting information:

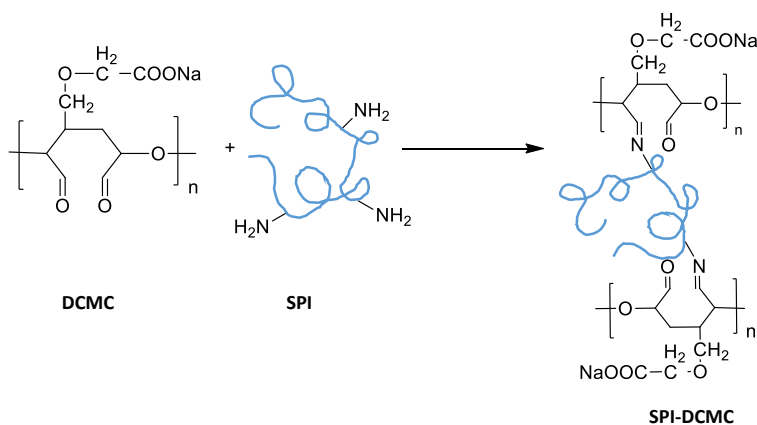


Figure S 2.1 The crosslinking chemistry of DCMC with SPI

Determination of residual primary amine:

The free α -amino concentrations in the film casting solution were quantified by ninhydrin colorimetric assay⁸⁵⁻⁸⁶. Specifically, film casting solution was seasoning for 3 days allowing the crosslinking reaction complete. Then, 300 μ L such film casting solution was mixed with 1.7 mL water and 1 mL 2% ninhydrin solution (1g ninhydrin (AC415720100, Acros), 50 mL alcohol, 1.5 mL acetic acid). Samples were heated at 80°C for exact 10 min, cooled in ice water, mixed with 5 mL ethanol, and centrifuged at 4k rpm for 5 min. The supernatant was collected, and optical absorbance at 570 nm was measured using a double beam spectrophotometer (VWR UV6300PC). The content of free amino groups were then determined by reference to a standard curve derived from lysine solutions.

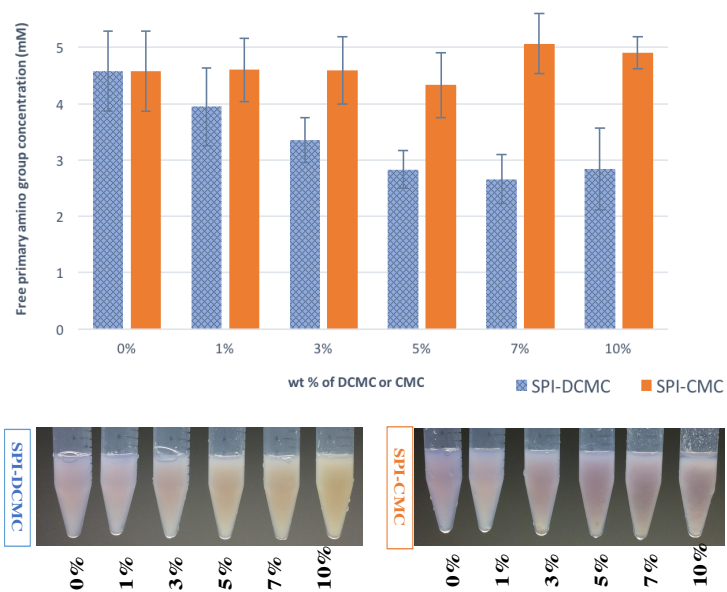
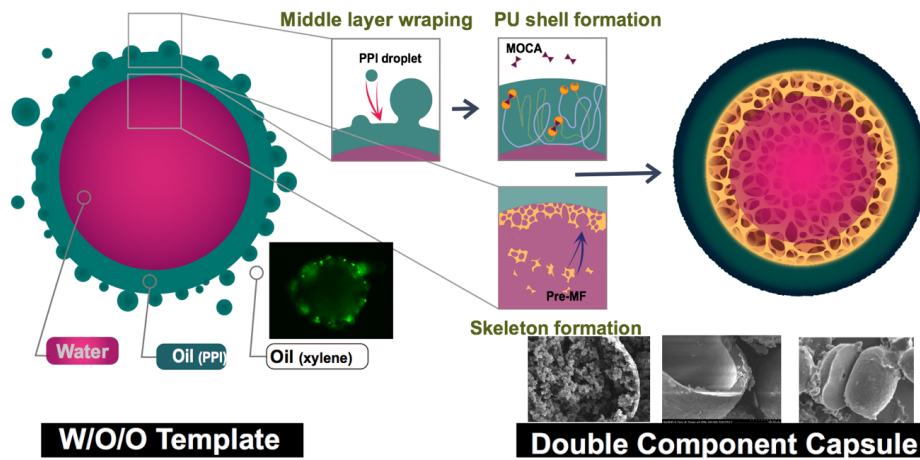


Figure S 2.2 Concentration of residual primary amino group after the DCMC or CMC treatment (top), and the typical colorimetric reaction (bottom).

CHAPTER THREE

3. ENCAPSULATING HYDROPHILIC SOLUTION BY PU-PMF DOUBLE COMPONENT CAPSULE BASED ON WATER-IN-OIL-IN-OIL EMULSION TEMPLATE



In this chapter, we demonstrate an effective method to encapsulate hydrophilic payload, in particularly, the formaldehyde. Formaldehyde is a promising healing agent for the protein-based resin due to its high efficiency of crosslinking and bonding capacity. In this study, encapsulation of water solution was achieved by use of polyurethane-poly(melamine-formaldehyde) (PU-PMF) dual-component capsules based on the W/O/O emulsion template, whose middle oil layer hosted the PU (external shell) forming reaction. The internal PMF skeleton, fabricated concurrently by condensation polymerization, provided additional mechanical support. Therefore, the formaldehyde has dual roles : (1)

as the inner PMF shell forming material and (2) the residual formaldehyde in the capsule as the healing agent. The resultant capsules exhibited dense and spherical shape, low permeability, and diameter of $\sim 50 \mu\text{m}$, making them suitable for self-healing applications. Remarkably, the interfacial tension was found to be the driving factor in the formation of W/O/O template. This micro-encapsulation system, and its fabrication methods, have the strong technical potential for use in industrial applications.

3.1 Introduction

Encapsulation of aqueous cargo is a widely-acknowledged challenge^{40, 87-88} despite its tremendous industrial value for numerous applications, ranging from self-healing and drug-delivery to cosmetics and pesticides. A stark contrast is the considerable success of encapsulation of hydrophobic cargo on the basis of oil-in-water (O/W) emulsion.^{30, 33, 42, 89} A good example of such O/W emulsion is the preparation of PU capsule,⁴² in which isocyanate (in the dispersive oil phase) and polyol (in the continuous aqueous phase) meet and react at the water/oil interface, and subsequently form the PU capsule with a dense, thick and robust shell.^{33, 89} Unfortunately, such facile interfacial polymerization route has proved to be ineffective when applied to the inverse emulsion (water-in-oil, W/O) for encapsulating a hydrophilic substance.²⁹ While other aqueous encapsulation strategies, such as self-assembly⁹⁰ and layer-by-layer polyelectrolyte deposition,⁵³ have been continuously developed,⁸⁸ these strategies bring with them inherent and unavoidable disadvantages, such as small dimensions ($\sim \text{nm}$ range),^{87, 91} atypical capsule architecture,^{29, 59} and fragility of shells.⁵⁷ This impedes their use for self-healing applications, where larger

diameters ($\sim 50 \mu\text{m}$), robust shells, and low permeability are required for the subsequent procedure and healing reagent release kinetics.⁹² Till now, no alternative has been designed to fabricate capsules for self-healing purposes that are as good as those obtained via interfacial polymerization.

The setback in aqueous core encapsulation via interfacial polymerization is hypothesized to be due to failure in synthesizing large molecular PU as the shell material. In the water-in-oil emulsion (inverse emulsion), chain extender remained confined within the dispersed water phase, which led to a high concentration of chain extender at the O/W interface. This terminated the chain extension reaction on a frequent basis, resulting in the obtainment of short PU molecules. In contrast, in the case of a oil-in-water emulsion, the presence of isocyanate in high concentration at W/O interface allows for hydrophobic payload encapsulation to be easily undertaken.

Based on this hypothesis, a pre-shell region with high isocyanate concentration was deemed to be a desirable locus to host the shell formation reaction. However, engineering a uniform, continuous liquid layer wrapping around individual aqueous droplets is technically challenging. For instance, mono-dispersed W/O/W double emulsion droplets were fabricated through use of sophisticated micro-fluids, with polymeric vesicles formed via solvent evaporation within its middle oil phase.⁹³ A simpler route – via addition of a pre-fabricated O/W emulsion into a second oil continuous phase – led to the formation of “capsule cluster”,⁹⁴ as opposed to the desired individual double emulsion architecture. Similarly, “vesicle” with aqueous core enclosed by dual layers of amphiphilic molecules could only generate nano-sized capsules, accompanied with its inherent risk of leakage

despite having been engineered to possess a thicker, cross-linked outer layer.⁹⁵ To the best of our knowledge, there exists no facile and effective route to prepare durable capsules based on this double-layer emulsion concept.

3.2 Results and Discussion

To illustrate this W/O/O concept, herein, we demonstrate an effective approach to engineer an isocyanate-rich phase wrapping around each individual aqueous droplet. Such a layer was achieved by adding polymeric isocyanate suspension (PPI suspension) to the Pickering pre-emulsion (W/O template emulsion). Driven by interfacial tension, PPI droplets attach to the surface of W/O template emulsion, fuse together, and form a coating layer, within which, the subsequent PU forming reaction was triggered by the addition of chain extender – 4,4'-methylenebis(2-chloroaniline) (MOCA) – to the continuous oil phase, as illustrated in Figure 1. By using this method, the W/O/O template was obtained on the basis of W/O template and PPI wrapping. In order to track the core substance, fluorescent rhodamine B water solution was chosen as the dispersive phase.

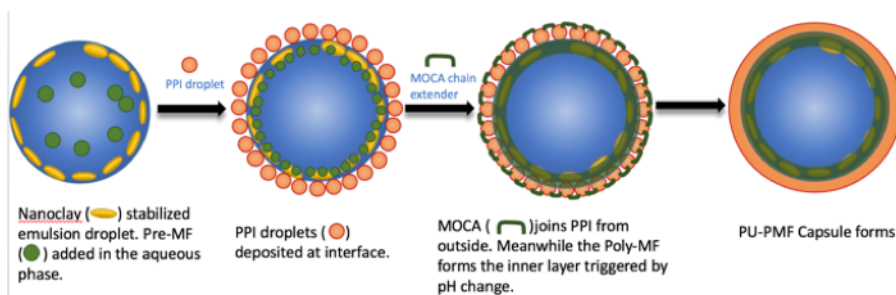


Figure 3.1 Schematic of PU-PMF capsule formation. PPI drop-lets migrate to the interface of water droplet where they fuse, spread and engulf water droplets to form isocyanate-rich layer as the locus of the consequent PU shell-forming reaction.

In this study, W/O emulsion template was stabilized by surface-modified montmorillonite (Cloisite 20), well-known as “Pickering emulsion” for its remarkable stability (> 16 h) and tunable droplet size via variation in species and load of nanoparticles (Table S1 & Figure S2-3).⁹⁶ Meanwhile, integrated solid particles in the shell imparted benefits of high leakage resistance,⁵⁹ capsule stability, and high shell strength⁹⁷ – aspects desirable for encapsulation. Benefitting from these advantages, shell formation chemistry was prominently investigated in this study.

The “isocyanate-rich layer” (middle oil layer, Figure 2-D) consist of a pre-polymeric isocyanate named “PPI” [M_n = 1149 Da, M_w/M_n = 1.43, NCO content ~ 20 %] that was synthesized from 1,4-butanediol in presence of excess TDI, as described in literature⁸⁹. PPI was found to be soluble in cyclohexanone, but the solution was observed to turn turbid upon the dropwise addition of xylene, provided the ratio of volume of xylene-to-cyclohexanone was greater than 1.25:1, which indicated the formation of stable (>12 h) PPI suspension (adding the PPI into the xylene led to a rapid precipitation). Further, mixing this turbid PPI suspension with the Pickering template emulsion led to the obtainment of a transparent supernatant after the settling of heavier template droplets, as shown in Figure 3.2. Hence, we hypothesized that PPI droplets attached to the surface of W/O template droplets – a hypothesis that was later confirmed visually through microscopy and fluoroscopy. As shown in Figure 3.2-B insert, black specks were observed to appear on the emulsion surface, and were identified as PPI by fluoroscopy (Figure S 3.7). Fluorescence-labelled PPI was found to form a green corona wrapping around the aqueous droplet with

very few visible free aggregations in the continuous phase, indicating the majority of PPI was on the O/W interface. Moreover, W/O/O template droplets displayed corrugated and wrinkling surfaces, indicating a formation of a complete membrane probably due to the slow isocyanate-water PU forming reaction. The PPI complete wrapping was further confirmed by the SEM image of the lyophilized W/O/O template, which was stabilized by MOCA (the “PU layer” specimen whose FITR was presented in Figure 3.2-C). Debris of spheres are observed in Figure 3.2-C. Thus, the existence of the PPI layer (the middle oil phase) is highly possible, which can be visualized by florescent microscopy, or through its reaction with the internal or external substance (water or MOCA) that form a substantial layer and was observed by optical microscopy or SEM. The formation of isocyanate (PPI)-rich layer is the basis of the “W/O/O template” hypothesis.

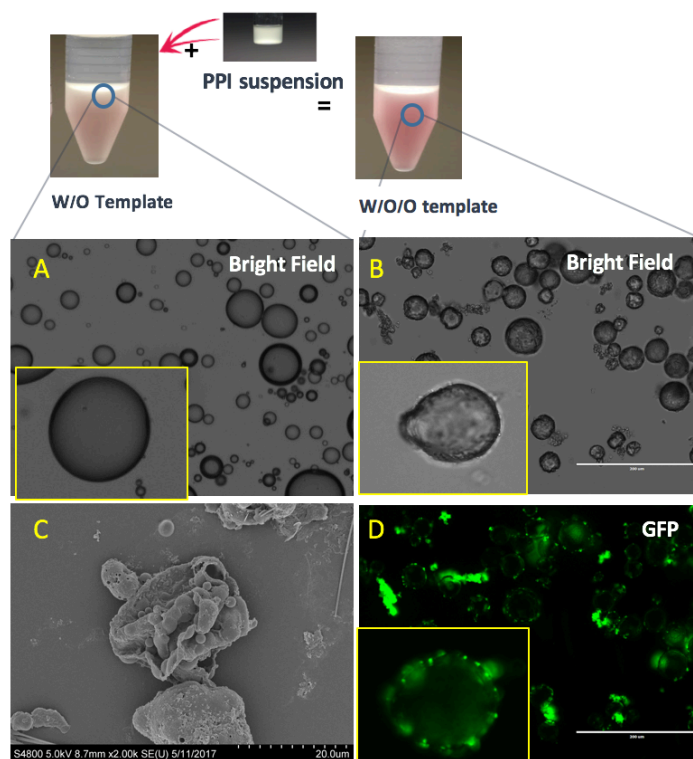


Figure 3.2 Characterization of emulsions templates. Optical and florescence images of the W/O template droplet (A) and W/O/O template droplet with labelled PPI (B,D). The latter displayed corrugated and wrinkling surfaces with the PPI middle oil layer fluorescently visible. Scale bars are 200 μm . SEM image of lyophilized W/O/O template stabilized by MOCA (C). Scale bar is 20 μm .

In a system composed of three mutually immiscible liquids, the process in which liquid 3 (PPI in this study) “engulfs” liquid 1 (water in this study) droplet to form a shell-core suspension in liquid 2 (continuous oil phase in this study) was rationalized thermodynamically, as per the minimum total free energy rule.⁹⁸ By defining the spreading coefficients (S_i) as ($S_i = \gamma_{jk} - \gamma_{ij} - \gamma_{ik}$), the final configuration (completely engulfing, partially engulfing or non-engulfing) can be predicted roughly by the three S_i values ($>$ or $<$ 0)^{47, 98-100}. For a better understanding of the formation of outer PPI layer, interfacial tension of water (1), oil phase (2) and PPI (3) were determined by drop shape analysis, and

obtained as: $\gamma_{12} = 20.56$, $\gamma_{13} = 13.89$, and $\gamma_{23} = 14.10$ (mN/m), based on which the spreading coefficients were calculated and obtained as: $S_1 = -20.35$, $S_2 = -20.77$ and $S_3 = -7.42$. Although the resultant values referred to a partially engulfing conformation (rather than complete engulfing), they indicated poor interaction between water and oil (based on the large γ_{12} value) and high affinity between PPI and water as well as PPI and oil phases (exhibited by small values of γ_{13} and γ_{23}), which were hypothesized as the driving factors favoring the enlargement of the contact area, eventually leading to the formation of shell-core morphology.

Although the designed isocyanate-rich layer gives a chance to synthesize a stronger PU shell, our final objective of the capsule holding the aqueous payload in extreme conditions could not be achieved only through the use of the afore-described route. The resultant PU capsules were observed to be still vulnerable to the drying process, and eventually collapsed. Thus, the multiple-layer strategy was employed to utilize the advantages it offers with regard to improving mechanical properties⁴². This was done by fabricating an additional PMF internal lining underneath the PU layer through a two-step chemistry¹⁰¹⁻¹⁰² (Figure S 3.11). Briefly, water soluble pre-MF oligomer was synthesized, subsequent to which its cross-linking was triggered by lowering the pH value of the solution. Following this, activated pre-MF was added to the water phase during the preparation of W/O emulsion. Pre-MF showed growth in size, depositing on the (internal) interface of droplets, undergoes continuous cross-linking, and eventually forms the PMF network that lined the capsule.

The most directly observed consequence of the addition of PMF lining was an improvement in capsule strength, which helped prevent their collapse while keeping their spherical shape intact throughout the drying process. A shell-core image was observed under the microscope, as shown in Figure 3.3. Fluorescent cargo (rhodamine B) depicted its occupying region that was confined by a thin shell layer with a distinct transmission.

Contrary to the impression given by optical images, SEM images of the cross-section revealed an atypical “capsule” structure (capsule_E6), showing solid surface and a porous occupied core (Figure 3.4-E). Also, a flexible “skin” was observed when the capsule was crushed, indicating a multi-layer structure, as shown in Figure 4-C. We assumed the dense surface layer and the porous internal material to be PU and PMF respectively. The tiny bulges on the surface might be associated with the deposition of PPI droplets, as was observed previously under the microscope (Figure 3.2-B).

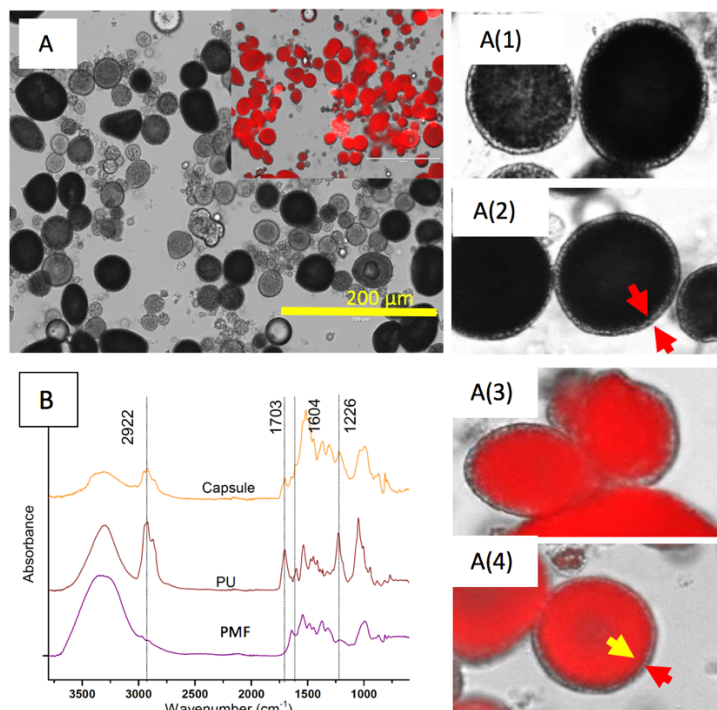


Figure 3.3 Microscopy of double component capsule (suspension of xylene). Shell-core structure is visible under bright field (A). Rhodamine cargo is visible under fluorescent microscopy (A-insert). Arrows indicate the position of the “shell” of sample E6. FTIR spectra of capsule, PU, and PMF (B).

FTIR aids in the determination of overall capsule composition, as shown in Figure 3.3-B. Furthermore, spectra of cured aqueous phase (without encapsulation) and single layer PU capsule (PU shell, no PMF) has been shown for reference. Some distinct peaks of either PU or PMF were observed in the capsule spectra, including characteristic urethane peaks ($\sim 1700 \text{ cm}^{-1}$ and $\sim 1600 \text{ cm}^{-1}$), and C-H stretching vibration ($\sim 2922 \text{ cm}^{-1}$) that can be attributed to MOCA or BD segment of PPI indicating the dual component of capsules.

Interesting, various capsule interiors were fabricated by varying the parameters related to the PMF forming such as formaldehyde-to-melamine (F/M) ratio, and pH value on the basis that they determine the functionality, structure and reactivity of the pre-MF molecule involved in the subsequent cross-linking reaction.¹⁰² In this study, distinct hollow,

solid filled, or porous-filled capsule structures with different shell thickness were observed, as shown in Figure 3.4. The typical capsule morphology with a dense and neat shell ($3.12 \pm 0.72 \mu\text{m}$) was achieved (Figure 3.4-F). It is beyond the scope of this communication to investigate the mechanism and techniques to manipulate the interior morphology. However, it is worthy to note that, a study on the morphology of the PMF capsule prepared in W/O was barely reported probably due to the lack of stable and robust platform, as the W/O/O template developed by this study.

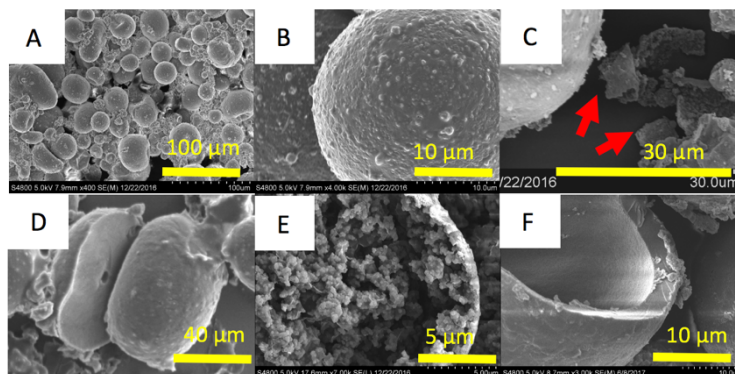


Figure 3.4 SEM image of the external appearance of double component capsules (A & B), and cross section exhibiting hollow (F capsule_B_{PH6}), porous filled (E, capsule_E6) and solid filled (D, capsule_A6) structures. Exfoliated skins (C, I) indicates the multi-layer structure. Detailed synthesis parameters are presented in supporting document.

PU and PMF layers were not added together in a simple, independent manner. To ascertain the nature of reactions involved in capsule fabrication, reactants were screened by removing one reactant in each batch. This confirmed the critical roles of MOCA, PMF, and PPI in capsule formation, as no capsule could be obtained upon the absence of either of these three substances (as shown in Figure S 3.12). Therefore, two possible chemistries will not be considered as the main reason for the capsule formation otherwise undermine

the significance of this study: one, capsules were formed due to the reaction between isocyanate and pre-MF without the help of MOCA;⁴² and two, capsules formed from the PMF itself in the reverse emulsion.⁹⁴ It is challenging to identify whether these aforementioned cross reactions exist by spectra, such as NMR or IR, due to the similarity of the reactants. However, use of this screening methodology, combined with the FTIR data and the multi-layer shell structure (as shown in Figure 3.4-C) clarify the critical roles of PPI-MOCA and PMF reactions in capsule formation.

For a potential micro-container, low permeability is no less important than structural stability. Hence, in this communication, a preliminary loading capacity test was performed to demonstrate the low permeability. Double component capsules were completely dried on the glass slide under controlled conditions (at 20 °C, 35 % humidity) for 7 days, and rolled by another glass slide. The payload, whose hydrophilic nature was confirmed by the drop test, was released from the capsule, and observed clearly under the microscope to demonstrate its excellent low permeability.

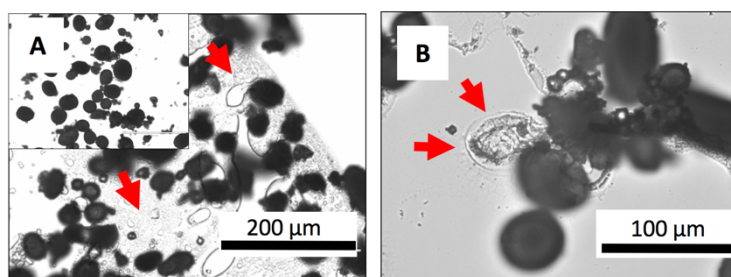


Figure 3.5 Aqueous cargo released after glass slide rolling. Optical images of (A-insert): intact dried capsules; (A) and (B): broken capsules; arrow: released water.

3.3 Conclusion

Based on these results, we concluded that the dual-component capsules were composed of an external PU layer and a porous-yet-stiffer PMF skeleton. The two components proved complementary to each other, with the PMF skeleton providing mechanical support, and the external PU layer providing isolation against leakage.

For the first time, effective encapsulation of hydrophilic payload was thus accomplished based on W/O/O template by integrating two classical capsule formation chemistries – PU interfacial polymerization and PMF *in-situ* polymerization – with critical modifications. For PU shell formation, isocyanate-rich pre-layer was achieved by taking advantage of interfacial tension that minimized overall free energy and eventually led to the novel W/O/O conformation. The advantages of this structure, with isocyanate confined in the middle layer, were: (1) High isocyanate concentration that facilitated synthesis of high molecular weight PU molecule; and (2) Possibility of external addition of chain extender (e.g. MOCA), thus avoiding any interference with the reactive/sensitive payload – the inherent drawback with the conventional route. Further improvement in mechanical properties was accomplished by incorporating PMF lining under the PU layer. A multilayer structure, composed of a dense external PU layer and PMF skeleton was obtained, with PU and PMF respectively performing complimentary roles of insulation and improving mechanical stability. The resultant capsule with tunable internal architecture was observed to withstand ambient drying process and hold the hydrophilic payload.

Future research efforts will be directed towards fabricating robust PU capsules based on W/O/O emulsion template without the use of any supporting internal lining, for which possible solutions include the use of alternative PU monomers and external coatings.

3.4 Support information

Experimental part

All materials and reagents were obtained from commercial suppliers and used in the as-obtained state without subjecting them to further purification. Micro-granulated nanoclay (Cloisite 10A, 15, 20, and Cloisite Ca⁺⁺) were obtained as generous gifts from BYK Additives & Instruments. Polymethylene-polyphenylene-isocyanate (PMPPI, M_w = 340, 372986) and polyisobutylene (PIB, 181463) were purchased from Sigma Aldrich. 1,4-butanediol (BD, AAL0349130), 1,4-diazabicyclo-2,2,2-octane (DABCO, AAA1400314) and xylene (AA16371K2) were purchased from Fisher Science. 4,4'-methylenebis(2-chloroaniline) (MOCA) was purchased from TCI America, while triethylenediamine (TEDA) was purchased from Huntsman.

Instrumentation

Attenuation Total Reflectance-Fourier Transform Infra-red (ATR-FTIR) Spectroscopy was performed on a Thermo-Nicolet Magna 550 FTIR Spectrometer in combination with a Thermo Spectra Tech Foundation Series Diamond ATR accessory with an angle of incidence of 50°. ATR-FTIR spectra were obtained for MOCA, dry PU-PMF capsule, PMF and PU resins, where PMF resin is the aqueous phase of cured pre-PMF

capsule, processed using pre-PMF. PU resin was obtained from the capsule prepared through PPI deposition-and-MOCA method.

Optical and fluorescent microscope images were acquired using a fluorescence microscope (AMF-4306; EVOS Fl, AMG) under four image channels: (a) Bright-field; (b) DAPI (excitation 360 nm, emission 447 nm); (c) GFP (excitation 470 nm, emission 525 nm); and (d) RFP (excitation 530 nm, emission 593 nm). Xylene suspension drop of the capsule was observed on a glass slide.

Scanning Electron Micrograph (SEM) (Hitachi, S-4800) was used to visualize the sample surfaces. Samples were coated with a gold layer prior to imaging. To observe a cross-section of the samples, the capsule was first dried in air on the glass slide mounted on the stage, and then rolled/crashed with another glass slide.

Interfacial tension between immiscible liquids was measured using a drop shape analysis system (Easy Drop DSA 100, Kruss, Germany) at 23.5 °C. A drop of higher density was generated using a syringe needle (1.82 mm in diameter). Video recording was employed to capture the shape of the drop as it came in contact with the solution in the reservoir. Interfacial tension was measured by fitting the shape and dimensions of the actual drop with the theoretical drop profile base obtained via Laplace equation on capillarity.

Reaction mechanism employed by the interfacial reaction:

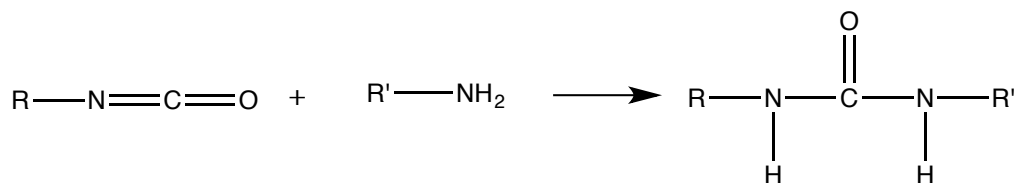


Figure S 3.1 Schematic presentation of the reaction between amine (e.g. MOCA) and an isocyanate (e.g. PPI and TDI)

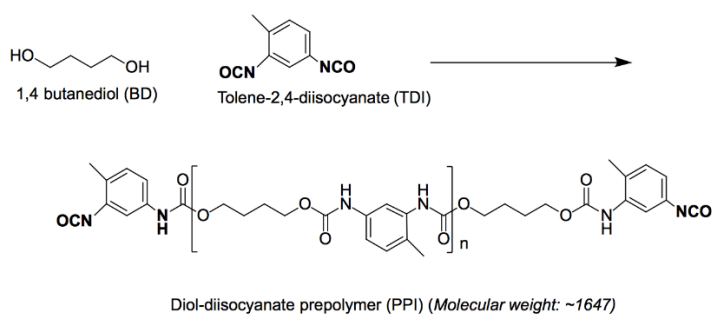


Figure S 3.2 Schematic representation of the synthesis PPI

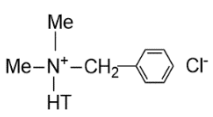
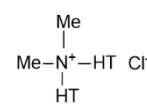
Evaluation of the stabilization of the Pickering pre-capsule.

Emulsion stabilization via Pickering mechanism is based on the contact angle of the interface (liquid-liquid-solid powder). Partial wetting by both oil and water phase drives solid powders irreversibly towards the interface, subsequently helping the emulsion stabilize efficiently.¹⁰³ The crucial role of hydrophobic/hydrophilic properties of the powder in stabilizing the Pickering emulsion has been well demonstrated in the literature.^{87,}
¹⁰⁴ For instance, through surface modification, emulsion forming capability of propyl- and octadecyl-functionalized silica⁸⁷ has shown significant improvement. Under the strategy employed in this study, particles are modified such that they are partially wettable by both

oil and water phases (contact angle: $\theta \cong 90^\circ$), thus accumulating at the interface and consequently stabilizing oil-water dispersion¹⁰⁴. In general, hydrophilic particle (i.e. $\theta < 90^\circ$) stabilize the emulsion, while hydrophobic particles (i.e. $\theta > 90^\circ$) stabilize the inverse emulsion.^{87, 103}

Emulsion ability of various unmodified (Cloisite Ca⁺⁺) and hydrophobically-modified organoclay platelets (Cloisite 10A, 15 and 20) were evaluated in this study. These organically modified clays were prepared through an ion-exchange reaction between sodium montmorillonite (Na-MMT) and ammonium surfactants by BYK Additives & Instruments¹⁰⁵. Physical properties of these clays have been summarized in Table S1.

Table S 3.1 Characteristics of hydrophobically modified nanoclay

Commercial designation	Surfactant used to make the clay	Surfactant loading in modified clay / MER (mequiv./100 g of clay)	Typical dry particle size (d50) / μm ^a	Interlayer spacing (d001) / nm ^b	Weight loss percentage at 550 °C
Cloisite Ca ⁺⁺	None	NA	<10	1.55	2.33
Cloisite 10A	Benzyl(hydrogenated tallow alkyl) dimethyl salt 	125 d	<10	1.9	34.95
Cloisite 15	Bis(hydrogenated tallow alkyl) dimethyl salt	unknown	<10	3.63	43.02
Cloisite 20		unknown	<10	3.16	36.55

^aThe typical particle size values are reported by BYK Additives & Instruments;

^bThe interlayer spacing values are reported by BYK Additives & Instruments;

^cMe, HT represent methyl, hydrogenated tallow of mainly 18 carbons with the majority of the double bonds hydrogenated.

^dValues are reported by literature.

The main differences among those organoclays were their surfactant loading, presented as cation exchange capacity (ECE). While the manufacturer has provided ECE values for the earlier product lines, ECE values for these current products have not been released by them. However, ECE can be estimated by using isothermal TG and the linear correlation between the mass of organic/MMT (g/g) and d-spacing (nm), as illustrated by Cui et. Al.¹⁰⁵

Organoclay-stabilized Pickering emulsions were observed under the optical microscope prior to the addition of isocyanate (Figure S 3.3). Capsules were observed to be stable for up to 16 h, indicating effective stabilization of the emulsion by organoclay. Unmodified nanoclay (Cloisite Ca⁺⁺) failed to assist in the formation of capsules, indicating the essential role of surface modification of clay in the formation of Pickering emulsion. Capsule size was significantly influenced by the nature and quantity of nanoclay species used. For self-healing purposes, capsules with diameters of ~ 50 μm have been reported as favorable.⁹² Thus, Cloisite 20 was added in amounts ranging from 3.2 mg to 6.4 mg and evaluated for its performance in subsequent experiments in this study.

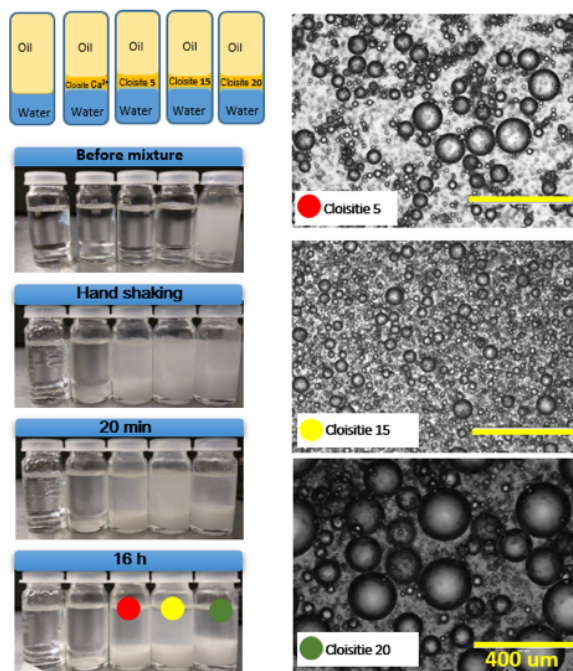


Figure S 3.3 Preparation of inverse Pickering emulsions (W/O template emulsion)

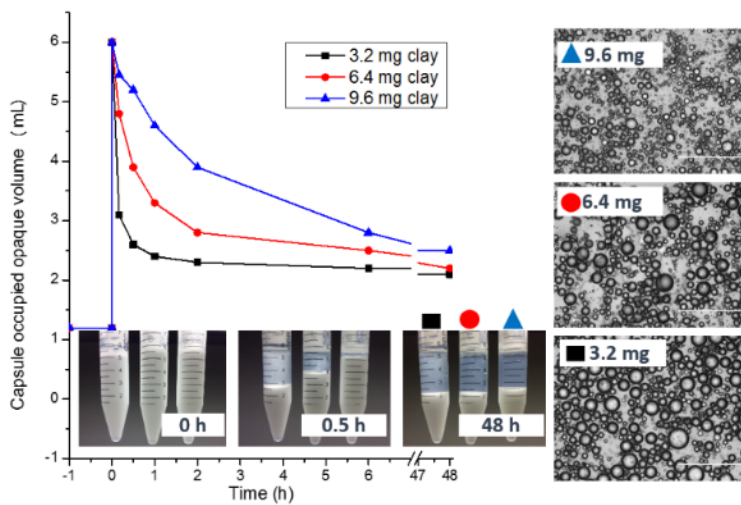


Figure S 3.4 The effect of Cloisite 20 load on the template-emulsion. The scale bar is 200 μm .

Preparation of Pickering capsules by applied conventional route inversely.

Attempts to encapsulate the aqueous payload by applying the inverse of the conventional route did not help in getting a robust capsule. The optimized process is described below.

Three kinds of solutions were prepared. In the first solution (Solution I – oil phase), PIB (polyisobutylene) was dissolved in 4.65 mL xylene. The second solution (Solution II – aqueous phase) contained 1.2 mL of water (H₂O). In the third solution (Solution III – isocyanate), CNO groups provided by PMPPI or TDI were dissolved in 0.78 mL of xylene using DABCO as a catalyst. Cloisite (6.4 mg) was dissolved in Solution I and the solution was sonicated for 5 min. Inverse emulsions were prepared by pouring Solution II into the mixture of Solution I and Cloisite clay. The combined mixture was subjected to vigorous hand shaking for ~ 5 min to pre-mix, after which Solution III was added drop-wise to it under continuous stirring.

According to literature, capsule parameters such as morphology, size and strength (based on emulsions) are related to a number of processing and constituent parameters, such as agitation speed, oil/water volume ratio, temperature, and chemical components. In this study, the synthesis process used to fabricate capsules was used in a manner to optimize these different processing and constituent parameters. These included the concentration of BD and TDI, processing temperature, amount of Cloisite 20 and catalyst added, and the nature of isocyanate species (e.g. TDI and PMPPI). However, the capsule did not show significant improvement in its strength. Hence, the collapse of capsules remained unavoidable through mere change in above-mentioned parameters.

Typical optical microscopy images are presented in Figure S5. As can be seen, nearly all the capsules eventually collapsed, and it was technically difficult to evaluate their strength given their fragile nature. However, the debris of collapsed capsules displayed different morphologies, ranging from containing small pieces to having regular round shape, and from being dark to very light in color. Through the use of subjective rate and gray analysis via image analysis software (“ImageJ”), it was found that use of higher processing temperature (40 °C), and concentration of isocyanate/polyol was essential to the formation of a darker, regular round-shaped capsule upon drying in air. An optimized process has been specified in Table S 3.2.

Table S 3.2 Typical recipe for conventional method

Cloisite 20	Condition	PID in Solution 1	TDI	PMPPPI	BD
6.4 mg	40°C/ overnight	1.3%	0.276 g	0.0402 g	60 μ L

Compared with the pre-emulsion, the size and size distribution of the drop showed significant variation, probably due to change in viscosity of the aqueous phase as a result of variation in BD content. The existence of smaller and larger capsules, prepared by the interfacial reaction, indicated that droplets broke and coalesced during capsule membrane formation. Despite the existence of large amounts of small particles (size < 20 μ m), a majority of the aqueous cargo was observed to be encapsulated in bigger capsules (size of ~ 80-200 μ m).

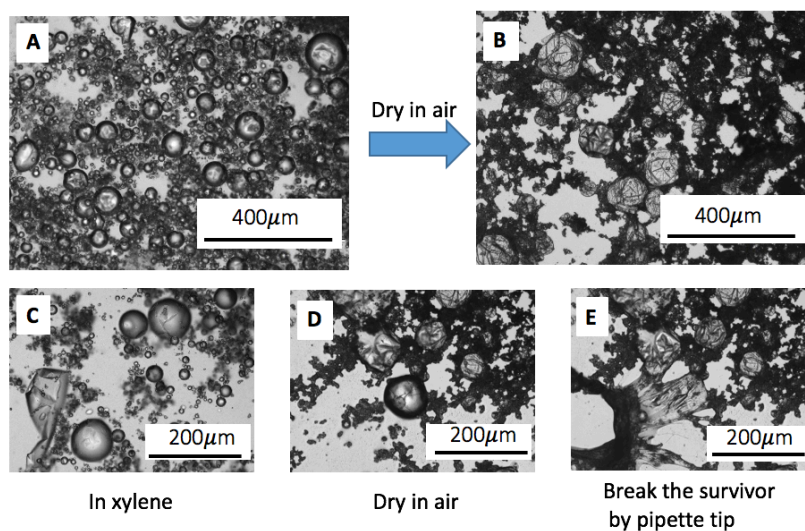


Figure S 3.5 Capsules fabricated by TDI-BD interfacial polymerization on the basis of W/O emulsion (A) collapsed during the in air drying process (B). Optimizing parameters (see Table S2) led to appearance of few survivor capsule after drying (D), and can be torn by pipette tip (E), showing the elastic and soft texture of capsule shell.

Synthesis of BD-TDI pre-polymer

Polymeric isocyanate (PPI) was prepared as per methods reported in the literature. Briefly, 12.65 g TDI was dissolved in 25 mL cyclohexanone in a 100 mL round-bottom flask, and the mixture was subjected to magnetic stirring at 80 °C. After this, 4.5 g of BD was slowly added to this solution and the reaction was allowed to continue for 24 h. Subsequently, the solution was distilled at 100 °C under pressure of 5 Torr for 5 h to cyclohexanone and excess amount of TDI. The final product obtained was a yellowish liquid with high viscosity, and its molecular weight was determined using GPC and reported in

Table S 3.3.

Table S 3.3 Molecular weight of the polymeric isocyanate (PPI)

Retention Time (min)	Mn (Daltons)	Mw (Daltons)	Mz (Daltons)	Polydispersity	Mz/Mw
10.845	1149	1647	2478	1.433620	1.504765

This high-viscosity polymeric isocyanate was observed to be soluble in cyclohexanone but insoluble in xylene. In a separate experiment, 0.2 g of this polymeric isocyanate (PPI) was dissolved in 1 mL of cyclohexanone, and xylene was added dropwise to this solution. Upon the volume of xylene reaching 1.25 mL and above, the solution changed from being transparent to becoming opaque (as shown in Figure S-6), indicating phase separation and the formation of PPI emulsion. The addition of this PPI emulsion (0.1 g) to the template emulsion followed by vigorous hand-shaking led to the obtainment of the template emulsion-PPI system, which has transparent supernatants after the sedation of heavier aqueous droplets.

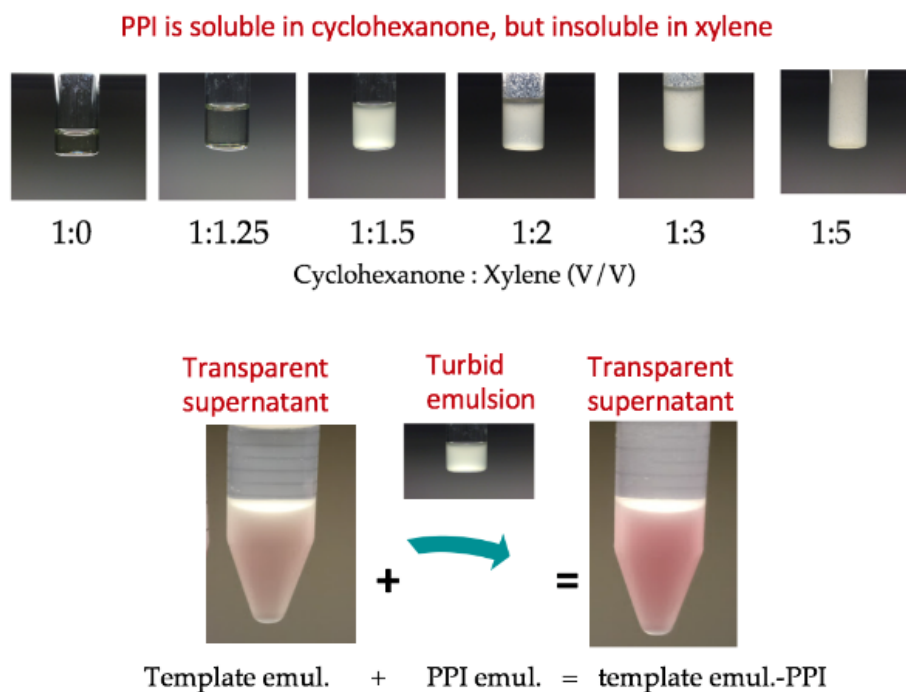


Figure S 3.6 PPI precipitates out from its cyclohexanone solution upon addition of xylene

To trace the PPI content in the template emulsion-PPI system, fluoresceinamine (Acros, MFCD00005052) was tagged to PPI molecules. Specifically, 1 mg of fluoresceinamine was dissolved in PPI solution (0.1 g of PPI in 500 L cyclohexane) and conjugated at room temperature for ≥ 2 h with occasional gentle agitation. One drop of this PPI-fluorescent solution was observed on a glass slide under the EVOS F1 digital inverted microscope. To confirm the formation of PPI-fluorescence conjugate, a large quantity of xylene was used to wash the PPI droplet on the slide; the result was obtainment of PPI precipitate on the slide (see Figure S 3.7).

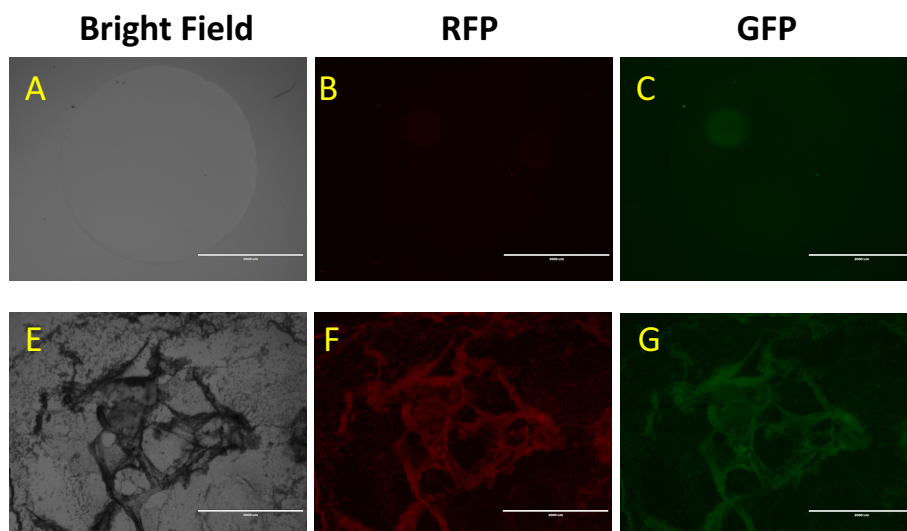


Figure S 3.7 The fluorescent microscope image of a drop of PPI-Fluor solution (A-C) and its precipitate residual after xylene wash on the slide (E-G). Scale bar = 2000 μm

Fluorescence signals of PPI-fluorescent solution were observed in RFP and GFP channels. After washing with xylene, the fluorescence image clearly indicated precipitation of PPI, indicating the success of their conjugation.

Preparation and characterization of “PPI-warping” capsules.

PPI layer outside the Pickering emulsion is proposed in this study as the location of the shell-forming reaction. Pre-emulsion was first prepared as described earlier: Briefly, 6.4 mg of Cloisite 20, 3.5 mL xylene and 1.15 mL PIB-xylene solution (1.3 wt. % of PIB) were mixed in a 15 mL centrifuge tube, followed by ultra-sonication for 5 min. After this, 1.2 mL aqueous solution (containing 0.5 mg of Rhodamine as a tracer) was added, and the tube was shaken vigorously by hand to obtain the pre-emulsion.

To ensure the deposition of PPI on the surface of the aqueous droplet, PPI emulsion was processed by adding 625 μL xylene into the PPI solution (containing 500 μL cyclohexane and 0.1 g PPI, fluorescence labeled or unlabeled). Such PPI emulsion was then poured to the previous pre-emulsion, followed by vigorous hand-shaking. At first, adhesion was observed, but this seemed to mitigate with the further shaking of the solution. Further, fine particles could be observed with naked eyes in the emulsion system. Such emulsion exhibited more reddish color compared to the pre-emulsion without any PPI layer (as shown in Figure S 3.6), probably due to change in refraction upon the presence of PPI layer.

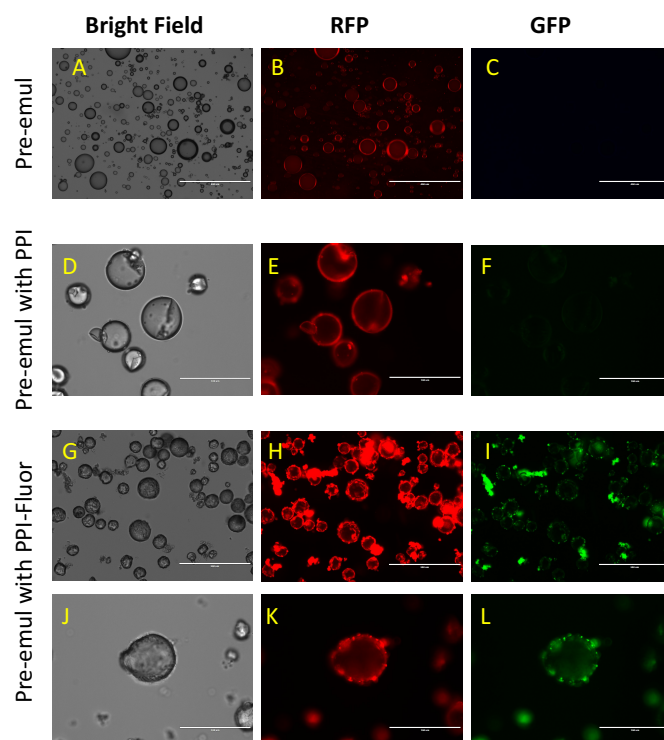


Figure S 3.8 The fluorescent microscope image of pre-emulsion (A-C, scale bar 400 μm), pre-emulsion with PPI (D-F, scale bar = 100 μm), and pre-emulsion with PPI-fluorescence (G-I, scale bar 200 μm , J-L, scale bar 100 μm). Red color indicates the aqueous payload and PPI, and green color indicates PPI

Fluorescence-labeled PPI (PPI-Fluor) was clearly observed on the surface of the template emulsion under the fluorescence microscope. Under the bright field channel, template emulsion-PPI droplets exhibited corrugated and rough surface (as shown in Figures S-8D, S-8G and S-8J), which was significantly different from the template emulsions without any PPI wrapping (Figure S8-A). Under the GFP channel, such small particles – attached to the droplet surfaces – were clearly observed and identified as PPI. Small and free particles not attached to droplet surfaces were also observed in both template emulsion-PPI (fluorescence unlabeled) and template emulsion-PPI (fluorescence labeled) samples, which could be identified as free PPI conglomerate floating in the emulsion system.

Preparing capsule based on the PPI warped emulsion system (water-in-oil-in-oil system)

Chain extenders (e.g. MOCA, TEDA) were used to react with PPI at the O/O interface (e.g. xylene/PPI interface) of the synthesized PPI-wrapped capsule system (W/O/O system). Optimization of parameters (such as the concentration of MOCA or TEDA) did not help in fabricating stronger capsules, which collapsed upon the evaporation of xylene. Under an optical microscope, upon the evaporation of xylene phase, objects in round-like contour and dark color were observed, as shown in Figure S 3.9-B and S9-E. By comparing these images (Figure S 3.9-B and S9-E) with images in xylene solution (Figure S 3.9-A and S9-D), the possibility of them being capsules was excluded as the contours were not found to be superimposable. Hence, objects observed in the former set

of images were deemed to be those of solid and stiff capsule debris, accompanied with aqueous cargo leakage that was confirmed by fluoroscopy (C and F).

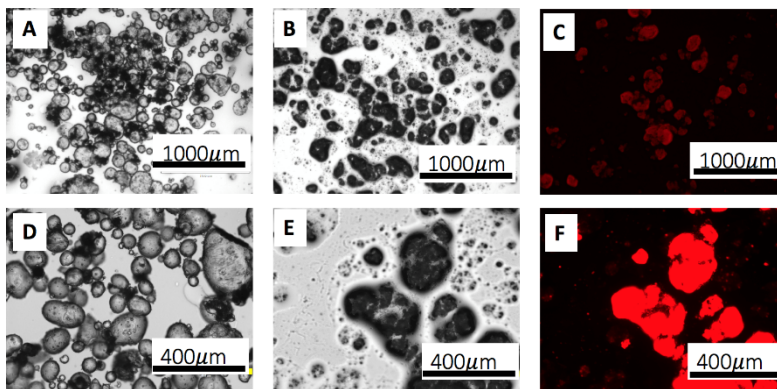


Figure S 3.9 Optical and fluorescent images of PPI-MOCA capsules prepared on the basis of W/O/O emulsion, in xylene solution (A &D) and after the evaporation of xylene (B,C,E &F). Black objects in B & E are deemed to be the debris of brittle and solid capsule debris, accompanied with the aqueous leakage.

Preparing multilayer poly(melamine formaldehyde)-polyurethane (PMF-PU) capsule

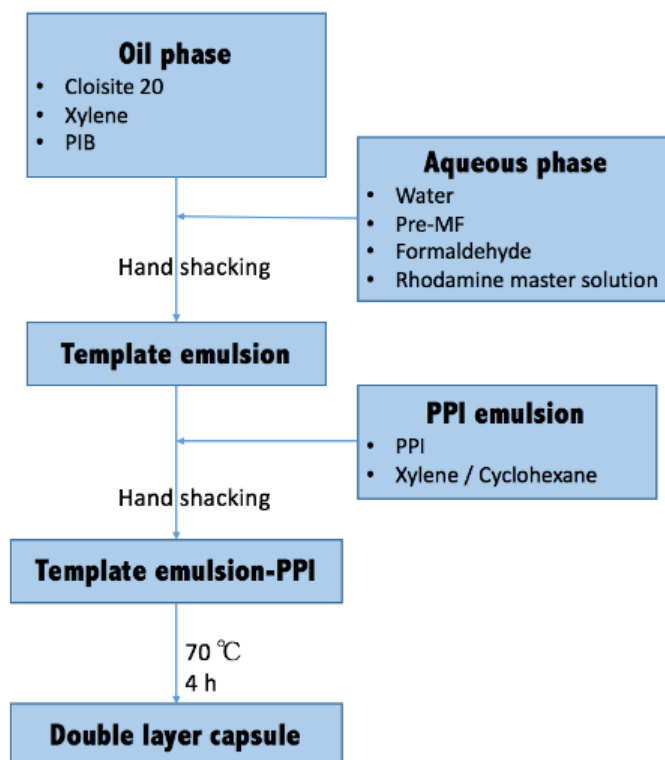


Figure S 3.10 Schematic presentation of capsulation via PU external layer and PMF skeleton

PMF-PU multi-layer capsule was fabricated by combining PMF (processed via *in-situ* polymerization) and PU (processed via interfacial polymerization), with the former forming the internal layer and the latter forming the external layer. To fabricate the PMF layer, pre-polymers of melamine and formaldehyde (pre-MF) were synthesized based on methods detailed in existing literature. Typically, melamine (3.79 g, 0.03 mol), formaldehyde (8.1 g, 0.1 mol) and water (5 mL) were mixed using magnetic stirring, after which pH of the solution was adjusted to 9.25. Subsequently, the temperature of the

solution was initially raised to 60 °C for 10 min, and then to 65 °C for another 10 min, until the solution became transparent in order to obtain the pre-MF solution (pre-MF master solution).

To prepare the aqueous phase, as-synthesized pre-MF, formaldehyde and water were mixed in a specific ratio (Optimized composition was listed in Table S 3.4), after which pH of the solution was adjusted to 3.20 by the addition of hydrochloric acid (HCl). This aqueous phase was subsequently emulsified with oil phase to make the capsule emulsion. Typically, 1.2 mL of as-prepared aqueous phase was mixed with 4.65 mL of the oil phase (consisting of 4.65 mL or 4 g of xylene, 0.3 wt. % PIB solution and 6.4 mg of Cloisite 20) in a 15 mL centrifuge tube. The mixture was emulsified with vigorous hand shaking for ~ 5 min. Isocyanate-rich wrapping layer was fabricated by simple addition of PPI emulsion (0.5 g of PPI in 1 mL of cyclohexanone and 1.25 mL xylene) followed by vigorous hand-shaking. The obtained emulsion was designated as “Emulsion A”.

External PU layer was fabricated by adding “Emulsion A” to xylene containing chain extender. In this work, triethylenetetramine (TETA, Huntsman) or 4,4'-methylenebis(2-chloroaniline) (MOCA, TCI Chemicals) were chosen as chain extenders. TETA and MOCA have multiple amine moieties that react with isocyanate to form PU¹⁰⁶. In a group of typical experiments (used to produce samples E1-E6), 1 mL of “Emulsion A” was added to 2 mL of MOCA's xylene solution (containing 0.038 g of MOCA or 2.80×10^{-4} mol $-NH_2$) and subsequently shaken vigorously via hand-shaking. This solution was designated as “Emulsion B”, and placed in a water bath at 70 °C for 4 h to ensure completion of the reaction.

The reaction accelerates due to use of elevated temperature, leading to the simultaneous formation of the internal PMF layer through cross-linking reaction among pre-MF oligomers. The chemistry of PMF formation has been elucidated in the previous studies¹⁰¹⁻¹⁰². Specifically, pre-MF oligomers were first synthesized under basic conditions, and subsequently, under high temperature, the presence of H⁺ ions triggered the cross-linking reaction. Pre-MF oligomers grew, deposited on the interface of emulsion droplets and continuously cross-linked to form the PMF network.

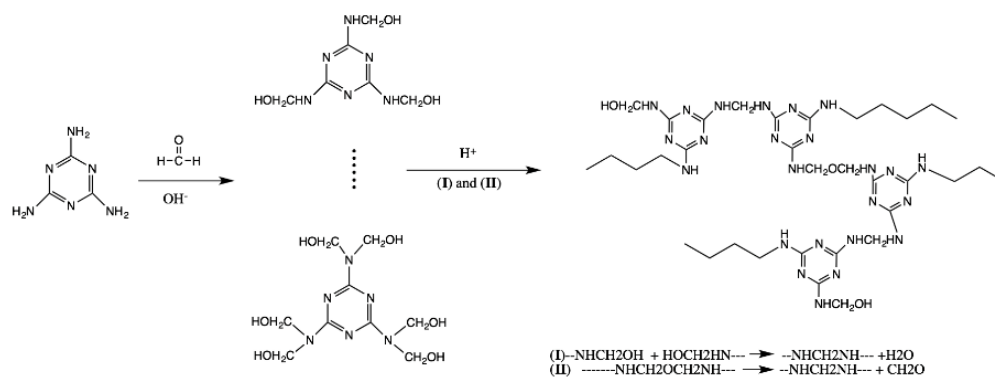


Figure S 3.11 Schematic of two-step poly(melamine-formaldehyde) formation chemistry

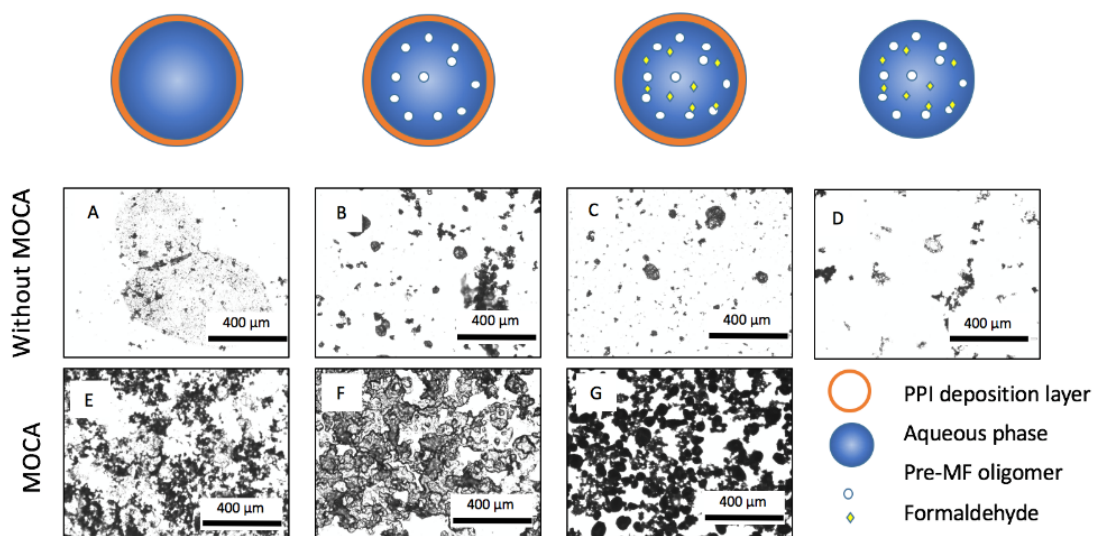


Figure S 3.12 Shell forming factors analysis. Optical images of dried capsule with different shell formation factors. Images are (A): template emulsion-PPI, (B): template emulsion-PPI with pre-MF in aqueous phase, (C): (B) with excessive formaldehyde, and (D): template emulsion with pre-MF and excess formaldehyde. (E), (F) and (G) samples were prepared same as (A), (B), (C) respectively, but adding MOCA as chain extender in the xylene phase. Results showed that, capsules can only be obtained in case (G), indicating MOCA, PPI, Pre-MF and excessive formaldehyde are critical factors to form robust capsules

Table S 3.4 Composition of multilayer PM-PU capsules

Sample	Aqueous phase composition				PH (step 1/ step 2)	W/O ^{a)} (V/ V)	Chain extender (g/2mL)
	Water (mL)	Formaldehyde (mL)	Rhodamine solution (mL) ^{c)}	Pre-PM master solution (mL) ^{b)}			
E4	2.0	1.0	0.5	1.5	9.25 / 3.20	1:3.8 8	0.038 (MOCA)
E6	0.5	2.5	0.5	1.5	9.25 / 3.20	1:3.8 8	0.038 (MOCA)
A5	0	0	0	5	9.25 / 3.20	1:3.8 8	0.038 (MOCA)
B _{PH6}	1.25	0	0	3.75	9.25 / 6.00	1:3.8 8	0.038 (MOCA)

^{a)} The composition of the oil phase was kept constant: 4.65 mL xylene (4 g), 1.3 wt.% PIB (0.052 g) and 6.4 mg Cloisite 20

^{b)} The starting concentration of the formaldehyde and melamine (master solution) were calculated to be 6.17×10^{-3} mol/mL, and 1.85×10^{-3} mol/mL.

^{c)} The concentration of rhodamine solution is 0.5 mg/mL

FTIR was used to confirm the composition of the multi-layer capsule. As can be seen from the FTIR spectra (Figure 3.3-B), the characteristic isocyanate peak (corresponding to $2100\text{-}2270\text{ cm}^{-1}$) was not observed, while the characteristic urethane peak (at ~ 1700 and 1600 cm^{-1}) was observed. A new strong peak was observed for the capsules at $\sim 2922\text{ cm}^{-1}$, which could be assigned to the C-H stretching vibration inherited from the MOCA and PPI (BD segment), while the peak at $\sim 1500\text{ cm}^{-1}$ could be assigned to the C-C aromatic stretch inherited from PPI (TDI segment) and MOCA. The peak at $\sim 813\text{ cm}^{-1}$ may be related to stretching vibration of C-Cl bond in MOCA.

CHAPTER FOUR

4. ENCAPSULATION OF HYDROPHILIC PAYLOAD BY PU-PMF CAPSULE: EFFECT OF SHELL FORMING CONTENT, PH VALUE AND TEMPERATURE ON CAPSULE MORPHOLOGY

This chapter is a continuation of the previous chapter.

Shell formation, or specifically PFM shell formation, has been extensively investigated in this chapter. Based on our previous observation, varying F/M ratio (formaldehyde: melamine ratio) of the feed material led to an unexpected internal morphology of the capsule. Variation in F/M ratio was found to cause variation in capsule conformation ranging from hollow to semi-filled and filled conformations. This phenomenon triggered our interest in further exploring the formed shell, as the understanding that can be gained through existing literature cannot be readily used to explain these observations.

4.1 Introduction

Encapsulation of liquid core is used in a wide variety of industries, such as cosmetics, drug delivery, anti-corrosion, food preservation and self-healing. By taking advantage of capsules, reactive reagents were preserved under its protective shell; sensitive chemicals were isolated from the environment and drugs were delivered in the capsule carrier to either pass through the physiological barrier or be endowed with controlled-release properties. Encapsulation can be effectively carried via emulsion, where the

payload is dissolved in the dispersed droplet, and shell formation reaction takes place at the droplet interface by either of interfacial polymerization, polymer precipitation or other methodologies. Thus, to encapsulate hydrophobic liquids such as epoxy⁴⁴, essence oil⁴³ and flame retardants¹⁰⁷, oil-in-water emulsion template has been appropriately employed. For instance, polyurethane (PU) or mechanically stronger PMF is the most common and effective capsule shells. PU capsule formed by interfacial polymerization contains two shell forming components: the water-soluble polyol, and oil-soluble isocyanate, both of which meet at the water/oil interface to eventually form the PU shell. For polymer deposition of PMF shell, a water-soluble precursor is crosslinked to form the water-insoluble polymer that gets deposited on the water/oil (W/O) interface to form the PMF shell. Capsules fabricated by these two methods usually exhibit neat and robust shells; hence, they are widely used.

However, encapsulation of hydrophilic payloads continues to remain a challenge. Employing the aforementioned protocols directly on water-in-oil emulsion template (inverse emulsion) usually leads to capsules with fragile nature, high permeability, and atypical shape, thus hindering their use for further applications. In our previous endeavor, a dual-component capsule containing a PU outer layer and PMF inner layer was fabricated based on a water-in-oil-in-oil (W/O/O) emulsion template, through which encapsulation of formaldehyde was achieved. Meanwhile, the effect of formaldehyde-to-melamine (F/M) ratio on capsule morphology was also observed, but its underlying mechanism was not elucidated.

In this study, we focus on the inner PMF layer as it determines the carrier capacity and release characteristics of the capsule. More importantly, payload and shell forming reaction coexist in the dispersive phase, indicating that direct exposure of the shell may cause negative interference on the payload. Hence, it is beneficial to understand the procedure of formation of PMF inner shell. Extensive previous studies have elucidated a two-stage chemistry of PMF synthesis: (1) Formation of water-soluble methylol melamines (pre-MF) by the addition of formaldehyde to melamine under basic condition, and (2) Crosslinking of methylol melamines by condensation reaction^{101-102, 108}. In the second stage, polymerization-induced phase separation occurred, and PMF precipitate from the solution, get deposited on the W/O interface, eventually forming the PMF shell. Various parameters have been observed to affect this reaction, such as pH of the solution, F/M ratio, temperature, and shell-forming materials. For instance, higher F/M ratio is expected to lead to more formaldehyde substitution and thus higher functionality and increase in crosslinking density. Studies on *in-situ* bulk polymerization have shown that high F/M ratio leads to high crosslinking rate¹⁰⁹, with the solution rapidly turning turbid¹⁰² and leading to the obtainment of the resultant resin with low hardness¹⁰². In addition, methylene bridge formation (stage 2) has shown higher reaction rate in acidic condition despite it could occur in wide range of pH (4 to 9)¹⁰⁹. Besides, the temperature has been found to influence not only the reaction rate but also the solubility of Pre-MF, e.g., high reaction temperature has been observed to retard the occurrence of turbidity¹⁰². Other studies carried out on the capsule have indicated that use of larger quantities of shell forming material leads to an increase in shell thickness, but probably up to a maximum limit¹¹⁰.

To date, PMF shell formation in the internal space of a droplet has not been investigated. This is probably due to the lack of a technique by which a robust, neat, and typical capsule can be fabricated. The route developed in our lab provides a platform on which features of the PMF shell formation could be systemically investigated. Such droplet-confined reaction shares similarity with its counterparts performed in bulk or direct emulsion, but has its distinct features, such as the severe fluctuation in concentration and pH, and the lack of shear stress. The main objective of this study was to analyze the effect of these factors on PMF reaction and geometry of formed capsule.

4.2 Experimental

Materials

Micro-granule nanoclay (Cloisite 20) was obtained from BYK Additives & Instruments. Polyisobutylene (PIB, 181463) was purchased from Sigma-Aldrich. Xylene (AA16371K2), 1,4-butanediol (BD, AAL0349130), and 1,4-diazabicyclo-2,2,2-octane (DABCO, AAA1400314) were purchased from Fisher Science. Triethylenediamine (TEDA) was purchased from Huntsman, while 4,4'-methylenebis(2-chloroaniline) (MOCA) was purchased from TCI America.

Table 4.1 Preparation parameters for different batches of microcapsules

Batch	Pre-MF master solution (mL)*	F/M ratio	PH	Temperature / °C
A1	0	3.3:1	9.25 / 3.2	70
A2	0.5	3.3:1	9.25 / 3.2	70
A3	1.25	3.3:1	9.25 / 3.2	70
A4	2.5	3.3:1	9.25 / 3.2	70
A5	3.75	3.3:1	9.25 / 3.2	70
A6	5	3.3:1	9.25 / 3.2	70
B _{pH3}	3.75	3.3:1	9.25 / 3.0	70
B _{pH4}	3.75	3.3:1	9.25 / 4.0	70
B _{pH5}	3.75	3.3:1	9.25 / 5.0	70
B _{pH6}	3.75	3.3:1	9.25 / 6.0	70
B _{pH6.6}	3.75	3.3:1	9.25 / 6.6	70
C _{30deg}	3.75	3.3:1	9.25 / 5.0	30
C _{50deg}	3.75	3.3:1	9.25 / 5.0	50
C _{70deg}	3.75	3.3:1	9.25 / 5.0	70

* Pre-MF master solution contained 3.79 g (0.03 mol) melamine, 8.10 g (0.1 mol) formaldehyde and 5 mL water.

Preparation of the microcapsules.

PMF-PU multilayer capsule was fabricated by combining PMF (obtained via *in situ* polymerization) and PU (obtained via interfacial polymerization), with the former constituting the internal layer and the latter forming the external layer. To fabricate the internal PMF layer, pre-polymer of melamine and formaldehyde (pre-MF) was synthesized based on previous literature with minor modifications⁹⁴. Typically, melamine (3.79 g, 0.03 mol), formaldehyde (8.1 g, 0.1 mol) and 5 mL water were mixed using magnetic stirrer. pH of the solution was then adjusted to 9.25, and its temperature was raised to 60 °C for 10 min followed by a further increase to 65 °C for another 10 min until the pre-MF solution became transparent (pre-MF master solution).

To prepare the aqueous phase, as-synthesized pre-MF, and water were mixed to a total volume of 5 mL (as listed in Table 4.1), and pH of the solution was adjusted to 3.20

by adding hydrochloric acid (HCl). This aqueous phase was emulsified with oil phase to make the capsule emulsion. Typically, 1.2 mL of as-prepared aqueous phase was mixed with 4.65 mL of oil phase – consisting of 4.65 mL xylene (4 g) with 0.33 wt. % PIB and 6.4 mg of Cloisite 20 in a 15 mL centrifuge tube. The mixture was emulsified with vigorous hand shaking for approximate 5 min. Isocyanate-rich warping layer was fabricated by adding PPI suspension (0.5 g PPI ($\sim 2.38 \times 10^{-3}$ mol CNO) in 1 mL cyclohexane and 1.25 mL xylene), followed by vigorous hand shaking. The obtained emulsion was designated as “Emulsion A”.

PU outer layer was fabricated by adding “Emulsion A” into xylene-containing chain extender. In this study, MOCA was chosen as the chain extender, as MOCA has multiple amine moieties that can react with isocyanate to form PU¹⁰⁶. In a set of typical experiments, one mL “Emulsion A” was added to 2 mL xylene solution of MOCA (0.038 g MOCA, 2.80×10^{-4} mol $-\text{NH}_2$) followed by vigorous hand shaking. Designated as “Emulsion B”, the obtained emulsion was placed in a water bath (temperature = 70°C) for 4 h to ensure completion of the reaction.

Accelerated by the elevated temperature, formation of the internal PMF layer occurred simultaneously through crosslinking reaction among pre-MF oligomers.

Dye load and PMF conversion

To determine the dye load and PMF conversion, dry capsules were ground in an agate mortar. Acetone was added to the ground powder to dissolve the payload. The suspension mixture was subjected to centrifugation at 5000 rpm for 3 min, and the

supernatant was collected to determine the amount of dye by UV absorbance. Sediment (shell material) was dried in a vacuum oven at 50 °C overnight to determine the PMF conversion – defined as the ratio of the amount of shell material to the amount of feeding material (melamine + formaldehyde amount).

Dye releasing

As a releasing model reagent, rhodamine B water solution (0.5 mg/mL) was encapsulated in the C70deg capsule. The produced capsules were added into 10 mL of acetone, water, and hexane respectively. At specific time intervals, the concentration of the dye was measured by UV absorbance.

Characterization techniques

Images of microcapsules were examined via fluorescence microscopy (AMF-4306; EVOS Fl, AMG). Emulsion template, synthesized capsule (in its xylene suspension), and the drying procedure in ambient condition were visualized under both bright fields.

Micromorphology of the capsules was investigated by using scanning electron micrograph (SEM) (Hitachi, S-4800). Voltage was adjusted from 5 kV to 3 kV or lower upon observing sample damage. Capsule suspension was dropped onto the silicon wafer, followed by sputter coating. To observe the cross-section of the capsule, capsules mounted on the silicon wafer were rolled by another wafer prior to sputter coating.

The overall composition of the capsule was characterized by Attenuation Total Reflectance-Fourier Transform Infrared Spectroscopy (ATR-FTIR, Thermo-Nicolet

Magna 550 in combination with a Thermo Spectra-Tech Foundation Series Diamond ATR accessory with an angle of incidence of 50°).

Thermo-gravimetric analysis (TGA) measurement was carried out by using TGA Q5000 instrument from room temperature to 800 °C at 10 °C/min under the nitrogen atmosphere (25 mL/min).

4.3 Results and discussions

The primary objective of this study is to understand the impact of different parameters on PMF internal shell formation on the basis of the W/O/O Pickering template. This study is based on the protocol that was developed in our previous study. Initially, stable W/O/O template was achieved by the active wrapping of an isocyanate layer around the primary W/O template. The middle oil layer was the locus of formation of the PU external shell, while dispersed droplet was the locus of formation of the internal PMF layer.

The overall composition of the dual-component capsule was elucidated by FTIR spectra (presented in Figure 4.1. PU spectra were obtained by assaying the #A1 capsule (Table 4.1) that was composed of only the external PU layer synthesized using MOCA and PPI. Before assaying, extensive xylene wash was performed on the #A1 capsule to eliminate any interference from residual MOCA. Likewise, non-encapsulated aqueous phase cured in a separate container was assayed and subjected to FTIR; it is named “PMF” in Figure 4.1. The disappearance of the characteristic isocyanate peak (2280 cm^{-1}) in PU indicated the consumption of isocyanate group of PPI. Generation of the urea peak ($\sim 1640\text{ cm}^{-1}$) was overlapped by the existing urethane peak in PPI ($\sim 1700\text{-}1600\text{ cm}^{-1}$), rendering

it border-like⁴⁰. These were substantial evidence of the occurrence of PU formation reaction (external layer formation). Moreover, feature peaks of both PU and PMF were both observed in the FTIR spectra of the capsule. Polyurethane peak ($\sim 1700\text{-}1600\text{ cm}^{-1}$) was not as pronounced in the FTIR spectra of capsules, probably due to its low proportion. However, the peak around 2922 cm^{-1} (that can be attributed to the C-H stretching vibration from MOCA and BD segment of PPI), and the peak around 1220 cm^{-1} (that corresponds to the C-O-C bond of PU) were clearly observed in the FTIR spectra of capsule, indicating the dual-components of the capsule (e.g., PU and PMF).

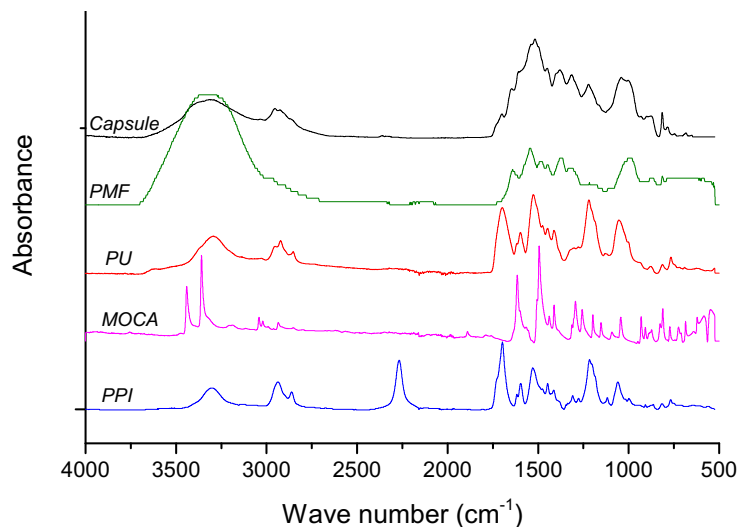


Figure 4.1 FTIR of capsule and its reactants

Three sets of capsules were fabricated containing different amounts of PMF shell forming material (ranging from 0 to 100 % with respect to the pre-MF master solution, has been described subsequently), different pH values of the solution in the second stage (ranging from 3.0 to 6.6), and different temperatures (ranging from 30 to 50°C). F/M ratio, another important factor in PMF synthesis, is, however, not reported in this study.

Reaction mechanism of PMF synthesis has been elucidated via a two-stage reaction (i.e., stage 1: methylation and stage 2: condensation). This reaction mechanism has been elucidated in detail in the previous literature^{44, 102, 108}, and therefore, has not been described in this work.

Effects of shell-forming materials

First, the effect of the amount of shell formation material (i.e., formaldehyde and melamine) was investigated. The molar ratio of formaldehyde-to-melamine was set to 3.3:1 (as per previous literature) which ensured a formation of the capsule shell on the basis of the direct emulsion template (O/W)⁴⁴. The concentration of pre-MF in the water phase was varied at 0, 10, 25, 50, 75 and 100 % of the master pre-MF solution. One of the direct consequences of change in the composition of the aqueous phase is the change in dimension of the emulsion templates. As can be seen in Figure 4.2, the size of Pickering emulsion template was observed to increase upon the increase of pre-MF content, probably due to the enhanced viscosity of the solution. The correlation between the viscosity of the dispersed phase and droplet size has been reported earlier¹¹¹ and can be understood as the increase in viscosity inhibiting the break-up during collision leading to the growth in emulsion droplet size. In this study, the frequency peak showed a shift from ~ 25 μm to ~ 50 μm with the increase in pre-MF content while exhibiting a bimodal distribution during the transition. This could be explained as the merging of initial droplets during the collision, followed by its non-breakage due to the enhanced viscosity.

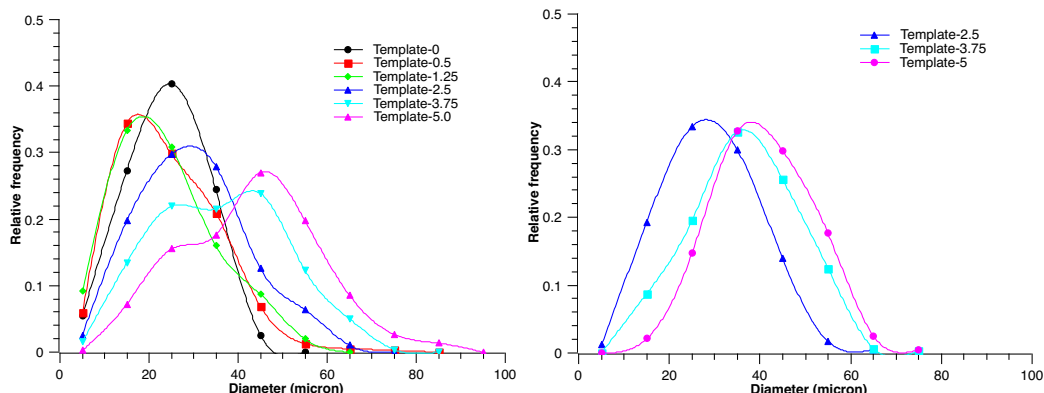


Figure 4.2: Size distribution curves of template emulsion ($n \sim 400$, droplets were measured in optical microscopy images), and size distribution curves of final capsules ($n \sim 300$, measured in SEM image) obtained with different pre-MF content.

The effect of pre-MF content on the morphology of final capsules was studied via the SEM images. As shown in Figure 4.3, capsules withstood the drying process in ambient condition and retained their spherical morphology only above a certain critical content of PMF forming materials. It should be noted that failure in the obtainment of spherical capsules (as per SEM image) does not indicate a failure in the fabrication of capsules. Capsules in xylene suspension could be observed by optical microscopy but were seen to collapse during xylene evaporation owing to their weak structure. Without the PMF lining under the PU layer, capsules (#A1) were found to collapse, leaving behind an amorphous substance as observed by SEM (Figure 4.3-a). This substance was earlier confirmed to be polyurethane (PU) by FTIR (Figure 4.1) – the substance constituting the external layer of dual-composition capsules. The increase in the pre-MF material was found to lead to the obtainment of stiffer spherical capsules that could be observed by SEM. The addition of pre-MF (at 10 % of master pre-MF content) was found to result in the obtainment of

capsules with stiffer structure, yet such capsules were not robust enough to support its spherical architecture, leaving behind a circle debris upon collapse, as shown in Figure 4.3-(b). The addition of 25 % pre-MF solution (at 25 % of master pre-MF content) led to capsules with a broad range of sizes, as shown in Figure 4.3-(c). Raspberry-like particles with rough skin may be due to the deposition of underdeveloped capsule or capsule debris.

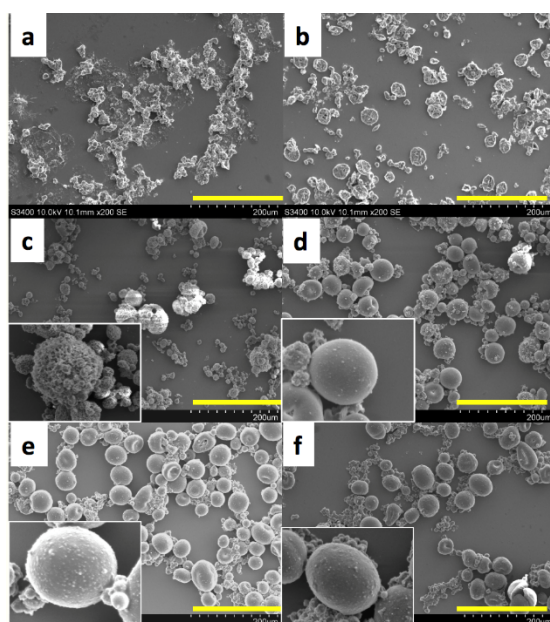


Figure 4.3: SEM images of capsules with F/M=3:1 but different pre-MF contents: a) 0 % master pre-MF (A1); b) 10 % master pre-MF (A2); c) 25 % master pre-MF (A3); d) 50 % master pre-MF (A4); e) 75 % master pre-MF (A5); f) 100 % master pre-MF (A6). All the scale bars are 200 μm .

Spherical capsules could only be obtained at the pre-MF concentration of > 50% of the master solution, as shown in Figure 4.3-(d) to (f). Capsules exhibited dense and neat external surface and were found to be robust enough to withstand the ambient environment after the evaporation of xylene. The increase in the pre-MF concentration of capsules was found to increase the capsule diameter (Figure 4.2-(b)). Compared with emulsion templates

which they were developed from (Figure 4.2-(a)), the shape of corresponding frequency curves overlapped nicely, indicating that the dimension of Pickering emulsion droplets determined the dimensions of the final capsule.

An entity is called a “capsule” only upon the presence/existence of a cavity. Representative cross-section image of A4 could not be obtained, probably due to its lower stiffness. In contrast, A5 and A6 capsules were observed to be easy to crush, indicating their higher stiffness, as shown in Figure 4.4. The effect of pre-MF content can be seen, with an increase in pre-MF content resulting in an increase in shell thickness. The shell thickness of A5 capsule was estimated to be $\sim 3.12 \pm 0.72 \mu\text{m}$ by use of ImageJ software, whereas A6 capsule showed varying cross-section morphology, ranging from capsules with $5.73 \mu\text{m}$ -shell to completely filled particles, with the latter more commonly observed, as shown in Figure 4.4-b1. Successful capsule formation revealed two facts: first, the feasibility to fabricate typical capsules on the basis of inverse emulsion (W/O/O), unlike counterparts manufactured via conventional W/O template that usually exhibit loose nature in texture and, thus, exhibit inherent permeability⁹⁴. Furthermore, deposition of PMF favors the droplet interface in a confined environment where no shear force was applied. Thus, as a starting point, processing parameters (e.g. pH and temperature) were investigated based on the composition of A5.

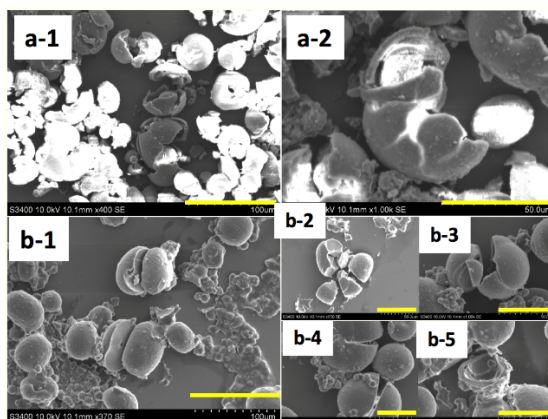


Figure 4.4: SEM image of the cross-section of A5 (a-1 & a2) and A6 (b-1 to b-5) capsule. Capsules are crushed by a silicon wafer. Scale bars are 100 μm for a-1 and b-1, 50 μm for the rest.

Effects of PH value

Interference between the payload and shell forming reaction is a primary concern when both of them are present in the dispersed phase. For the typical PMF shell forming protocol performed based on the O/W template⁴⁴, condensation step was carried out under acidic condition (pH \sim 3-5), under which, pH sensitive payloads may lose their function. Hence, milder conditions in the dispersed phase are favorable in stage 2, in which payloads are supposed to be added. In this study, stage 2 was carried out in a series of pH conditions (pH \sim 3.0, 4.0, 5.0, 6.0, and 6.6), as shown in Table 1, and synthesized capsules were named as B_{pH3} to B_{pH6.6} respectively.

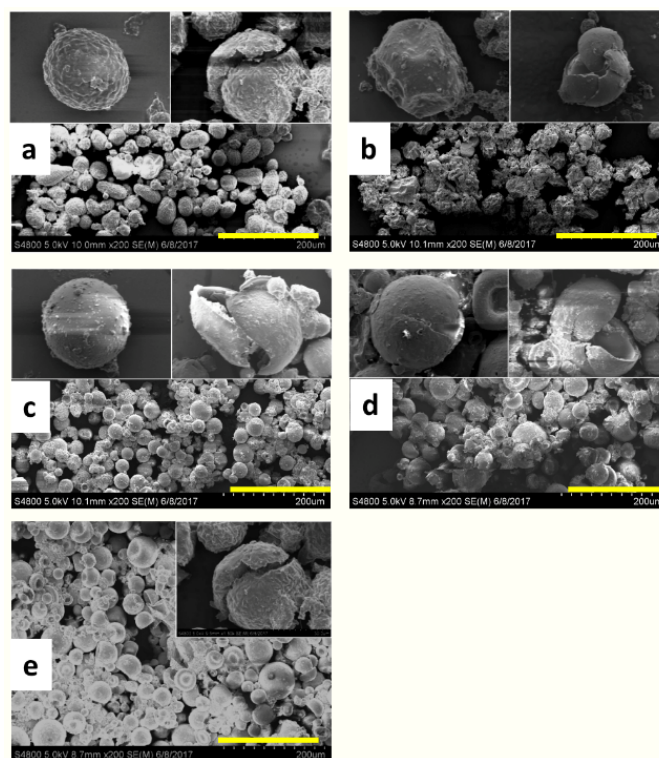


Figure 4.5 SEM of capsules prepared with different pH. Step 2 was carried out in pH = 3.0 (a, capsule B_{pH3}), 4.0 (b, capsule B_{pH4}), 5.0 (c, capsule B_{pH5}), 6.0 (d, capsule B_{pH6}) and 6.6 (e, capsule $B_{pH6.6}$). Surface feature and crushed capsule are presented as inserts respectively. Scale bars are 200 μm .

Distinct surface features and cross-section of capsules was observed by SEM, as shown in Figure 4.5. We hypothesized that differences in capsule morphology, for both the external surface as well as internal architecture, are associated with the confinement of PMF reaction in the emulsion droplet. As a reference, parallel *in-situ* bulk polymerization under corresponding conditions (i.e., concentration, composition, temperature, named as R_{pH3} to $R_{pH6.6}$ where “R” is short for Resin) was carried out in a plastic tube to mimic the reaction in the emulsion droplet. R_{pH3} , R_{pH4} , and R_{pH5} were observed to solidify within 5 min at 70 °C while exhibiting distinct texture. R_{pH3} was found to be transparent and brittle,

while R_{pH4} was observed to be hard and opaque. R_{pH5} was observed to be white in color and porous while possessing stable dimension – all of which could be observed by naked eyes. R_{pH6} and $R_{pH6.6}$ were not observed to solidify as a whole entity but were found to turn turbid at ~ 10 min and ~ 30 min respectively. Following this, the white substance was found to accumulate on the internal surface of the tube wall, resulting in a white hard lining against the wall, leaving transparent liquid in the middle space.

Reactions in emulsion droplets may take place in an analogous manner, and this can affect the morphology of capsules. Capsules prepared in $pH = 3$ (B_{pH3}) exhibited shriveled external surface (Figure 4.5-a), which was believed to be the consequence of the drying process. This was supported by optical images in which smooth profile of capsule was observed to become rough after the evaporation of xylene (image not shown). Oval shape reflected the occurrence of PMF polymerization prior to the emulsion becoming stable, thereby “freezing” the shear-induced elongation. For B_{pH4} , a large number of capsules were observed to be lacking any external PU layer (Figure 4.5-b) – a phenomenon that we could not explain. Typical spherical capsules with smooth skin were observed when pH of the solution was controlled at 5.0 and 6.0. $B_{pH6.6}$ capsules showed less mechanical stability, along with spherical shape in xylene suspension (observed in the optical image, not shown) that collapsed upon drying and exhibited bowl-like conformation, as shown in (Figure 4.5-e). To observe the cross-section, capsules were dried under ambient condition and crushed by a silicon wafer. However, for capsules B_{pH3} and B_{pH4} , few broken capsules were observed. The high impact resistance may have been inherited from the precursor materials (due to their high resistance properties) and particle architecture (cavity filled),

as shown in Figure 4.5- right insert. In contrast, for capsules $B_{\text{pH}5}$ and $B_{\text{pH}6}$, plenty of crushed capsules were observed with the typical hollow structure, neat internal surface and thin shell (1~4 μm thickness).

Considering the phenomenon observed in the plastic tube, it can be likely concluded that pH of the solution has a strong effect on the PMF forming reaction and the architecture of the final capsule. Based on observations above, lower pH probably led to a rapid crosslinking and tended to result in a bulk resin. This may also occur within the emulsion droplet and justified the generation of a cavity-filled particle, as was observed for capsules $B_{\text{pH}3}$ and $B_{\text{pH}4}$. The reaction was so rapid that the oval droplet was found to “solidify” even before it stabilized, leading to the obtainment of an elliptical capsule for $B_{\text{pH}3}$. pH was observed to exhibit a pronounced effect on the clarity of dried PMF aerogel¹¹². The increase in pH of the solution from 3.0 to 5.0 was found to result in a transition from the transparent stiff gel ($R_{\text{pH}3}$) to the white porous rigid foam ($R_{\text{pH}5}$), indicating the change in the microstructure and phase morphology of the PMF¹¹². Although characterization of the PMF resin at the molecular level remains challenging¹¹³, the fact that foam dimension showed stability ($R_{\text{pH}5}$) in comparison to the visible shrinkage of the bulk resin during the condensation step ($R_{\text{pH}3}$ & $R_{\text{pH}4}$) indicates distinct PMF microstructure forming process. This is especially evident in $R_{\text{pH}6}$ and $R_{\text{pH}6.6}$ where visible particles were observed to form in the system and accumulate on the internal surface of the plastic wall. Therefore, folds and creases on the capsule $B_{\text{pH}3}$ surface can be interpreted as the consequence of shrinkage of its solid bulk core. During the drying process, vapor-liquid interface recedes, causing an increase in tensile stress that causes the polymeric network to collapse¹¹⁴. In contrast, at

higher pH, PMF particle was found to deposit gradually within the droplets and form dense and stiff shells, along with less integration of water within the PMF network, thereby eliminating the shrinkage during the drying process. However, when the reaction was undertaken at neutral pH (for instance, 6.6 in this study), low reaction rate and possible low PMF conversion led to the incomplete formation of the PMF internal shell, resulting in its collapse after drying.

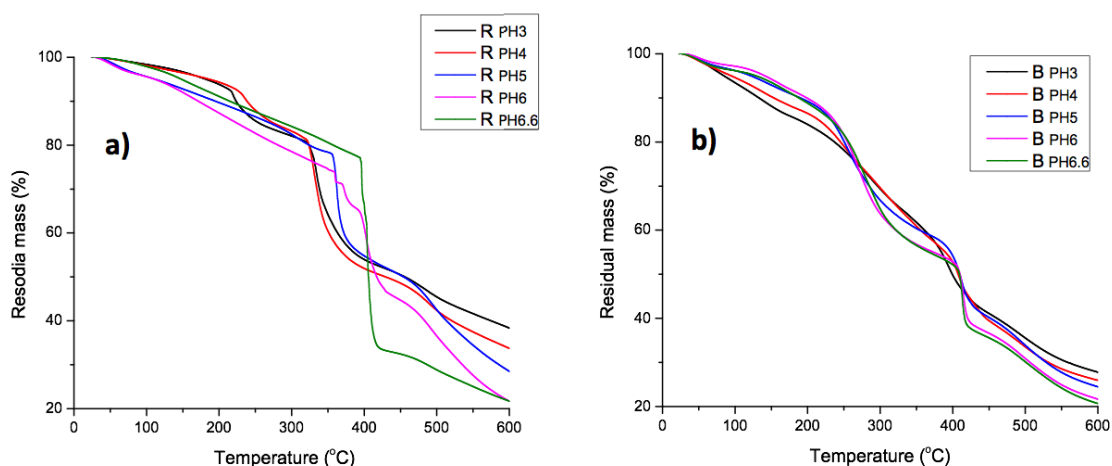


Figure 4.6: TGA thermograms of capsule (right) and PMF resin (left).

TGA thermograms of capsules (Figure 4.6-B) and corresponding PMF resin (Figure 4.6-A) revealed the similarity of PMF synthesis reaction carried out in the micro-droplet and *in-situ* bulk polymerization. Thermal behavior of PMF resin is complicated, as the post-pot reaction occurring during its heating is accompanied by molecular elimination. Multi-stage weight loss behavior of PMF has been observed in earlier studies⁸⁹. Each stage is correlated to specific reactions involved in PMF synthesis. For instance, the stage around 160 °C on the TGA thermogram corresponds to the elimination of formaldehyde via reverse methylation reaction, along with the elimination

of water due to condensation^{41, 108}. Similarly, weight loss above 350°C is associated with the breakdown of methylene bridges, and that above 400°C corresponds to slow thermal degradation of the triazine ring^{41, 108}. When compared with cured PMF, partially cured PMF resin has been observed to exhibit more pronounced weight loss at ~ 160 °C and ~ 350 °C, and the stage around ~ 350°C has been found to shift towards higher temperature⁴¹, which is in good agreement with the phenomenon observed in Figure 4.6-A. Thus, it can be interpreted that pH of the solution affects the molecular structure of PMF resin, with a higher pH leading to a sparser PMF network. This trend, e.g. the stage shift and weight loss at ~ 350 °C, is also observed in thermograms of capsules (Figure 4.6-B) despite the reduced significance of PMF resin. The opposite trend observed at the lower temperature (~160 °C) associated with weight loss can be interpreted as the loss of weight due to aqueous payload evaporation, reflecting that the capsule is more efficient in bearing loads when prepared in higher pH condition. In summary, PMF formation under higher pH conditions (such as ~ 5.0) would be favorable in the formation of a dimensional stable capsule.

Temperature effect

The initial intention of the temperature study was to investigate the effect of PMF formation rate on the morphology of the prepared capsule. As an easily controlled parameter, temperature effect was observed to be pronounced in batch PMF synthesis in the plastic tube, in which the white solid bulk was observed to form within 5 min at 70 °C,

whereas at 50 and 70 °C, white solid particles were found to occur at 10 min and 30 min respectively, but did not show any solidification to form a bulk material (data not shown).

Experimental conditions for preparing capsules were kept identical as those of basic design while varying the temperature in condensation stage (30, 50 and 70 °C), as summarized in Table 1. External and cross-section morphology of capsules are presented in Figure 4.7. Capsules obtained at the lower temperature (30 and 50 °C) exhibited bowl-like shape, as clearly shown in Figure 4.7-a, which is analogous with capsules B_{pH6} and B_{pH6} (**Error! Reference source not found.**-b & e) fabricated in more neutral conditions. This phenomenon can again be explained by the same consideration as presented above, i.e., factors (low temperature and low pH value) that led to a low conversion of PMF, resulting in an incomplete formation of the internal PMF layer and subsequent collapse of capsules during the drying process. The collapsed morphology was not observed when the temperature was increased in our study to 70 °C (Figure 4.7-c), indicating that a more stable structure was achieved probably due to complete formation of the internal PMF layer. Moreover, the surface of collapsed capsule remained intact, showing the flexible nature of the capsule shell, which can be attributed to the flexible PU external layer synthesized by MOCA and PPI. A slight increase in thickness of the capsule shell was observed with increase in temperature, as shown in Figure 4.7-d. Shell thickness and thickness-to-diameter (T/D) ratio of capsules with a typical diameter between ~ 32 - $44 \mu m$ were measured. Typical thickness of C_{30deg} , C_{50deg} , and C_{70deg} was measured as $1.02 \pm 0.18 \mu m$, $1.12 \pm 0.19 \mu m$ and $1.19 \pm 0.19 \mu m$ respectively, and T/D ratio was calculated as $3.6 \pm 0.7\%$, $3.5 \pm 0.5\%$, $3.5 \pm 1.1\%$, respectively.

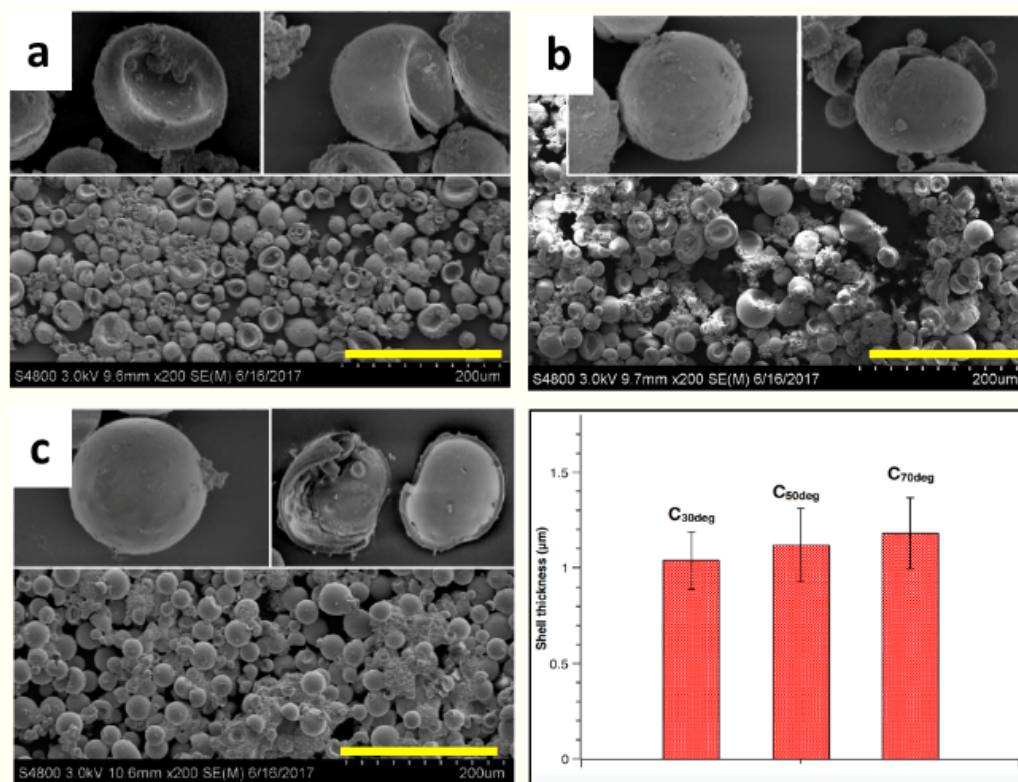


Figure 4.7. SEM image of capsules prepared at 30°C (a), 50°C (b) and 70°C (c). Inserts include break capsules. The thickness of capsules' shell (d).

Permeability and releasing behavior

As a potential micro-container, permeability is essential for capsules. Thus, the release behavior of prepared capsules was investigated. Herein, fluorescent rhodamine B aqueous solution was encapsulated in the dual component capsules under optimized encapsulation conditions. The diffusion rate of rhodamine B in water was investigated.

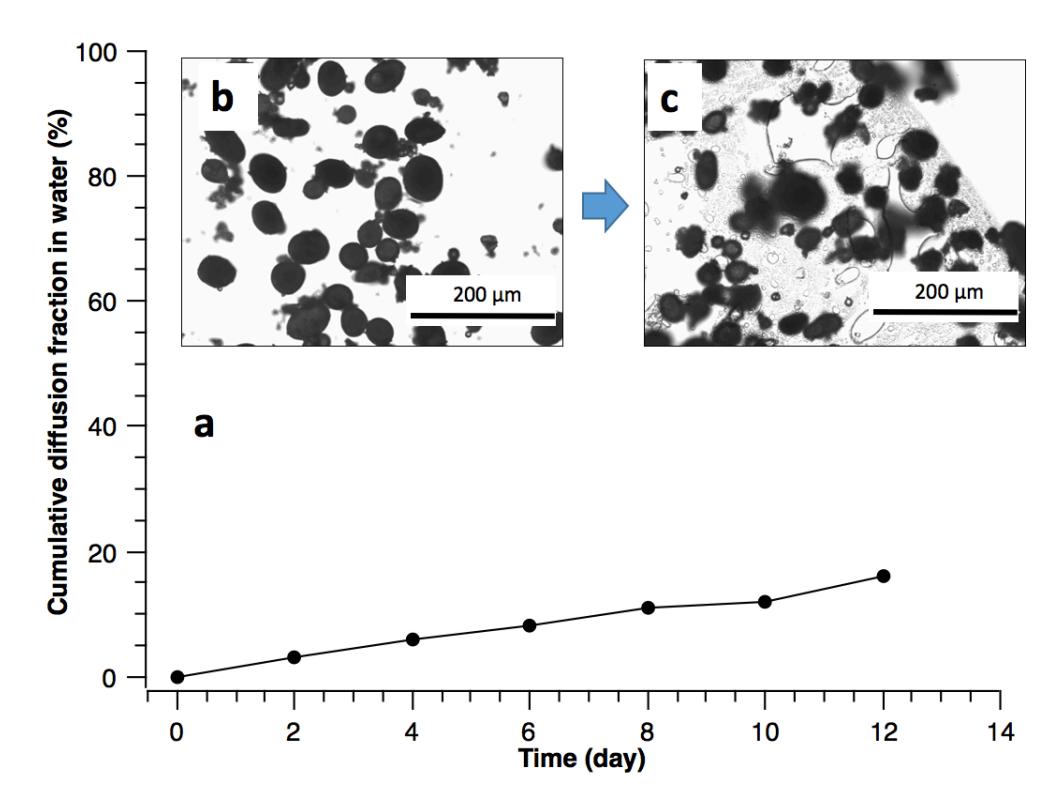


Figure 4.8 Diffusion profile of rhodamine B from the capsule in water (a). Encapsulated solution released after the crush (b &c)

Capsules ($C_{70\text{deg}}$) were dried in the controlled condition (i.e., 20 °C, 35 % humidity) for seven days and crushed by silicon wafer on the glass slide. Observed under the optical microscope, the liquid was released as shown in Figure 1.8 (b and c). The release properties of the capsule were investigated by tracing the loaded fluorescence dye. As shown in Figure 1.8-a, the diffusion of the rhodamine B in water is relatively slow. Given that the water can wet the PU substance and PMF well, and the rhodamine B has a high solubility in water⁹⁴, the low diffusion rate could attribute to the low permeability of the capsule.

4.4 Conclusion

PU-PMF dual component capsules with typical and robust shell were fabricated with the aim of encapsulating the hydrophilic payload. Selected parameters that can influence PMF synthesis in in-situ bulk polymerization were found to affect capsule formation in the micro-droplet, and eventually, determine its morphology. By controlling temperature, formaldehyde and melamine content, and pH conditions, capsule size, shell thickness and its internal/external morphology were adjusted. A protocol was also provided to manufacture capsules with a regular surface, dense shell, and mild pH condition. Capsule size was found to be determined by the Pickering emulsion, and shell thickness was found to be related to PMF synthesis that in turn was affected by the shell forming material and temperature. Thermal behavior of the capsule, studied using TGA, revealed that the effect of pH on capsule morphology was related to the density of the methylene bridges. In sum, this study provides a protocol to encapsulate hydrophilic payload within a capsule.

CHAPTER FIVE

5. CONCLUSION AND FUTURE WORK

5.1 Conclusion

In this dissertation, we provide solutions to address two critical problems that are related to the fabrication of protein-based resin. Our solution employs the crosslinking technique to improve mechanical properties, while applying self-healing technique to remedy the brittleness caused by crosslinking.

We demonstrate a method to improve properties of SPI films by DCMC crosslinking. DCMC treatment led to significant increase in tensile strength (~ 218 %) and simultaneous improvement in both water resistance and thermal stability. Effective generation of crosslinking network via aldehyde-amine reaction is believed to be the reason for these improvements, which are also observed to be related to DCMC content, and are accompanied by the consumption of primary amine groups in the system. Excellent performance of SPI-DCMC system is believed to be due to good compatibility between SPI and DCMC. Unlike other protein bio-based crosslinking systems, granules and phase separation phenomenon were not observed in SEM images of SPI-DCMC films. In summary, DCMC crosslinking was an efficient method for obtaining fully bio-based, biodegradable SPI films with low cytotoxicity.

We propose in this work that the tendency of cracking due to crosslinking can be alleviated by employing the self-healing system. Based on the distinct features of the protein-based material, a single capsule self-healing system with formaldehyde as self-healing reagent was designed. Encapsulating the hydrophilic formaldehyde was

challenging. For the first time, effective encapsulation of hydrophilic payload was accomplished based on W/O/O template by integrating two classical capsule formation chemistries – PU via interfacial polymerization and PMF via in-situ polymerization – with critical modifications. For PU shell formation, isocyanate-rich pre-layer was achieved by taking advantage of interfacial tension that minimized overall free energy and eventually led to the novel W/O/O conformation. The advantages of this structure, with isocyanate confined in the middle layer, were: (1) High isocyanate concentration that facilitated synthesis of high molecular weight PU molecule; and (2) Possibility of external addition of chain extender (e.g. MOCA), thus avoiding any interference with the reactive/sensitive payload – an inherent drawback of the conventional route. Further improvement in mechanical properties was accomplished by incorporating PMF lining under the PU layer. A multilayer structure, composed of a dense external PU layer and PMF skeleton, was obtained with PU and PMF respectively performing complementary roles of insulation and improving mechanical stability. The resultant capsule with tunable internal architecture was observed to withstand ambient drying process and hold the hydrophilic payload.

Based on the protocol, we focused on fabricating capsules with robust structure, dense shell, and typical structure. Selected parameters that can influence PMF synthesis in in-situ bulk polymerization were found to affect capsule formation in the micro-droplet, and eventually determine its morphology. By controlling temperature, formaldehyde-to-melamine content ratio and pH conditions, capsule size, shell thickness and its internal/external morphology were adjusted. A protocol was also developed and provided to manufacture capsules with a regular surface, dense shell, and mild pH condition. Capsule

size was found to be determined by the Pickering emulsion, while shell thickness was observed to be related to PMF synthesis, which in turn was affected by shell forming material and temperature. Thermal behavior of the capsule, studied using TGA, revealed that the effect of pH on capsule morphology was related to the density of methylene bridges.

5.2 Future work

Shell wall refinement

Although we have provided a protocol to encapsulate formaldehyde in this dissertation, the more significant value of the W/O/O template is its potential to prepare capsule with single PU layer without containing the internal PMF skeleton. If this were to be realized, it might be an extremely facile solution to encapsulate hydrophilic loads. The interference of shell forming reaction with the payload can then be smartly eliminated, since in this work, PU shell forming occurred only in the middle oil layer of the double emulsion droplet. Currently, double emulsion concept can only be realized via microfluidic technique, which has limited potential to be applicable for mass production. Improvement in the strength of PU shell can be achieved by optimization of PU components (i.e., soft segment, stiff segment, and crosslinking reagents) or additional coating from the external side of capsules.

Self-healing evaluation

Self-healing evaluation was not performed in this dissertation due to the huge amount of systematic evaluations required for the conversion of the capsule to self-healing system. These assessments include, but are not limited to, the bonding capacity of the capsule shell to the protein matrix, deposition of capsules in matrix materials, and optimization of the viscosity of the payload, all of which can impact healing efficiency of the system.

6. REFERENCES

- (1) Meier, M. A.; Metzger, J. O.; Schubert, U. S., Plant oil renewable resources as green alternatives in polymer science. *Chemical Society Reviews* 2007, 36 (11), 1788-1802.
- (2) Biermann, U.; Friedt, W.; Lang, S.; Lühs, W.; Machmüller, G.; Metzger, J. O.; Ruesch gen Klaas, M.; Schaefer, H. J.; Schneider, M. P., New syntheses with oils and fats as renewable raw materials for the chemical industry. *Angewandte Chemie International Edition* 2000, 39 (13), 2206-2224.
- (3) Pillai, C.; Prasad, V.; Sudha, J.; Bera, S.; Menon, A., Polymeric resins from renewable resources. II. Synthesis and characterization of flame-retardant prepolymers from cardanol. *Journal of Applied Polymer Science* 1990, 41 (9-10), 2487-2501.
- (4) Gandini, A.; Belgacem, M., Recent contributions to the preparation of polymers derived from renewable resources. *Journal of Polymers and the Environment* 2002, 10 (3), 105-114.
- (5) Raquez, J.-M.; Deléglise, M.; Lacrampe, M.-F.; Krawczak, P., Thermosetting (bio) materials derived from renewable resources: a critical review. *Progress in Polymer Science* 2010, 35 (4), 487-509.
- (6) Rosenthal, F., Cottonseed meal in phenolic plastics. *Industrial & Engineering Chemistry* 1942, 34 (10), 1154-1157.
- (7) Andresen, C.; Demuth, C.; Lange, A.; Stoick, P.; Pruszko, R., Biobased automobile parts investigation. *A Report Developed for the USDA Office of Energy Policy and New Uses* 2012.
- (8) Paetau, I.; Chen, C.-Z.; Jane, J.-L., Biodegradable plastic made from soybean products. 1. Effect of preparation and processing on mechanical properties and water absorption. *Industrial & engineering chemistry research* 1994, 33 (7), 1821-1827.
- (9) Sue, H.-J.; Wang, S.; Jane, J.-L., Morphology and mechanical behaviour of engineering soy plastics. *Polymer* 1997, 38 (20), 5035-5040.
- (10) Kumar, R.; Choudhary, V.; Mishra, S.; Varma, I.; Mattiason, B., Adhesives and plastics based on soy protein products. *Industrial crops and products* 2002, 16 (3), 155-172.
- (11) Vaz, C. M.; van Doeveren, P. F.; Yilmaz, G.; De Graaf, L. A.; Reis, R. L.; Cunha, A. M., Processing and characterization of biodegradable soy plastics: Effects of

- crosslinking with glyoxal and thermal treatment. *Journal of applied polymer science* 2005, 97 (2), 604-610.
- (12) Fraenkel-Conrat, H.; Olcott, H. S., Reaction of formaldehyde with proteins VI. cross-linking of amino groups with phenol, imidazole, or indole groups. *Journal of Biological Chemistry* 1948, 174 (3), 827-843.
- (13) Sun, S.; Song, Y.; Zheng, Q., Morphologies and properties of thermo-molded biodegradable plastics based on glycerol-plasticized wheat gluten. *Food Hydrocolloids* 2007, 21 (7), 1005-1013.
- (14) Hernandez-Munoz, P.; Kanavouras, A.; Villalobos, R.; Chiralt, A., Characterization of biodegradable films obtained from cysteine-mediated polymerized gliadins. *Journal of agricultural and food chemistry* 2004, 52 (26), 7897-7904.
- (15) Gennadios, A.; Handa, A.; Froning, G. W.; Weller, C. L.; Hanna, M. A., Physical properties of egg white– dialdehyde starch films. *Journal of Agricultural and Food Chemistry* 1998, 46 (4), 1297-1302.
- (16) Dou, Y.; Huang, X.; Zhang, B.; He, M.; Yin, G.; Cui, Y., Preparation and characterization of a dialdehyde starch crosslinked feather keratin film for food packaging application. *Rsc Advances* 2015, 5 (34), 27168-27174.
- (17) Martucci, J.; Ruseckaite, R.; Vazquez, A., Creep of glutaraldehyde-crosslinked gelatin films. *Materials Science and Engineering: A* 2006, 435, 681-686.
- (18) Bourtoom, T., Edible films and coatings: characteristics and properties. *International Food Research Journal* 2008, 15 (3), 237-248.
- (19) Xie, D.-Y.; Song, F.; Zhang, M.; Wang, X.-L.; Wang, Y.-Z., Soy protein isolate films with improved property via a facile surface coating. *Industrial Crops and Products* 2014, 54, 102-108.
- (20) Hernández-Muñoz, P.; Villalobos, R.; Chiralt, A., Effect of cross-linking using aldehydes on properties of glutenin-rich films. *Food Hydrocolloids* 2004, 18 (3), 403-411.
- (21) Krochta, J. M.; Mulder-Johnston, D., Edible and biodegradable polymer films: challenges and opportunities. *Food technology (USA)* 1997.
- (22) Rhim, J.-W.; Gennadios, A.; Weller, C. L.; Cezeirat, C.; Hanna, M. A., Soy protein isolate–dialdehyde starch films. *Industrial Crops and Products* 1998, 8 (3), 195-203.
- (23) Martucci, J.; Ruseckaite, R., Tensile properties, barrier properties, and biodegradation in soil of compression—Molded gelatin-dialdehyde starch films. *Journal of Applied Polymer Science* 2009, 112 (4), 2166-2178.
- (24) Anjali, T., Modification of carboxymethyl cellulose through oxidation. *Carbohydrate polymers* 2012, 87 (1), 457-460.

- (25) Pratama, P. A.; Sharifi, M.; Peterson, A. M.; Palmese, G. R., Room temperature self-healing thermoset based on the Diels–Alder reaction. *ACS applied materials & interfaces* 2013, 5 (23), 12425-12431.
- (26) Schoth, A.; Landfester, K.; Muñoz-Espí, R., Surfactant-free polyurethane nanocapsules via inverse pickering miniemulsion. *Langmuir* 2015, 31 (13), 3784-3788.
- (27) Sauvant-Moynot, V.; Gonzalez, S.; Kittel, J., Self-healing coatings: An alternative route for anticorrosion protection. *Progress in Organic Coatings* 2008, 63 (3), 307-315.
- (28) Takahashi, M.; Taguchi, Y.; Tanaka, M., Microencapsulation of hydrophilic solid powder as a flame retardant with epoxy resin by using interfacial reaction method. *Polymers for Advanced Technologies* 2010, 21 (3), 224-228.
- (29) McIlroy, D. A.; Blaiszik, B. J.; Caruso, M. M.; White, S. R.; Moore, J. S.; Sottos, N. R., Microencapsulation of a reactive liquid-phase amine for self-healing epoxy composites. *Macromolecules* 2010, 43 (4), 1855-1859.
- (30) Koh, E.; Lee, S.; Shin, J.; Kim, Y.-W., Renewable polyurethane microcapsules with isosorbide derivatives for self-healing anticorrosion coatings. *Industrial & Engineering Chemistry Research* 2013, 52 (44), 15541-15548.
- (31) Koh, E.; Kim, N.-K.; Shin, J.; Kim, Y.-W., Polyurethane microcapsules for self-healing paint coatings. *RSC Advances* 2014, 4 (31), 16214-16223.
- (32) Stoessel, P. R.; Krebs, U.; Hufenus, R.; Halbeisen, M.; Zeltner, M.; Grass, R. N.; Stark, W. J., Porous, water-resistant multifilament yarn spun from gelatin. *Biomacromolecules* 2015, 16 (7), 1997-2005.
- (33) Yang, J.; Keller, M. W.; Moore, J. S.; White, S. R.; Sottos, N. R., Microencapsulation of isocyanates for self-healing polymers. *Macromolecules* 2008, 41 (24), 9650-9655.
- (34) Caruso, M. M.; Blaiszik, B. J.; Jin, H.; Schelkopf, S. R.; Stradley, D. S.; Sottos, N. R.; White, S. R.; Moore, J. S., Robust, double-walled microcapsules for self-healing polymeric materials. *ACS applied materials & interfaces* 2010, 2 (4), 1195-1199.
- (35) Gao, Z.; Wang, W.; Zhao, Z.; Guo, M., Novel whey protein-based aqueous polymer-isocyanate adhesive for glutam. *Journal of Applied Polymer Science* 2011, 120 (1), 220-225.
- (36) Meng, L. M.; Yuan, Y. C.; Rong, M. Z.; Zhang, M. Q., A dual mechanism single-component self-healing strategy for polymers. *Journal of Materials Chemistry* 2010, 20 (29), 6030-6038.
- (37) Bouchemal, K.; Briançon, S.; Perrier, E.; Fessi, H.; Bonnet, I.; Zydowicz, N., Synthesis and characterization of polyurethane and poly (ether urethane) nanocapsules

- using a new technique of interfacial polycondensation combined to spontaneous emulsification. *International Journal of Pharmaceutics* 2004, 269 (1), 89-100.
- (38) Rosenthal, A.; Chang, T., The incorporation of lipid and Na⁺-K⁺-ATPase into the membranes of semipermeable microcapsules. *Journal of Membrane Science* 1980, 6, 329-338.
- (39) Janssen, L.; Te Nijenhuis, K., Encapsulation by interfacial polycondensation. I. The capsule production and a model for wall growth. *Journal of membrane science* 1992, 65 (1-2), 59-68.
- (40) Kuypers, S.; Pramanik, S. K.; D'Olieslaeger, L.; Reekmans, G.; Peters, M.; D'Haen, J.; Vanderzande, D.; Junkers, T.; Adriaensens, P.; Ethirajan, A., Interfacial thiol–isocyanate reactions for functional nanocarriers: a facile route towards tunable morphologies and hydrophilic payload encapsulation. *Chemical Communications* 2015, 51 (87), 15858-15861.
- (41) Alič, B.; Šebenik, U.; Krajnc, M., Microencapsulation of butyl stearate with melamineformaldehyde resin: Effect of decreasing the pH value on the composition and thermal stability of microcapsules. *Express Polymer Letters* 2012, 6 (10).
- (42) Yi, H.; Yang, Y.; Gu, X.; Huang, J.; Wang, C., Multilayer composite microcapsules synthesized by Pickering emulsion templates and their application in self-healing coating. *Journal of Materials Chemistry A* 2015, 3 (26), 13749-13757.
- (43) Fei, X.; Zhao, H.; Zhang, B.; Cao, L.; Yu, M.; Zhou, J.; Yu, L., Microencapsulation mechanism and size control of fragrance microcapsules with melamine resin shell. *Colloids and Surfaces A: Physicochemical and Engineering Aspects* 2015, 469, 300-306.
- (44) Ollier, R. P.; Alvarez, V. A., Synthesis of epoxy-loaded poly (melamine-formaldehyde) microcapsules: Effect of pH regulation method and emulsifier selection. *Colloids and Surfaces A: Physicochemical and Engineering Aspects* 2017, 520, 872-882.
- (45) Tiarks, F.; Landfester, K.; Antonietti, M., Preparation of polymeric nanocapsules by miniemulsion polymerization. *Langmuir* 2001, 17 (3), 908-918.
- (46) Berg, J.; Sundberg, D.; Kronberg, B., Microencapsulation of emulsified oil droplets by in-situ vinyl polymerization. *Journal of microencapsulation* 1989, 6 (3), 327-337.
- (47) Loxley, A.; Vincent, B., Preparation of poly (methylmethacrylate) microcapsules with liquid cores. *Journal of colloid and interface science* 1998, 208 (1), 49-62.
- (48) Dowding, P. J.; Atkin, R.; Vincent, B.; Bouillot, P., Oil core/polymer shell microcapsules by internal phase separation from emulsion droplets. II: controlling the release profile of active molecules. *Langmuir* 2005, 21 (12), 5278-5284.
- (49) Dowding, P. J.; Atkin, R.; Vincent, B.; Bouillot, P., Oil core– polymer shell microcapsules prepared by internal phase separation from emulsion droplets. I.

Characterization and release rates for microcapsules with polystyrene shells. *Langmuir* 2004, 20 (26), 11374-11379.

(50) Atkin, R.; Davies, P.; Hardy, J.; Vincent, B., Preparation of aqueous core/polymer shell microcapsules by internal phase separation. *Macromolecules* 2004, 37 (21), 7979-7985.

(51) Caruso, F.; Trau, D.; Möhwald, H.; Renneberg, R., Enzyme encapsulation in layer-by-layer engineered polymer multilayer capsules. *Langmuir* 2000, 16 (4), 1485-1488.

(52) Antipov, A. A.; Sukhorukov, G. B., Polyelectrolyte multilayer capsules as vehicles with tunable permeability. *Advances in colloid and interface science* 2004, 111 (1), 49-61.

(53) Donath, E.; Sukhorukov, G. B.; Caruso, F.; Davis, S. A.; Möhwald, H., Novel hollow polymer shells by colloid-templated assembly of polyelectrolytes. *Angewandte Chemie International Edition* 1998, 37 (16), 2201-2205.

(54) McClements, D. J., *Nanoparticle-and microparticle-based delivery systems: Encapsulation, protection and release of active compounds*. CRC Press: 2014.

(55) Yuan, L.; Liang, G.; Xie, J.; Li, L.; Guo, J., Preparation and characterization of poly (urea-formaldehyde) microcapsules filled with epoxy resins. *polymer* 2006, 47 (15), 5338-5349.

(56) Jin, H.; Mangun, C. L.; Stradley, D. S.; Moore, J. S.; Sottos, N. R.; White, S. R., Self-healing thermoset using encapsulated epoxy-amine healing chemistry. *Polymer* 2012, 53 (2), 581-587.

(57) Li, J.; Hughes, A. D.; Kalantar, T. H.; Drake, I. J.; Tucker, C. J.; Moore, J. S., Pickering-emulsion-templated encapsulation of a hydrophilic amine and its enhanced stability using poly (allyl amine). *ACS Macro Letters* 2014, 3 (10), 976-980.

(58) Chen, P. W.; Cadisch, G.; Studart, A. R., Encapsulation of aliphatic amines using microfluidics. *Langmuir* 2014, 30 (9), 2346-2350.

(59) Yeom, C.; Oh, S.; Rhim, J.; Lee, J., Microencapsulation of water-soluble herbicide by interfacial reaction. I. Characterization of microencapsulation. *Journal of applied polymer science* 2000, 78 (9), 1645-1655.

(60) Rhim, J.-W.; Lee, J. H.; Ng, P. K., Mechanical and barrier properties of biodegradable soy protein isolate-based films coated with polylactic acid. *LWT-Food Science and Technology* 2007, 40 (2), 232-238.

(61) Kurniawan, L.; Qiao, G. G.; Zhang, X., Chemical modification of wheat protein-based natural polymers: grafting and cross-linking reactions with poly (ethylene oxide) diglycidyl ether and ethyl diamine. *Biomacromolecules* 2007, 8 (9), 2909-2915.

- (62) Wilson, R. H., Utilization and toxicity of dialdehyde-and dicarboxyl-starches. *Experimental Biology and Medicine* 1959, 102 (3), 735-737.
- (63) Gennadios, A.; Handa, A.; Froning, G. W.; Weller, C. L.; Hanna, M. A., Physical properties of egg white-dialdehyde starch films. *Journal of Agricultural and Food Chemistry* 1998, 46 (4), 1297-1302.
- (64) Su, J.-F.; Huang, Z.; Yuan, X.-Y.; Wang, X.-Y.; Li, M., Structure and properties of carboxymethyl cellulose/soy protein isolate blend edible films crosslinked by Maillard reactions. *Carbohydr. Polym.* 2010, 79 (1), 145-153.
- (65) Dyatlov, V.; Gumnikova, V.; Grebeneva, T.; Kruppa, I.; Rustamov, I.; Kireev, V.; Maleev, V., Study of the chemical structure of dialdehyde carboxymethyl cellulose produced by periodate oxidation under different conditions. *International Polymer Science and Technology* 2015, 42 (4), T19.
- (66) Mu, C.; Guo, J.; Li, X.; Lin, W.; Li, D., Preparation and properties of dialdehyde carboxymethyl cellulose crosslinked gelatin edible films. *Food Hydrocolloids* 2012, 27 (1), 22-29.
- (67) Varma, A.; Kulkarni, M., Oxidation of cellulose under controlled conditions. *Polymer Degradation and Stability* 2002, 77 (1), 25-27.
- (68) Brandenburg, A.; Weller, C.; Testin, R., Edible films and coatings from soy protein. *Journal of food Science* 1993, 58 (5), 1086-1089.
- (69) Mo, X.; Sun, X., Plasticization of soy protein polymer by polyol-based plasticizers. *Journal of the American Oil Chemists' Society* 2002, 79 (2), 197-202.
- (70) Hermanson, G. T., *Bioconjugate techniques*. Academic press: 2013.
- (71) Smith, M.; Verbeek, C. J. R.; Lay, M., Non-isothermal curing of DGEBA with bloodmeal-based proteins. *Ind. Eng. Chem. Res.* 2015.
- (72) Jongjareonrak, A.; Benjakul, S.; Visessanguan, W.; Prodpran, T.; Tanaka, M., Characterization of edible films from skin gelatin of brownstripe red snapper and bigeye snapper. *Food Hydrocolloids* 2006, 20 (4), 492-501.
- (73) Bertelsen, G.; Skibsted, L., Photooxidation of oxymyoglobin. Wavelength dependence of quantum yields in relation to light discoloration of meat. *Meat Science* 1987, 19 (4), 243-251.
- (74) Djenane, D.; Sánchez-Escalante, A.; Beltrán, J.; Roncalés, P., Extension of the retail display life of fresh beef packaged in modified atmosphere by varying lighting conditions. *Journal of Food Science* 2001, 66 (1), 181-186.
- (75) Pan, H.; Jiang, B.; Chen, J.; Jin, Z., Blend-modification of soy protein/lauric acid edible films using polysaccharides. *Food chemistry* 2014, 151, 1-6.

- (76) Park, S.; Bae, D.; Rhee, K., Soy protein biopolymers cross-linked with glutaraldehyde. *Journal of the American Oil Chemists' Society* 2000, 77 (8), 879-884.
- (77) Vieira, M. G. A.; da Silva, M. A.; dos Santos, L. O.; Beppu, M. M., Natural-based plasticizers and biopolymer films: A review. *Eur. Polym. J.* 2011, 47 (3), 254-263.
- (78) Arib, R.; Sapuan, S.; Ahmad, M.; Paridah, M.; Zaman, H. K., Mechanical properties of pineapple leaf fibre reinforced polypropylene composites. *Materials & Design* 2006, 27 (5), 391-396.
- (79) Lovinger, A. J.; Williams, M., Tensile properties and morphology of blends of polyethylene and polypropylene. *Journal of Applied Polymer Science* 1980, 25 (8), 1703-1713.
- (80) Bigi, A.; Cojazzi, G.; Panzavolta, S.; Rubini, K.; Roveri, N., Mechanical and thermal properties of gelatin films at different degrees of glutaraldehyde crosslinking. *Biomaterials* 2001, 22 (8), 763-768.
- (81) Wang, L.; Xiao, M.; Dai, S.; Song, J.; Ni, X.; Fang, Y.; Corke, H.; Jiang, F., Interactions between carboxymethyl konjac glucomannan and soy protein isolate in blended films. *Carbohydrate polymers* 2014, 101, 136-145.
- (82) HERNANDEZ-MUÑOZ, P.; Hernandez, R. In *Heat curing of wheat gluten gliadin and glutenin films*, 2002 Annual Meeting and Food Expo-Anaheim, California, 2002.
- (83) Stuchell, Y. M.; Krochta, J. M., Enzymatic treatments and thermal effects on edible soy protein films. *J. Food Sci.* 1994, 59 (6), 1332-1337.
- (84) P Henandez-Munoz, P.; Hernandez, R. In *Heat curing of wheat gluten gliadin and glutenin films*, 2002 Annual Meeting and Food Expo-Anaheim, California, 2002.
- (85) Yao, C.-H.; Liu, B.-S.; Chang, C.-J.; Hsu, S.-H.; Chen, Y.-S., Preparation of networks of gelatin and genipin as degradable biomaterials. *Mater. Chem. Phys.* 2004, 83 (2), 204-208.
- (86) Martinez, A. W.; Caves, J. M.; Ravi, S.; Li, W.; Chaikof, E. L., Effects of crosslinking on the mechanical properties, drug release and cytocompatibility of protein polymers. *Acta Biomater.* 2014, 10 (1), 26-33.
- (87) Schoth, A.; Landfester, K.; Munoz-Espi, R., Surfactant-free polyurethane nanocapsules via inverse pickering miniemulsion. *Langmuir* 2015, 31 (13), 3784-3788.
- (88) Yow, H. N.; Routh, A. F., Formation of liquid core-polymer shell microcapsules. *Soft Matter* 2006, 2 (11), 940-949.
- (89) Koh, E.; Baek, S.-Y.; Kim, N.-K.; Lee, S.; Shin, J.; Kim, Y.-W., Microencapsulation of the triazole derivative for self-healing anticorrosion coatings. *New J. Chem.* 2014, 38 (9), 4409-4419.

- (90) Velev, O.; Nagayama, K., Assembly of latex particles by using emulsion droplets. 3. Reverse (water in oil) system. *Langmuir* 1997, *13* (6), 1856-1859.
- (91) Voorn, D.; Ming, W.; Van Herk, A., Polymer-clay nanocomposite latex particles by inverse pickering emulsion polymerization stabilized with hydrophobic montmorillonite platelets. *Macromolecules* 2006, *39* (6), 2137-2143.
- (92) Rule, J. D.; Sottos, N. R.; White, S. R., Effect of microcapsule size on the performance of self-healing polymers. *Polymer* 2007, *48* (12), 3520-3529.
- (93) Hayward, R. C.; Utada, A. S.; Dan, N.; Weitz, D. A., Dewetting instability during the formation of polymersomes from block-copolymer-stabilized double emulsions. *Langmuir* 2006, *22* (10), 4457-4461.
- (94) Yang, Y.; Ning, Y.; Wang, C.; Tong, Z., Capsule clusters fabricated by polymerization based on capsule-in-water-in-oil Pickering emulsions. *Polymer Chemistry* 2013, *4* (21), 5407-5415.
- (95) Samanta, A.; Tesch, M.; Keller, U.; Klingauf, J. r.; Studer, A.; Ravoo, B. J., Fabrication of Hydrophilic Polymer Nanocontainers by Use of Supramolecular Templates. *J. Am. Chem. Soc.* 2015, *137* (5), 1967-1971.
- (96) Bon, S. A.; Chen, T., Pickering stabilization as a tool in the fabrication of complex nanopatterned silica microcapsules. *Langmuir* 2007, *23* (19), 9527-9530.
- (97) Jagtap, S. B.; Mohan, M. S.; Shukla, P. G., Improved performance of microcapsules with polymer nanocomposite wall: Preparation and characterization. *Polymer* 2016, *83*, 27-33.
- (98) Torza, S.; Mason, S., Three-phase interactions in shear and electrical fields. *Journal of Colloid and Interface Science* 1970, *33* (1), 67-83.
- (99) Wang, Y.; He, J.; Liu, C.; Chong, W. H.; Chen, H., Thermodynamics versus kinetics in nanosynthesis. *Angewandte Chemie International Edition* 2015, *54* (7), 2022-2051.
- (100) Kim, J. W.; Cho, J.; Cho, J.; Park, B. J.; Kim, Y. J.; Choi, K. H.; Kim, J. W., Synthesis of Monodisperse Bi-Compartmentalized Amphiphilic Janus Microparticles for Tailored Assembly at the Oil–Water Interface. *Angewandte Chemie International Edition* 2016.
- (101) Palanikkumaran, M.; Gupta, K. K.; Agrawal, A. K.; Jassal, M., Highly stable hexamethylolmelamine microcapsules containing n-octadecane prepared by in situ encapsulation. *Journal of applied polymer science* 2009, *114* (5), 2997-3002.
- (102) Lee, H.; Lee, S.; Cheong, I.; Kim, J., Microencapsulation of fragrant oil via in situ polymerization: effects of pH and melamine-formaldehyde molar ratio. *J. Microencaps.* 2002, *19* (5), 559-569.

- (103) Binks, B. P., Particles as surfactants—similarities and differences. *Current Opinion in Colloid & Interface Science* 2002, 7 (1), 21-41.
- (104) Schulman, J. H.; Leja, J., Control of contact angles at the oil-water-solid interfaces. Emulsions stabilized by solid particles (BaSO₄). *Transactions of the Faraday Society* 1954, 50, 598-605.
- (105) Cui, L.; Khramov, D. M.; Bielawski, C. W.; Hunter, D.; Yoon, P.; Paul, D., Effect of organoclay purity and degradation on nanocomposite performance, Part 1: Surfactant degradation. *Polymer* 2008, 49 (17), 3751-3761.
- (106) Shirasaka, H.; Inoue, S.-i.; Asai, K.; Okamoto, H., Polyurethane urea elastomer having monodisperse poly (oxytetramethylene) as a soft segment with a uniform hard segment. *Macromolecules* 2000, 33 (7), 2776-2778.
- (107) Luo, W.-j.; Yang, W.; Jiang, S.; Feng, J.-m.; Yang, M.-b., Microencapsulation of decabromodiphenyl ether by in situ polymerization: preparation and characterization. *Polymer degradation and stability* 2007, 92 (7), 1359-1364.
- (108) Merline, D. J.; Vukusic, S.; Abdala, A. A., Melamine formaldehyde: curing studies and reaction mechanism. *Polym. J.* 2013, 45 (4), 413-419.
- (109) Nastke, R.; Dietrich, K.; Reinisch, G.; Rafler, G.; Gajewski, H., The initial stage of the reaction of melamine with formaldehyde. *Journal of Macromolecular Science—Chemistry* 1986, 23 (5), 579-596.
- (110) Long, Y.; York, D.; Zhang, Z.; Preece, J. A., Microcapsules with low content of formaldehyde: preparation and characterization. *Journal of Materials Chemistry* 2009, 19 (37), 6882-6887.
- (111) Tan, J.; Li, C.; Zhou, J.; Yin, C.; Zhang, B.; Gu, J.; Zhang, Q., Fast and facile fabrication of porous polymer particles via thiol–ene suspension photopolymerization. *RSC Advances* 2014, 4 (26), 13334-13339.
- (112) Pekala, R.; Alviso, C.; Kong, F.; Hulsey, S., Aerogels derived from multifunctional organic monomers. *J. Non-Cryst. Solids* 1992, 145, 90-98.
- (113) Coullerez, G.; Léonard, D.; Lundmark, S.; Mathieu, H. J., XPS and ToF-SIMS study of freeze-dried and thermally cured melamine-formaldehyde resins of different molar ratios. *Surf. Interface Anal.* 2000, 29 (7), 431-443.
- (114) Ren, H.; Zhu, J.; Bi, Y.; Xu, Y.; Zhang, L.; Shang, C., Rapid fabrication of low density melamine–formaldehyde aerogels. *J. Porous Mater.* 2017, 1-8.